esa
european space agency
agence spatiale européenne

SCI(88)4
October 1988

QUASAT

A SPACE VLBI SATELLITE

REPORT ON THE PHASE A STUDY

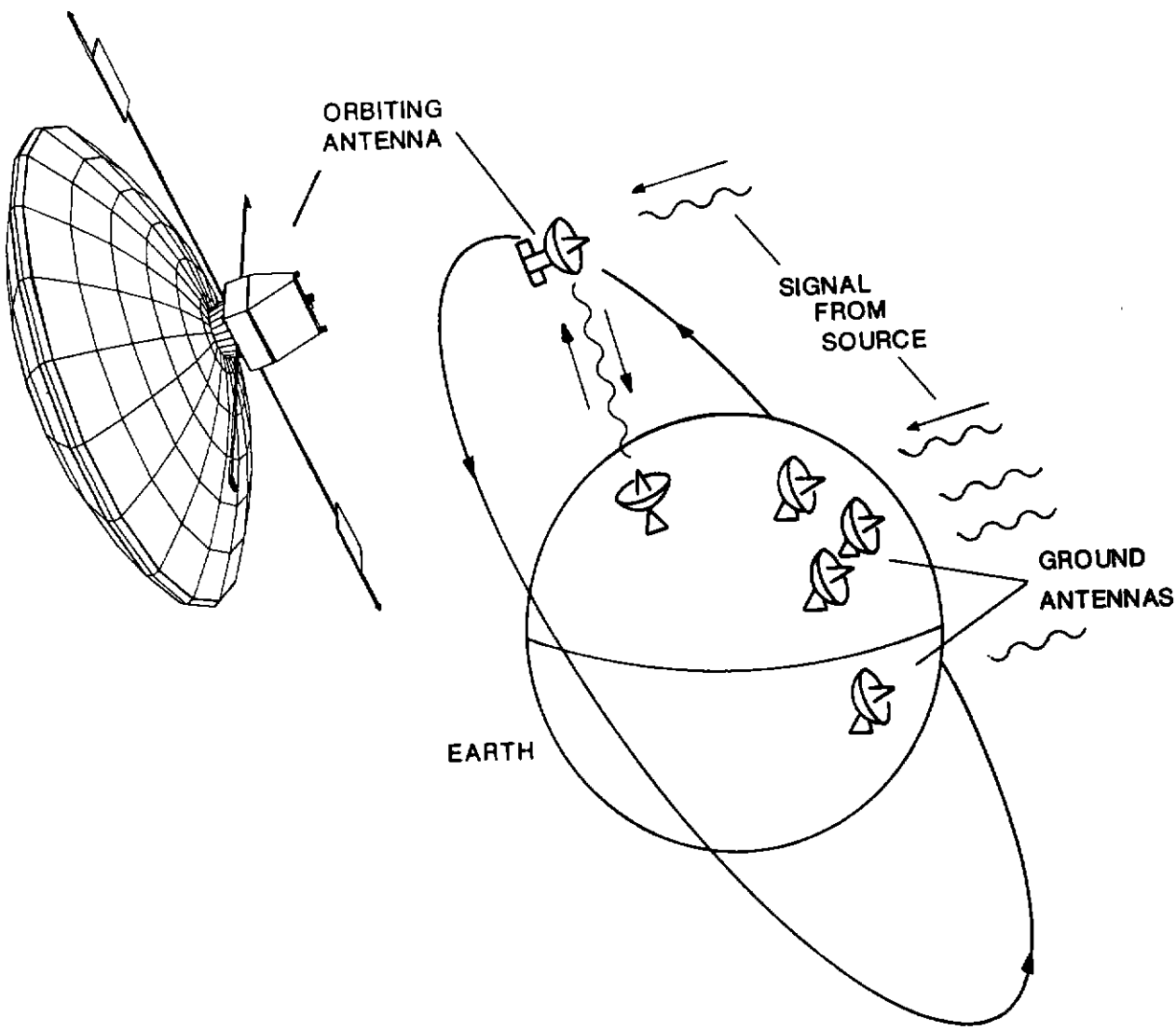

Quasat mission summary

Objective	Very-Long-Baseline Interferometry (VLBI) K-band (22 GHz) dual polaristion C-band (5 GHz) bandwidth: 64 MHz L-band (1.6 GHz) UHF (327 MHz) bandwidth: 4 MHz
Payload	15 m aperture, inflatable, space-rigidised. Feeds for four frequencies. Radio-astronomy receivers
Launch Mass	1298 kg (incl. 85 kg adaptor)
Payload Mass	160 kg (incl. 124 kg reflector)
Propellant Mass	434 kg (hydrazine)
Size/Envelope	Width: 2.1 m (launch configuration) Height: 4.8 m (launch configuration) Deployed reflector diameter: 16 m Reflector focal length: 5.85 m
Spacecraft Type	Three-axis stabilised
Pointing Accuracy	30 arcsec
Power Consumption	600 W
Telemetry	Science data: Ku-band, 144 Mbit/s Command and housekeeping: Ku-band, 2 kbit/s LEOP and emergencies: S-band, 2 kbit/s
Payload Thermal Control	K-band and C-band pre-amplifiers cooled to 80 K by Stirling-cycle coolers
Launcher	Ariane-4, dual-launch Lower passenger (Spelda 20)
Initial Orbit	Geostationary Transfer Orbit (GTO)
Operational Orbit	Perigee: 5000 km Apogee: 36 000 km Inclination: 30° Period: 12.1 h
Ground Stations	ESA Ku-band stations (to be developed) Alternative: Deep-Space Network (DSN)
Operational Mode	Pre-planned
Design Lifetime	2 yr (Consumables: 5 yr)

FOREWORD

Many radio sources are unresolved on the longest interferometer baselines possible on Earth. Their further study requires the longer baselines only provided by a radio telescope as interferometer element in space. Several concepts for orbiting radio telescopes operating with ground based VLBI networks were in consideration in the early 1980's, culminating in the QUASAT concept which is the subject of this Phase A report.

Following agreement on the scientific objectives and the mission concept, the QUASAT proposal was submitted to ESA in 1982 by Dr. R. T. Schilizzi for a group of European, American and Australian radio astronomers. From its inception, the project was studied as a joint ESA/NASA project; ESA and NASA carrying out parallel assessment studies in the 1983-1985 period. Australia also expressed interest in participating in QUASAT. The European and US concepts were reviewed by the scientific community during a Workshop held 1984 in Gross-Enzersdorf, Austria (ESA SP-213).

Because of the global character of VLBI activity, extensive discussions on possible modes of coordination and cooperation took place not only between ESA and NASA but also ESA and Interkosmos (USSR), and ESA and ISAS (Japan). These discussions have continued within the Inter - Agency Consultative Group (IACG) where a working group on space VLBI has been set up.

In parallel with these activities, ESA was preparing its Long Term Plan for science, *Horizon 2000*. In this plan the idea of fixed budget allocations was presented. QUASAT, as a cooperative venture, was classified as a medium sized mission ("blue box"). Following presentation of the ESA Assessment study to the science community in February 1986, the Science Programme Committee gave approval in April 1986 for a Phase A study of a cooperative ESA/NASA QUASAT mission.

However, in the summer of 1986, after the Challenger disaster, NASA found itself unable to support the anticipated schedule for cooperation on the QUASAT study. Following the recommendations of a "Tiger Team" appointed by the Astronomy Working Group to appraise the situation, ESA then re-oriented its study of QUASAT toward an ESA-led mission concept that would not necessarily involve the same level of NASA participation. At this time the National Research Council of Canada also expressed interest in the project. US, Canadian and Australian representatives have participated as full members of the ESA study team.

The ESA QUASAT mission concept described in this report was studied at Phase A level with industry, in cooperation with US, Canadian and Australian scientists and engineers. The industrial study was carried out between May 1987 and May 1988 by a consortium consisting of Aeritalia, British Aerospace, Erno, Fokker, Inta, Matra and Saab Space. The study has been supported by technical development work done on the antenna by Contraves and on the feed by CSELT.

From the start of the ESA QUASAT Phase A Study, the cooperative scenario with the US and Canada has been well identified. In parallel to the ESA study efforts, NASA and Canada have studied their proposed areas of support. Because of budgetary constraints, Australian support will not include any involvement on the spacecraft except the payload. Representatives of the ground systems (EVN, NRAO and the AT) have been involved in the study and have expressed their intent to provide observing time for operation with QUASAT. The cooperation regarding the ground systems are described in the main report which reflects the ESA stand-alone scenario. A description of the potential ESA-led cooperation with NASA and Canada has been attached to this report as an appendix.

In writing this report, the science team has been supported by colleagues around the world. References to published work have, for the most part, been excluded from the text for ease of reading.

The European members of the ESA QUASAT Science Team are:

B. Anderson	University of Manchester (UK)
A. van Ardenne	Radiosterrenwacht, Dwingeloo (NL)
A. Baudry	Observatoire de l'Université de Bordeaux (F)
A. Benz	Institut für Astronomie, ETH, Zürich (CH)
R. S. Booth	Onsala Space Observatory (S)
A. Ferrari	Instituto di Fisica Generale, Torino (I)
D. W. Murphy	University of Manchester (UK)
E. Preuss	Max-Planck-Institut für Radioastronomie, Bonn (D)
R. T. Schilizzi	Radiosterrenwacht, Dwingeloo (NL)
G. Tofani	Osservatorio Astrofisico di Arcetri, Firenze (I)
P. N. Wilkinson	University of Manchester (UK)

The non European members are:

B. F. Burke	Massachusetts Institute of Technology, Cambridge (USA)
J. F. Jordan	Jet Propulsion Laboratory, California Institute of Technology, Pasadena (USA)
J. S. Levy	Jet Propulsion Laboratory, California Institute of Technology, Pasadena (USA)
R. A. Preston	Jet Propulsion Laboratory, California Institute of Technology, Pasadena (USA)
T. H. Legg	National Research Council, Ottawa (CAN)
D. Morton	National Research Council, Ottawa (CAN)
D. N. Cooper	CSIRO, Epping (AUS)
D. L. Jauncey	CSIRO, Canberra (AUS)

Substantial contributions to this report have been provided by:
L. D'Addario, W. A. Baan, N. Bartel, J. A. Biretta, A. G. de Bruyn, B. K. Dennison, P. J. Diamond, I. Fejes, R. Freeland, D. A. Graham, K. I. Kellermann, A. Marscher, G. K. Miley, J. M. Moran, R. L. Mutel, G. Pilbratt, M. J. Reid, N. Renzetti, D. H. Roberts, R. E. Spencer, J. Springett, R. G. Strom, S. Weinreb, K. J. Wellington and J. Wilcher.

The ESA personnel responsible for the study are:
A. Hawkyard (*Study Manager*), J. W. Cornelisse (*Deputy Study Manager*) and U. O. Frisk (*Study Scientist*).

Requests for further information or additional copies of this report should be adressed to the Study Scientist or the Study Manager:

U. O. Frisk
Astrophysics Division
Space Science Department
ESTEC, Postbus 299, 2200 AG Noordwijk
The Netherlands

A. Hawkyard
Future Science Projects
Scientific Programme Directorate
ESTEC, Postbus 299, 2200 AG Noordwijk
The Netherlands

r to the Secretary of the Astronomy Working Group:

S. Volonte'
European Space Agency
8-10, rue Mario-Nikis
F-75738 Paris Cedex 15
France

Contents

List of Tables

List of Figures

EXECUTIVE SUMMARY

During the past 20 years, radio astronomers have developed the very-long-baseline interferometry (VLBI) technique to the point that the longest baselines available on Earth are now in regular use to make high resolution measurements on a wide variety of celestial radio sources. In this way, angular resolutions of 0.3 milliarcsec are achieved, resolutions which are more than three orders of magnitude greater than for individual optical telescopes on the Earth and two orders of magnitude greater than for the Hubble Space Telescope. But despite this resolution, unresolved radio components are found. By adding a radio telescope in space, the longer baselines needed to investigate their structure can be achieved.

This Phase A study has been carried out for an ESA-led mission to launch QUASAT, a free flying satellite carrying a radio telescope in an elliptical orbit around the Earth. From this orbit it will be used to make interferometer observations of radio sources primarily with the major ground-based VLBI networks in Europe, USA and Australia. Altogether telescopes in some 20 countries are expected to take part in QUASAT observation. QUASAT is unique amongst space science missions in that the space element has little scientific value in itself — it is only in interferometric combination with the ground-based VLBI arrays that it breaks new instrumental ground, providing high quality images of radio sources with a five-fold increase in angular resolution.

The main goal of the QUASAT mission is to probe the nuclei of radiogalaxies and quasars more deeply and with greater detail than is possible with ground-based networks alone. Ground-based VLBI has already played an essential role in establishing the current paradigm for the central parsec in active nuclei. With QUASAT, structures on scales expected for the accretion disks around massive black holes will be observable in nearby active nuclei. Such observations will add to our understanding of the physical processes responsible for the generation of enormous energies within regions light days across, the channelling of part of that energy into highly collimated (probably relativistic) jets, and the interaction of these jets with thermal plasma in the broad optical emission line region. QUASAT images will provide a framework for the interpretation of continuum outbursts from IR to mm wavelengths which are believed to be related to shock processes at the base of the jets. It will also be possible to observe galactic and extragalactic H_2O and OH maser sources in much finer detail than hitherto and to clarify their role as signposts of star formation in the galaxy. Observations of statistical parallax in H_2O masers in nearby galaxies will lead to a direct measurement of the distances to these objects. The flares (and possibly the quiescent emission) of radio stars can be monitored to give unique information on emission mechanisms in these objects.

On these small scales, changes in radio structures are to be expected in response to surges in the energy release processes, proper motion of the emitting regions at relativistic speeds along the jets, and evolution of the emitting regions themselves. Tracing these changes in both galactic and extragalactic sources through repeated multi-frequency imaging in total intensity and polarisation will be one of the primary tasks of QUASAT, and should provide unique information on the structure, the kinematics, the magnetic field, and the thermal electron distribution in a wide variety of astrophysically important objects on linear scales of great interest.

The choice of orbit is a trade-off between the desire for higher angular resolution and the ability to make images of the compact sources detected. The factor of five increase in angular resolution chosen for QUASAT over the Earth-based arrays is a good compromise in these respects. QUASAT will provide strikingly better images than any other currently proposed space VLBI mission.

The satellite will be launched by Ariane 4 in a dual-launch configuration and injected into a geostationary transfer orbit (GTO). Insertion into the operational orbit will take place after a

few revolutions in the GTO. The parameters of the orbit are: apogee altitude 35786 km, perigee altitude 5000 km, inclination 30° and period 12.11 hours.

The observing wavelengths are 1.35, 6, 18 and 92 cm in common with the standard wavelengths for the ground networks. At 1.35 cm the highest angular resolution on the stronger compact quasars and radio galaxies will be achieved, and at this wavelength H_2O maser sources can be observed. Observations at 6 cm provide for two to three times the sensitivity at 1.35 cm, at a resolution similar to 1.35 cm on the ground. Observations at 18 cm also have a similar sensitivity to 6 cm for continuum work and a resolution similar to 6 cm on the ground; OH masers are observed at 18 cm. The longest wavelength, 92 cm, is essential for studies of the interstellar medium; the resolution with QUASAT is similar to 18 cm on the ground. Typical observations will last from 3 to 48 hours.

The angular resolution of the QUASAT system at 1.35 cm will be 50 micro-arcseconds, corresponding in linear measure to 8×10^{12}cm (0.5 Astronomical Units) at the distance of the Galactic Centre, 4×10^{15}cm (1.5 light days) at the distance of the nearest radio galaxy, Centaurus A, and 5×10^{17} cm (0.15 pc) at the distance of most quasars. The angular and linear resolutions at the other observing wavelengths scale with the wavelength.

The overall sensitivity of a typical twelve-station VLBI array including QUASAT and one large diameter (> 70 m) antenna on the ground is sufficient to detect a 50 mJy compact component at 1.35 cm, a 20 mJy component at 6 and 18 cm, and an 85 mJy component at 92 cm in the basic 300 second integration necessary for self calibration. Image simulation studies have shown that an image built up over a 24 hour period will have a dynamic range off-source of 1000:1, which will allow detection of components in the field of view with flux densities down to 200μJy. This is comparable to current VLBI systems. With the surface brightness sensitivity of QUASAT, it is expected that at least 500 extragalactic objects will be mappable at 22 GHz, and at least 5000 at each of 5, 1.6 and 0.3 GHz.

The space-borne antenna will be capable of observing in both hands of circular polarisation simultaneously at any two of the wavelength complement, and will relay the received signals via a digital link directly to telemetry stations (ESA and/or NASA DSN) on the ground. A phase/frequency reference for the antenna in space, stable to about one part in 10^{14}, will be based on hydrogen maser oscillators on the ground and relayed directly to the satellite via a two-way link from the telemetry stations in turn. All communication with the space element will be through telemetry stations in the network using standard techniques.

After transmission to the ground, the signal will be recorded on magnetic tape in digital form, and transported to the central processing facility of the European or US VLBI array for correlation with similar tapes from the ground VLBI arrays. After correlation and calibration the data will be sent to the principal investigators for further analysis.

The major new aspect of the spacecraft is the deployable antenna. An Inflatable Space Rigidised Reflector manufactured by Contraves has been selected in view of its relatively high surface accuracy, low cost and mass, easy storage during launch and simple mechanical design and deployment concept. Following deployment of the antenna, both the spacecraft bus and the remainder of the payload will be located at the prime focus of the antenna.

A satisfactory design has been developed for the radio astronomy feed involving a coaxial waveguide feed at prime focus for the three shortest wavebands with four dipoles spaced around it to support the fourth waveband (92 cm). Polarisers are provided to separate the left and right hand circularly polarised signals. A focal distance to diameter ratio of 0.39 has been adopted for the antenna to provide the best overall performance with this feed.

Radio astronomy receivers using HEMT (High Electron Mobility Transistor) preamplifiers have been selected to amplify, with minimum noise, the very weak signals intercepted by the antenna.

The noise performance goals for QUASAT at 92 and 18 cm can be met without resort to active cooling. At 1.35 cm the goals can only be met by using long-life mechanical Stirling cycle coolers to cool the preamplifier, the transmission lines and the polarisers and, at 6 cm, the preamplifier. The expected physical temperatures achievable are 95 K and 150 K at 1.35 and 6 cm respectively, and 300 K at 18 and 92 cm.

The scientific Instrument namely the receivers with associated electronics and coolers, the feeds, will be provided by national institues. Following an open Announcement of Opportunity a consortium will be selected which will provide this complete package. The reflector will be procured by ESA.

The study has shown that the overall mission, which is based on current VLBI and spacecraft engineering practice, is technically feasible. Also, a successful "proof of concept" demonstration has been carried out by a JPL-led international team using the Tracking and Data Relay Satellite (TDRS). This satellite had a sensitivity about 20 times less than that expected for QUASAT.

Support for the QUASAT mission in terms of observing time on the ground VLBI systems and in use of the correlation facilities has been given by the managements of the ground arrays.

The operational management of QUASAT will include a Steering Group comprising appropriate representatives of the ground-based arrays and the space agencies with responsibility for reviewing the overall performance of the QUASAT system and initiating action where necessary. The managements of the ground-based VLBI arrays will be responsible for the operations of their individual telescopes and correlators. The Mission Control Centre (MCC) at ESOC will be responsible for the operation of the QUASAT spacecraft including its payload, and the telemetry station network. The MCC will monitor the performance of the spacecraft-ground signal link required for acquisition of the science data from the spacecraft. Following competitive selection a Science Operations Centre in Europe, located at a host institute, will be established for the smooth interfacing of the space and ground VLBI elements of the QUASAT system. Following open Announcements of Opportunity, observing proposals will be selected by a Proposal Evaluation Committee with a wide-ranging membership.

QUASAT will be operated in observatory mode with data correlation and ground-based observing being carried out for the astronomer "in absentia". The astronomer will receive calibrated interferometric data for further analysis at his or her institute or at the Science Operations Centre using standard software.

During the first few months of operation a science core program will be carried out. This program will be composed by a QUASAT Science Team including Principle Investigator representatives and Mission Scientists. Except during commissioning phase, the core program, and periods needed for functional verification and calibration, all time will be available as open observing time.

The QUASAT Phase A Study has shown that an interferometric system incorporating an orbiting radio telescope in a 12 hour orbit and existing ground-based VLBI arrays is feasible from the technical and managerial points of view. *It is the next logical step in the development of radio interferometry and will provide an unprecedented combination of angular resolution and image quality to tackle a wide range of astrophysical problems.*

Chapter 1

Introduction

The history of radio astronomy has been marked by a continuous series of discoveries of new astrophysical phenomena. Many of these discoveries have been instrumental in shaping our current view of the universe. The enormous power emitted by radio sources, galactic and extragalactic, was not foreseen in pre-radio astronomy days but it is now clear that high energy processes are common in astrophysics and that they occur in radio sources ranging from stellar to galactic dimensions. Radio astronomy played a vital role in the discovery of quasars. Galactic nuclei have been shown to be powerful centres of activity, in all likelihood associated with massive black holes. Radio images have shown ordered, collimated outflow of material from objects ranging in size from stars to galactic nuclei. Finally, the interstellar and circumstellar masers observed at radio wavelengths demonstrate that dense gas clouds can exhibit phenomena with an entirely unexpected degree of order and coherence.

The advance of modern astrophysics has been marked by three principal instrumental themes: increased sensitivity, improved spectral coverage, and higher angular resolution. Despite the intrinsic limits imposed by diffraction at longer wavelengths, the greatest improvements in angular resolution have come in radio astronomy, where the advance of interferometric techniques has produced dramatic increases in the angular resolution of radio images. This has been because of longer interferometer baselines; Very Long Baseline Interferometry (VLBI), which combines the outputs of radio antennas located as far apart as an Earth diameter, marks the greatest advance achieved so far in angular resolution. Current global VLBI arrays with up to 18 elements and effective diameters of some 8000 km reach sub- milliarcsecond angular resolution and are the largest telescopes which have ever looked into the depths of the universe. Accompanying this advance has been an increase in the quality of the images, as characterised by their dynamic range, the ratio of the brightest to faintest reliable features. This increase has come as a result of better aperture plane (or uv plane) coverage and improved image construction algorithms.

The angular resolving power of the current global VLBI network at 1.35 cm wavelength (0.3 milliarcsec) surpasses individual ground-based optical telescopes by more than three orders of magnitude and will surpass the Hubble Space Telescope by two orders of magnitude. This resolving power has led to many important discoveries, including apparent velocities in quasars and radio galaxies that exceed the speed of light, and highly collimated plasma jets in radio galaxies on scales of less than one parsec which are the bases of jets extending to several million parsecs. To a large extent it is the direct observational evidence from VLBI which has led to current ideas about compact "central engines" and bulk relativistic material motion in galactic nuclei. Within our home Galaxy, the powerful molecular masers, often associated with the star-formation process, have been shown to have complex spatial and velocity structure on very small scales which trace the winds of change in star formation. Active binary systems, such as the mass-transfer X-ray

objects, exhibit outbursts of radio noise. Even the nucleus of our Galaxy is sufficiently compact to require study by VLBI techniques.

As the body of discoveries from VLBI has grown, it has become clear that in nearly every compact source observed at centimetre wavelengths, there remains spatial structure which is unresolved with the best angular resolution achievable with antennas on Earth. To explore the smallest structures and thereby observe on scales which are likely to be of great importance for our understanding of the central regions of quasars and galaxies, the role of molecular masers in star formation and stellar evolution, and flaring processes on stars, substantially higher resolution, high quality images are essential. This can only be achieved by placing a radio telescope in space observing in interferometric mode with Earth-based VLBI arrays. *Space to ground VLBI is the next logical step in the development of radio interferometry. It will give angular resolutions and image quality orders of magnitude better than for any other astronomical instrument operating at any wavelength in the next 20 years.*

The elements of a space VLBI system are:

- An orbiting radio telescope with multi-frequency and polarisation capability.
- The ground VLBI networks or arrays which observe with the orbiting antenna.
- A network of telemetry stations to receive the down-linked signals from the orbiting antenna, and to relay stable reference frequency signals up to the satellite.
- The data processing facilities.

This Phase A Study report describes the results of a study of the QUASAT space VLBI system, an ESA-led international project to launch a free-flying satellite carrying a 15 metre diameter radio frequency antenna into Earth orbit. The major elements studied have been the spacecraft configuration, the science package (antenna, feeds and receivers), the orbits, the image quality and ground support.

During the Study, a "proof of concept" was carried out by a JPL-led international team using a 4.9 metre antenna on the US Tracking and Data Relay Satellite (TDRS) to successfully perform VLBI observations with antennas in Australia and Japan on baselines up to 2.16 Earth diameters. This has put the technical feasibility of space VLBI beyond doubt, and demonstrated quite clearly that many radio sources possess structure on scales accessible to QUASAT. It should be noted that the QUASAT spacecraft will be about 20 times more sensitive than TDRS.

Emerging from the phase A study is a clear idea of the advantages of going into space for VLBI - not only increased angular resolution combined with image quality comparable to the best achieved on current Earth-based VLBI systems, but also coverage of the sky in the equatorial and southern hemisphere, virtually unexplored with VLBI techniques.

By combining simultaneous space and ground measurements, QUASAT effectively builds a radiotelescope with a diameter of about 50000 km. It will have five times higher angular resolution than for Earth-based VLBI networks at the same wavelength. The potential effect of this higher resolution is demonstrated graphically by the comparison of interferometer beam sizes in Figure 1.1.

The angular resolution, the maximum size of source that can be mapped reliably, and the sensitivity for the proposed observing frequencies are listed in Table 1.1. Figure 1.2 compares the angular resolution of QUASAT with other radio instruments, and shows the linear resolution for observations of the Galactic Centre and 3C84 (NGC1275), a typical active galaxy. The linear resolution is, broadly speaking, < 1 AU for galactic objects, 0.001–0.1 pc ($3 \times 10^{15} - 3 \times 10^{17}$ cm) for nearby galaxies, and 0.3 pc (10^{18} cm) for very distant radio galaxies and quasars.

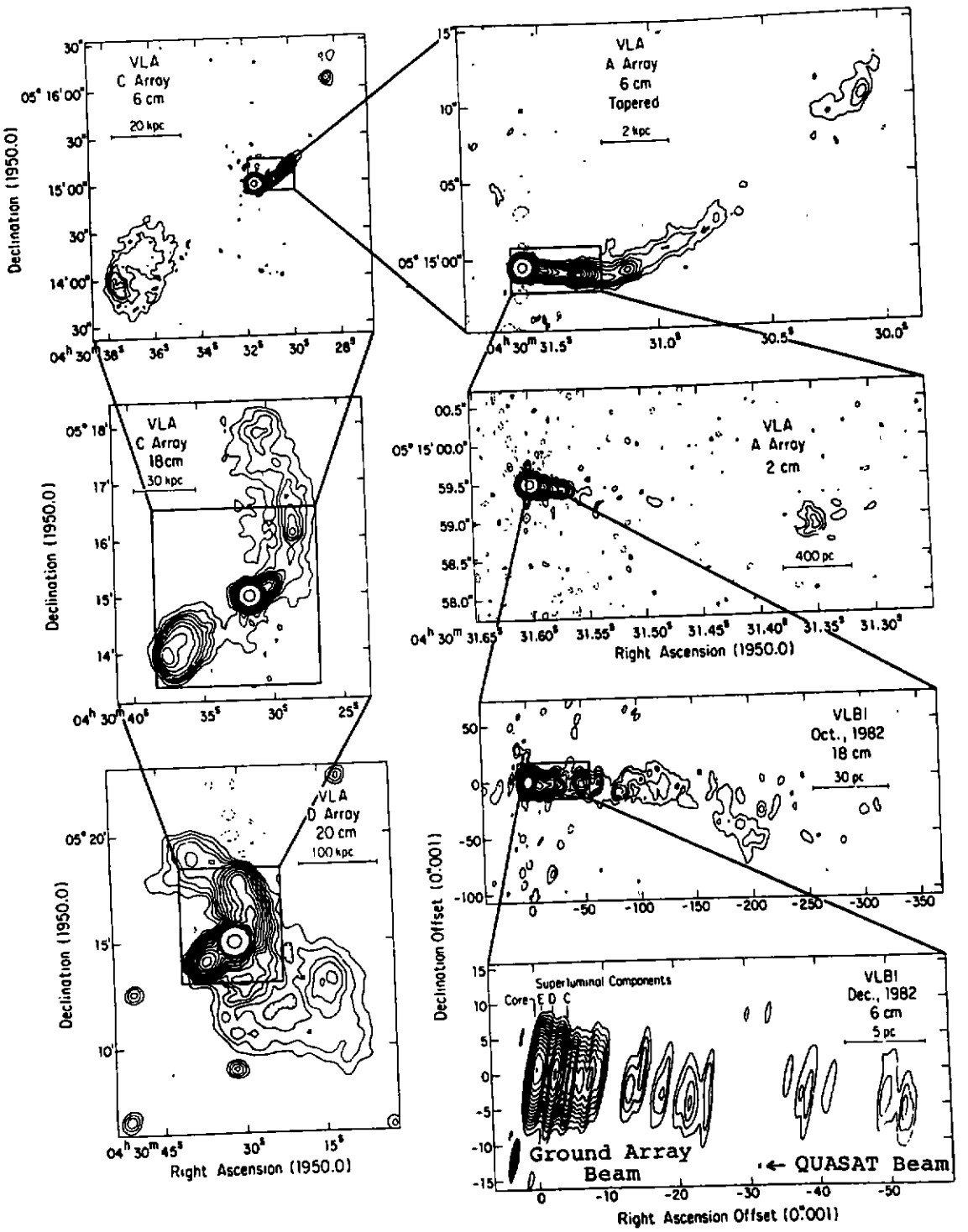

Figure 1.1: 3C120

A composite of radio pictures of 3C120 (0430+05) showing the emission structure on size scales ranging from 1 milli-arsec (pc) to 30 arcmin (kpc). The 5 GHz VLBI image (bottom right hand) will be greatly improved by using QUASAT. Compare the beam (point spread function) actually used with the one provided by QUASAT. The decrease in beam area demonstrated here is typical for objects at low declinations ($< 10°$) Adopted from Walker et al., ApJ **316**, 546, (1987).

Table 1.1: Angular resolution, maximum source size that can be mapped, and sensitivity

λ (cm)	Angular resolution[1] (micro-arcsec)	max source size (milli-arcsec)	RMS noise per pixel[2] (continuum)	RMS noise per spectral channel[3]	Frequency (GHz)
1.35	50	10	0.3 mJy	15 mJy	22.0-22.50
6	225	50	0.1	8	4.72-5.02
18	670	125	0.1	8	1.60-1.72
92	3410	675	0.6	-	0.324-0.328

1. this is the dimension of the synthesised beam (point spread function of the interferometer system). Information on size and position angle is in fact available on scales 2 to 3 times smaller than this.
2. for a 24 hour observation assuming there is a sufficiently strong feature (50 mJy at 1.35 cm, 20 mJy at 6 and 18 cm, and 85 mJy at 92 cm) present in the map to allow self-calibration.
3. for a 24 hour observation assuming there is a spectral feature present of sufficient strength (5 Jy at 1.35 cm and 2 Jy at 6 and 18 cm) to allow self-calibration.

The frequencies of observation chosen for QUASAT are 22, 5, 1.6 and 0.3 GHz. The maser line emissions at 22 GHz for H_2O and 1.6-1.7 GHz for OH dictate two of the frequency complement. 22 GHz is, at the same time, the highest operating frequency of the ground network for which there are telescopes of large collecting area and for which good sensitivity for both continuum and line can be achieved with a 15 metre diameter antenna in space.

Experience has shown that the most revealing radio images arise when there is a good match between resolution and surface brightness sensitivity but it is often impossible to predict in advance what the optimum observing frequency (and hence resolution) will be for a particular source. The third frequency of 5 GHz, approximately the geometric mean of the other two, has been chosen to fill the gap between 22 and 1.6 GHz, and provide a different combination of resolution and surface brightness sensitivity. 5 GHz will be particularly useful for imaging the optically thin jets in AGNs and is an optimum frequency for observing radio stars. On the ground, 5 GHz is one of the prime frequencies for high quality imaging since it is least affected by problems due to variations in atmospheric propagation delay. The lowest frequency, 0.3 GHz, is essential for studies of low frequency variable sources and the interstellar medium.

QUASAT at 5 GHz will have similar resolution to the global ground network at 22 GHz, and at 1.6 GHz a similar resolution to the ground network at 5 GHz. It will thus be possible for the first time to compare spectral and polarisation effects at different wavelengths at these extreme resolutions using simultaneous measurements. Such measurement yield important constraints on gas densities and magnetic fields in the compact cores. Simultaneity is essential since most, if not all, compact sources are variable.

The choice of orbit is a trade-off between the desire for higher angular resolution and the ability to make images of the compact sources detected. The factor of five increase in angular resolution chosen for QUASAT over the Earth-based arrays is a good compromise in these respects. A factor of ten or more increase necessarily would mean a highly eccentric orbit with high angular resolution achieved in one dimension only and poor image quality due to the absence of intermediate spacings. Simple size and orientation parameters may be derived but, from a highly elliptical orbit, imaging in the true sense is no longer possible. Larger orbits will also pose problems in detecting sources for systems having limited surface brightness sensitivity, and, also, at longer cm wavelengths sources will begin to be blurred by interstellar scattering.

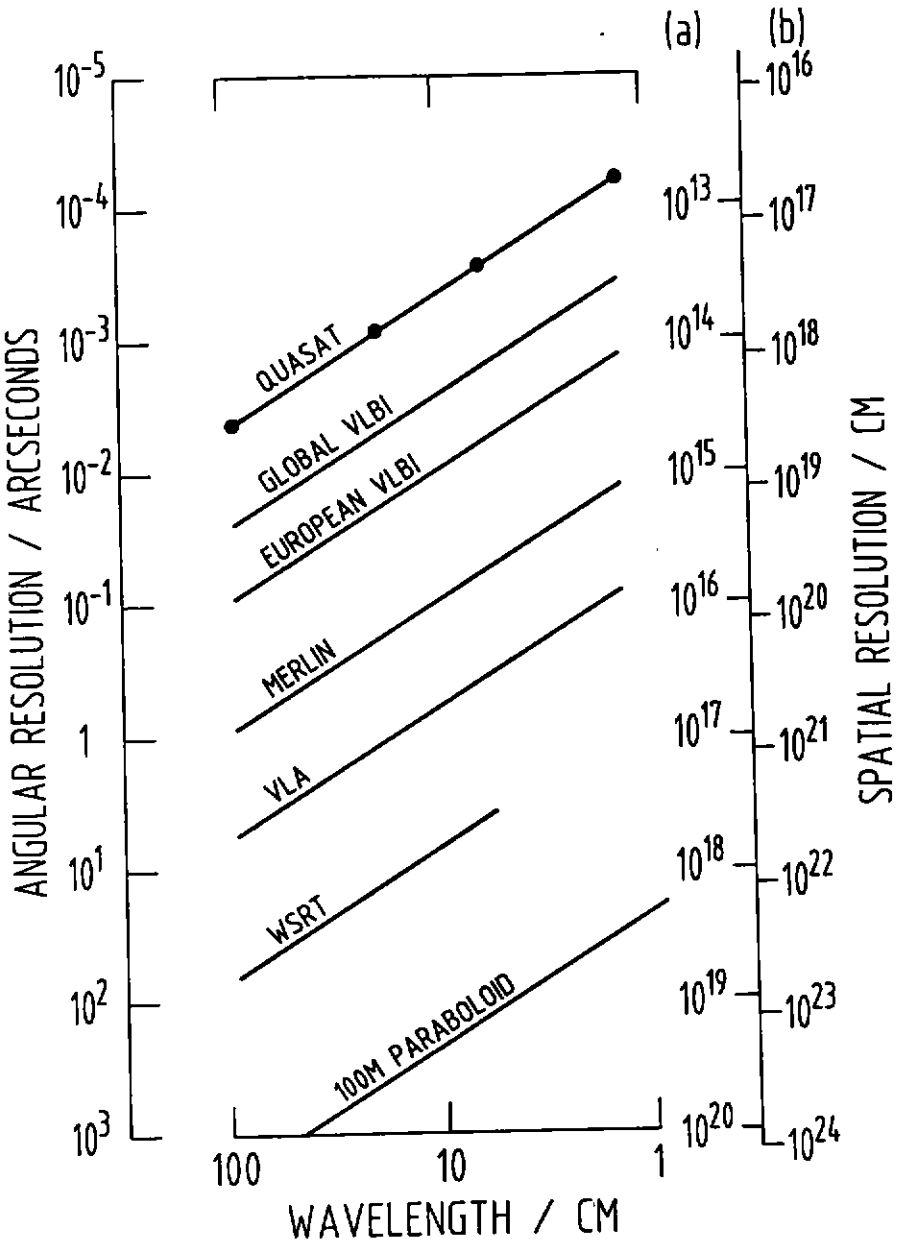

Figure 1.2: Angular resolution for some radio astronomical instruments.
Comparison of angular and spatial resolution of radio astronomical instruments for the wavelength range 1 to 100 cm. The angular resolution is given by wavelength divided by largest linear dimension of the telescope (diameter or interferometer baseline). The spatial resolution is given for a) the Galactic Centre (distance 7.1 kpc), and b) NGC1275=3C84 (distance 55 Mpc).

Current Soviet and Japanese plans include space missions which complement QUASAT, although these other missions, individually, have significantly less sensitivity and mapping capability than QUASAT. The Soviet mission, RADIOASTRON will be launched into a highly eccentric orbit with an apogee altitude of at least 75000 km, (and perhaps as high as 300000 km). The Japanese mission, VSOP, will be launched into a lower orbit (10000 km); cooperative observations between QUASAT and VSOP would enhance image quality as the lower flying Japanese satellite would fill in the holes in the QUASAT aperture plane coverage. The Inter-Agency Consultative Group (IACG)

has set up a panel on space VLBI to study the ramifications of a multi-satellite, multi-agency, space VLBI mission.

Extra angular resolution can also be achieved on the ground for flat spectrum continuum sources by going to shorter wavelengths. At 3 mm the angular resolution of ground-based VLBI networks is similar to QUASAT at 1.35 cm. Thus, simultaneous spectral index measurements will be possible, but only for a few strong active galactic nuclei since the 3 mm VLBI network is, and will remain, a factor of 20 less sensitive than QUASAT at 1.35 cm.

The QUASAT project is inherently international, and the VLBI community has an outstanding record of coordinating the activities of radio observatories in many different nations. Numerous international VLBI experiments have been successfully carried out, with radio telescopes in Australia, Brazil, Canada, China, England, Finland, France, Germany, India, Italy, Japan, the Marshall Islands (Kwajalein), the Netherlands, Poland, South Africa, the Soviet Union, Spain, Sweden, and the United States being involved at various times. While the space-based part of the QUASAT proposal involves a collaboration between ESA and other space agencies, the ground-based arrays are an essential component, and the necessary commitments of the European, U.S. and Australian ground-based VLB arrays have all been obtained.

The following sections of the report review all aspects of the QUASAT mission: the science objectives, the mission concept, the spacecraft system design including science payload, the mission ground support, the status and plans of the ground-based VLBI arrays, and the management of QUASAT operations. The report concludes with the development program for QUASAT, and some remarks on cooperation and coordination with other space agencies.

Chapter 2

Scientific Impact of QUASAT

2.1 Summary of scientific goals

QUASAT will add a new dimension to our understanding of high energy processes in celestial objects via detailed radio polarimetric imaging over a wide range of frequencies at resolutions as fine as 50 micro-arcsec. The immediate targets of observation are the compact high brightness temperature regions found in the nuclei of galaxies and quasars (AGNs), the molecular masers distributed throughout our own galaxy and detectable in many nearby galaxies, and the atmospheres and active regions of radio stars in our galaxy. QUASAT should advance our understanding of activity in AGN's, of relativistic bulk motion and collimated outflow in galactic nuclei and stars, of the physics of masers, and of energy release from flaring stars. Specific goals are summarised below and described in detail later in the chapter.

Extragalactic Studies

- the nature of the radio components associated with the central engines in AGN's, via detailed images at 50 μas resolution.
- the physics of the energy-carrying beams in radio sources; their structure, velocity, collimation and interaction with the broad and narrow line regions observed optically.
- the nature of radiation processes in compact radio sources, especially the link between synchrotron radiation and inverse Compton X-ray emission, via measurements of the brightness temperature and spectra of individual radio components.
- the large-scale geometry of the universe using the internal proper motions of distant superluminal quasars as a probe.
- the physical nature of the strong evolution with cosmic epoch exhibited by powerful radio sources, via radio images of high and low redshift objects.
- the nature of low-frequency variability in radio sources, via direct observations of their variable structure at low frequencies.
- the physical conditions in starburst nuclei from observations of megamasers.
- the physical characteristics and evolution of extragalactic radio supernovae, via observations of their structure in the first few years after outburst.
- the location of "dark" matter in the universe via detailed radio images generated by gravitational lenses.
- the measurement of the distances to the nearest galaxies in the Local Group via statistical parallax measurements in clusters of H_2O masers in their spiral arms.

Galactic Studies

- the physics of star-forming regions, via observations of the properties and motions of H_2O and OH masers in the innermost regions inaccessible by any other technique.
- the physics of stellar mass loss, from observations of OH and H_2O masers in circumstellar envelopes.
- the physics of the maser amplification process, from the measurement of the size, shape and kinematics of the maser spots.
- the physics of stellar binary systems which may contain small-scale versions of the central engines in AGN's.
- the distribution of turbulence in the interstellar medium and its effect on the propagation of radio waves through the Galaxy, via measurement of the apparent sizes of galactic masers, and of continuum radio components.
- the measurement of distances in the Galaxy from observations of statistical parallaxes in clusters of interstellar H_2O masers.

2.2 Active Galactic Nuclei

2.2.1 Introduction

One of the outstanding problems in extragalactic astronomy is to understand the nature of the source of energy for the violent activity displayed throughout the electromagnetic spectrum by the nuclei of a wide variety of galactic-sized objects. Quasars, blazars (i.e. optically violent variables (OVVs) and BL Lac objects), Seyfert galaxies, X-ray galaxies, radio galaxies, and, in milder form, in many less exotic galaxies like our own all have active nuclei and are known as AGNs. Radio, infrared (IR), optical and X-ray data combine in indicating an enormous total energy budget, sometimes equivalent to a significant fraction of the rest energy of 10^9 solar masses ($M_\odot$). Besides the extended radio structures (jets, lobes and hotspots), optical emission line profiles (in broad, narrow and extended emission-line regions (BLRs, NLRs and ELRs)) also suggest a strong, persistent dynamical activity characterized by supersonic outflows.

The radio galaxies ($\sim 10^{-4}$ of all galaxies), radio-loud quasars (a few percent of all quasars) and BL Lac objects form an important subclass of AGNs characterised by powerful non-thermal emission at centimetre wavelengths. This intense radio emission is agreed to be incoherent synchrotron radiation from ultra-relativistic charged particles gyrating in weak magnetic fields; emission is observed to arise on spatial scales smaller than 1 parsec (pc) and as large as 1 Mpc. As an example we can refer to 3C111 (Fig. 2.1) which is a luminous edge-brightened "classical" radio galaxy. It displays the three main components which are present in many extragalactic radio sources: (i) a compact radio core with a flat spectrum, (ii) a strongly collimated one-sided jet and (iii) two opposite extended lobes, $\sim$ 200 kpc apart. The source of the enormous energy required and

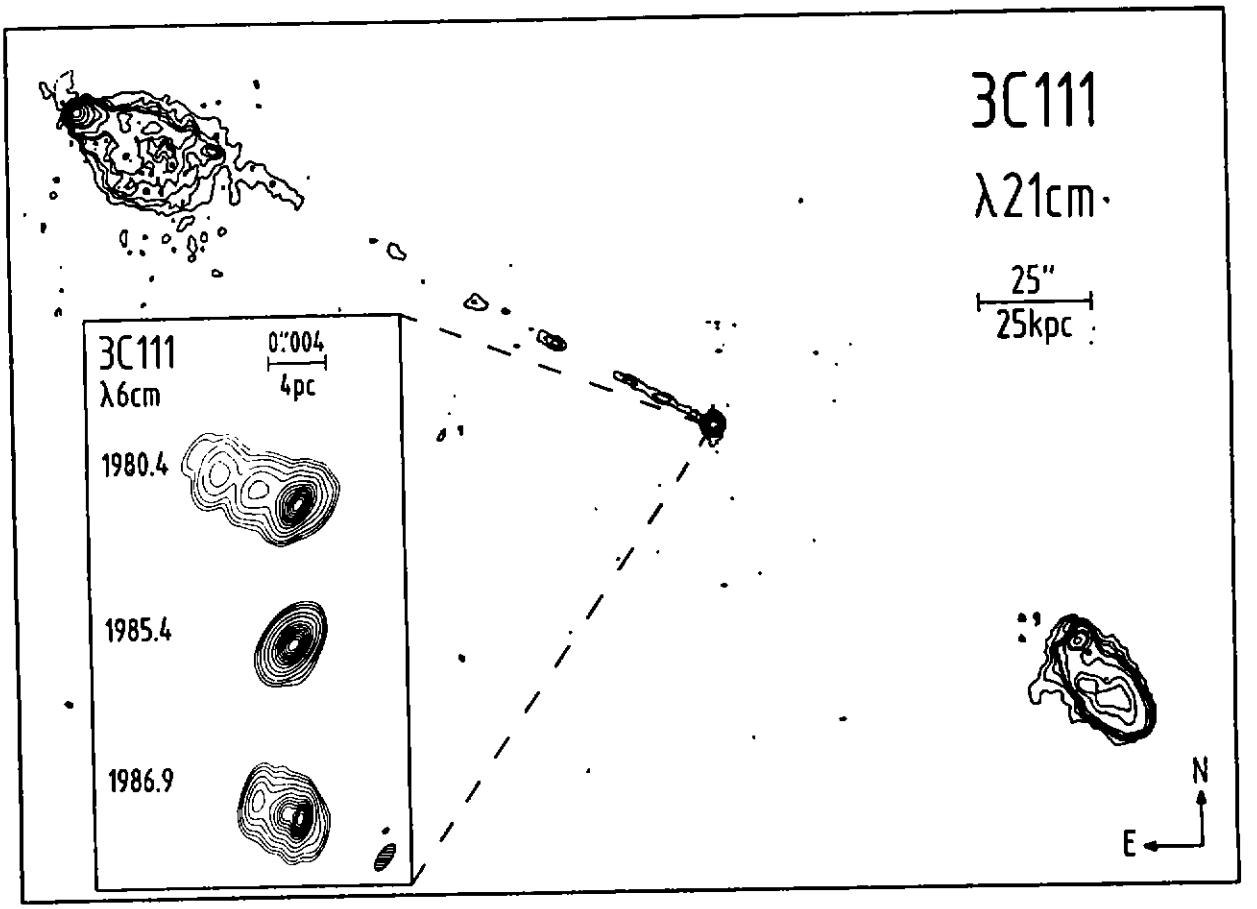

Figure 2.1: 3C111, a "classical" radio galaxy.

3C111, an example of a "classical" radio galaxy, mapped by the VLA at $\lambda = 21$ cm, and (inset) by VLBI at $\lambda = 6$ cm at several epochs. The bright, variable central component is coincident with a broad-line radio galaxy with $z = 0.0485$, giving a linear scale of 1 mas = 1 pc, for a Hubble constant of 65 $\mathrm{kms^{-1}Mpc^{-1}}$. The pc-scale structure of this radio core is strongly variable. If interpreted as propagation effects, the rapid changes imply a superluminal phenomenon. The synthesised beam of the ground VLBI network used to produce the sequence of VLBI images is shown in the lower right-hand corner of the inset together with the QUASAT beam (black dot) at the same frequency. Adapted from Linfield and Perley: 1984 (*Astrophys. J.* **279**, 60) and from Preuss et al.: 1988 (*IAU Symp. No. 129*, eds. M. J. Reid, J. M. Moran, Dordrecht, Reidel).

the manner which this energy is converted into relativistic particles remain tantalising problems, although the origin of the energy probably lies in a "central engine", possibly a supermassive black hole, within the nucleus. The compact central radio component is thought to be coincident with the inner nucleus; however, its size is unknown because the compact cores contain unresolved structure even at highest resolution yet attained. Generally speaking, the cores in quasars are much stronger than in radio galaxies.

Groundbased VLBI has already had a major impact on our understanding of the AGNs, including:

- The fact that cores remain unresolved on the longest Earth baselines. This is direct evidence that the central engine is smaller than $10^{17} - 10^{18}$ cm.

- The inference from the widespread occurrence of superluminal motion that matter is ejected with relativistic bulk velocities from the nuclei of these objects. This is the clearest indication at hand of the existence of a very deep potential well in, at least some, AGNs.
- The demonstration that the initial collimation of the energy-carrying beams in powerful radio sources occurs within 1 pc of the nucleus, and therefore cannot be due to the parent galactic interstellar medium.
- The discovery that the milli-arcsecond counterparts of one-sided arcsecond jets are always one-sided on the same side. This suggests there is a common cause of asymmetry from scales of less than 1 pc to much larger than 1 kpc in many sources.
- The discovery that the nuclear and the large-scale jet directions in double sources are well aligned. This shows that the outer jet axis is established not by the axis of the host galaxy but by the central engine, and suggests gyroscopic action of a rotating massive object.
- The discovery that radio continuum components always have brightness temperatures $T_B \leq 10^{12}$ K in AGNs. This is a strong indication that the nuclear radio emission is dominated by incoherent synchrotron emission. According to theory brightness temperatures $\gg 10^{12}$ K do not arise because of inverse Compton scattering of the radiating electrons.

The VLBI technique is, and will remain for many years, the only feasible way to image the very inner structure of galactic nuclei with any detail, and is therefore needed to study the basic physics of the central regions of galaxies. The direct resolution afforded by VLBI has already proven to be an invaluable complement to the detailed studies in the IR, UV, optical and X-ray bands.

QUASAT observations will allow us to achieve even greater angular resolution and to obtain direct, 20-100 μas limits on the size of the central radio emitting region in a wide variety of AGNs. With the resolution of QUASAT we reach very interesting physical scales in AGNs, i.e. $10^{15} - 10^{17}$ cm, depending on the redshift. In the case of the nearby radio galaxy Centaurus A, and the weak Seyfert I spiral M81, QUASAT will be sensitive to emission from a region about one light day (3×10^{15} cm) in size, and in the case of Centaurus A the flux density is known to vary on this timescale above 10 GHz. In general, *imaging observations with QUASAT will yield direct information about the total intensity distribution and polarization of radio continuum emission on similar scales to those causing most of the optical BLR emission, which may allow links between the properties of the emitting regions to be established.*

Candidate objects for QUASAT observations are those with flat or inverted radio spectra and sufficient flux density (20 mJy at 6 and 18 cm wavelength, 50 mJy at 1.35 and 85 mJy at 92 cm) in compact components for detection. Radio surveys at 22 GHz show that there are likely to be roughly 500 sources in the sky satisfying these criteria, while surveys at the lower frequencies show the expected numbers of observable sources are more typically 5000.

2.2.2 Current Views and Questions about the Central Parsec

In the usual picture of an active nucleus (Fig. 2.2) a supermassive, compact object, most likely a black hole, is located in the centre. It is surrounded by an accretion disk and further out by the optical broad and narrow emission-line regions, and has a radio jet blasting its way through from the centre along the axis of symmetry. There are two quite distinct ways in which massive black holes can generate the high luminosities observed: by accretion, or by having rotational energy tapped by electromagnetic processes. Accretion is thought to dominate in quasars with bright cores, whereas in strong radio galaxies with weak cores, the electromagnetic processes may be more important.

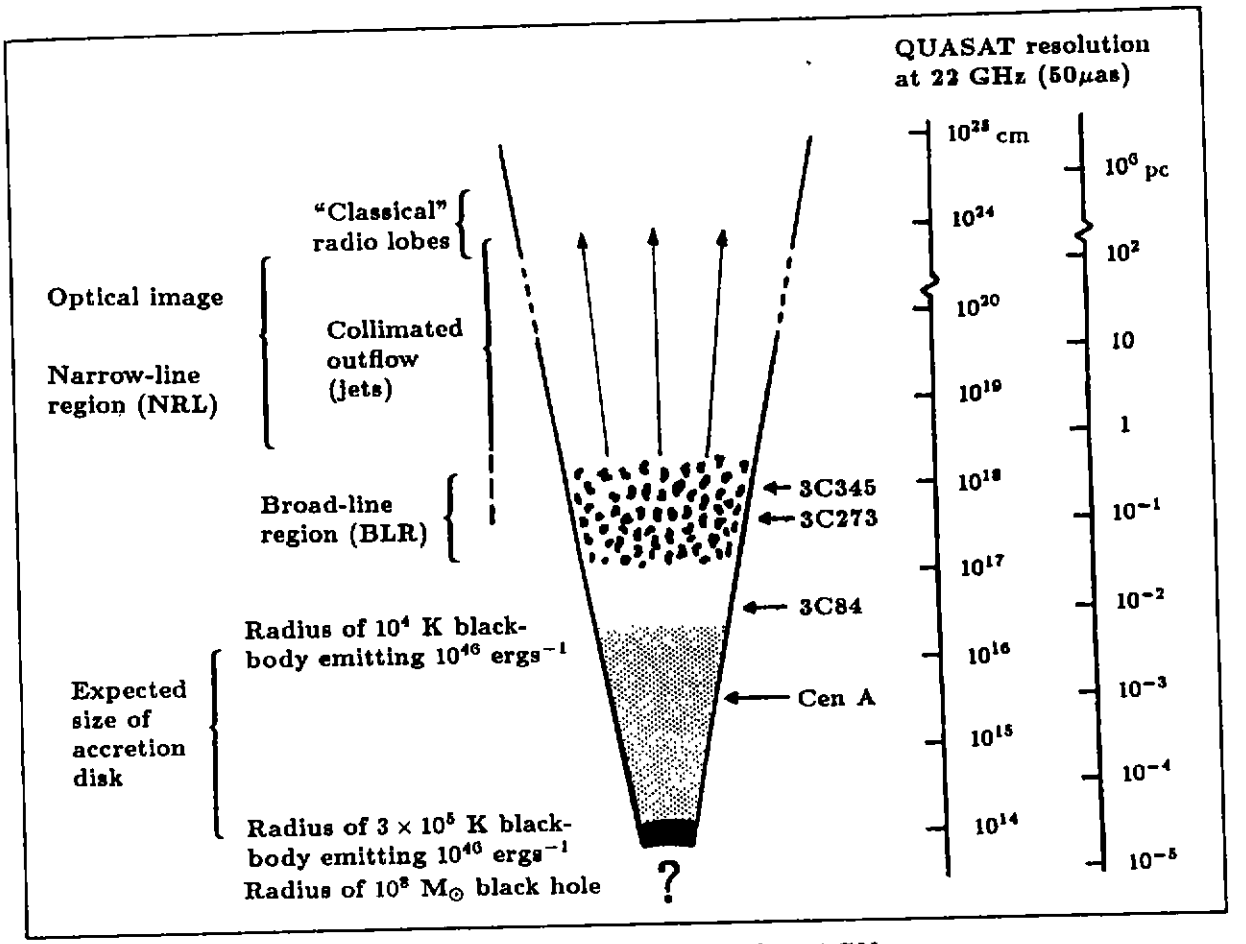

Figure 2.2: A typical model of an AGN.

A schematic "slice" through an AGN. If the primary power source involves a single mass of order 10^8 $M_\odot$ then general relativistic effects would be important within a few times R_S (where $R_S \simeq 3 \times 10^{13}$cm) and this object would dominate the gravitational field (yielding a potential well $\propto r^{-1}$) out to order 1 pc ($= 3 \times 10^{18}$ cm). On larger scales, interaction of the radiation and outflowing matter with the environment of the parent galaxy is the determinant factor. The QUASAT resolution at 22 GHz (50μas) is indicated for four sources: Centaurus A, distance 5 Mpc; 3C84, distance 53 Mpc; 3C273, z = 0.158; and 3C345, z = 0.595; Hubble constant 65 $kms^{-1}Mpc^{-1}$. Adapted from Rees: 1986 (*IAU Symp. No. 119*, eds. G. Swarup, V. K. Kapahi, Reidel, Dordrecht, p. 1).

The power produced is reprocessed and channelled into various energy bands, including kinetic energy of the beam. The details depend strongly on the conditions in the nuclear environment and the form of primary energy release. The source/observer geometry and the intrinsic conditions will cause the appearance of the AGN to vary when observed in various frequency bands.

If the central engine is radiating at the Eddington limit it can radiate 1.3×10^{38} $ergs^{-1}$ per $M_\odot$. Thus, a typical quasar radiating 10^{46} $ergs^{-1}$ would need a hole with a mass of $\sim 10^8$ $M_\odot$. If the energy release corresponds to ~ 0.1 of the rest mass energy of the accreted material, then there is a "critical" accretion rate (directly proportional to the mass of the hole) associated with the Eddington limit of $\sim 1.5 \times L_{Edd}/10^{46}$ $M_\odot yr^{-1}$. Thus, the typical quasar would consume ~ 1 $M_\odot yr^{-1}$, while 3C273 for example, whose output is about 10^{47} $ergs^{-1}$, would be consuming ~ 10 $M_\odot yr^{-1}$.

The Schwarzschild radius (R_S) of a black hole is 3 km per $M_\odot$ so that for a 10^8 $M_\odot$ hole,

$R_S \simeq 3 \times 10^{13}$ cm. Close to the black hole, 3–5 R_S, the ionised, accreting, gas becomes optically thick because of Thomson scattering and the rapidly infalling material gets in the way of the radiation diffusing outwards. This scale is beyond the reach of radio VLBI. A luminosity of $\sim 10^{46}$ ergs^{-1} emerging with a black-body spectrum from a region with dimension $\sim 10^{14}$ cm ($\sim 3R_S$), would correspond to a temperature of $\sim 3 \times 10^5$ K. The flux would therefore peak in the far UV, and be unobservable in the radio.

However, direct variability observations seem to show either intrinsically slow variations or larger sizes than 10^{14} cm. This suggests that there may be an optically thick medium surrounding the central energy source which thermalises the unknown original spectrum and dampens the expected rapid time variations. This may be an indication of the existence of an accretion disk, or torus, around the black hole. Simple spherical accretion is not a good model for a radio source where the energy outflow has to be collimated into the form of a radio jet. If the infalling gas has some angular momentum it will form an accretion disk. There are indications of optically thick accretion disks from observations of "blue bumps" in the optical spectra. The expected size of the accretion disk ranges from about 10 to perhaps 1000 R_S, that is from $3 \times 10^{14} - 3 \times 10^{16}$ cm for a 10^8 $M_\odot$black hole; note that 3×10^{16} cm is the radius of a 10^4 K black-body emitting 10^{46} ergs^{-1}.

Outside the accretion disk in the model is the BLR region, although there is accumulating evidence that part of the BLR emission emanates from the accretion disk itself. Models for the BLR, generally involving $10^7 - 10^8$ K (tenuous) gas confining $\simeq 10^4$ K (denser) line-emitting clouds, have had some success. It is now believed that the highly excited optical emission lines in the BLR are due to photoionization by the optical through X-ray continuum radiation, and that this continuum radiation arises either around the central source or at the base of the jets which have been revealed by the VLBI observations. Spectroscopic observations show that the BLR is extremely inhomogeneous and exhibits violent motions with velocities $\geq 10^4$ kms^{-1}. The geometry of the BLR is very uncertain and direct measurements must await the arrival of sensitive optical interferometry, almost certainly in space. The size of the region, inferred from the optical line intensity variations, ranges from a radius of 0.015 pc (5×10^{16} cm) for nearby low luminosity Seyferts to about 0.3 pc (10^{18} cm), or more, for the more distant luminous quasars. Further out there is the NLR region which is of galactic dimensions, reaching out to of the order of 1–10 kpc from the nucleus.

We emphasise that the above outline is, in fact, very speculative. Some of the factors still uncertain are:

- the nature of the primary source of power, and whether it is a single object.
- the mode of energy release from the central engine and how the primary radiation is reprocessed.
- the geometry of accreted material around the central massive object.
- where the acceleration and collimation of the relativistic plasma responsible for the observed radio radiation takes place.
- what governs the energetics, dynamics and geometry of the BLR, and what influence the radio jet has on the BLR.

High resolution radio observations have played a decisive role in the shaping the current picture despite its uncertainties. The availability of QUASAT observations promises to make a major leap forward possible in probing active galactic nuclei.

Fundamental astrophysical problems which QUASAT will attack include the following :

- What is the brightness temperature, size and shape of the central radio continuum source? Is the size scale that expected for an accretion disk or the optical broad-line region? How does it evolve? What is it? What does it tell us about the still hidden central engine?
- What are the mechanisms by which the jets are accelerated and collimated, and where does this all take place? What is the structure of the jets on scales smaller than the smallest currently observable?
- What evidence is there for interaction of the jets with the BLR, and what implications does this have for the structure and energetics of the BLR?
- What is the origin of the "knots" seen in the jets? What are their structures? How do they evolve with time and with distance along the jet? Are velocity changes observed in superluminally moving knots close to the cores?

To discuss the impact of QUASAT observations on AGNs, we assume in the following sections that a QUASAT AGN image at the highest resolution will bear generic relationship to the compact core/extended jet structures currently found on far larger angular scales. ***But, as with any telescope breaking new instrumental ground, we can expect much of QUASAT's contribution to astrophysics to be in discovering unexpected radio structures and in answering as yet unformulated questions.***

2.2.3 The Central Compact Radio Continuum Source

Flux Density Variations

The discovery of radio flux density variations in extragalactic objects more than 20 years ago first pointed to the presence of very compact structure which was later confirmed by VLBI. The same studies have also shown that rapid variability is very often correlated with high brightness temperature components and rapid structural changes including superluminal motion. Inferences from variability studies are therefore particularly relevant to QUASAT observations.

BLLac objects reveal the most violent and most rapid variations at radio wavelengths with timescales down to 1 hour. If these variations are intrinsic there may be structure on a scale of μas possibly requiring coherent emission mechanisms as well. If the variations are extrinsic, due perhaps to interstellar diffraction or refraction effects, the angular sizes still must be well below 0.1 mas. ***In either case, we need QUASAT at 1.35 cm to resolve or isolate the components responsible for such very rapid variations.***

Many AGNs vary in brightness at frequencies below 1 GHz, a phenomenon known as low frequency variability (LFV). Typical timescales are of the order a year. On the simplest assumptions this implies source sizes of light-years and brightness temperatures (inferred from variability timescales and distances) of $\sim 10^{14} - 10^{16}$ K, considerably greater than the inverse Compton limit. If this variability is intrinsic to these sources it would pose severe problems of interpretation. Possible explanations are bulk relativistic motion in these sources, but the required Lorentz factors are implausibly high (as are the bulk kinetic energies), or coherent radiation processes.

More likely LFV is not intrinsic but rather is a propagation effect caused by large-scale density fluctuations in the interstellar medium. Such "refractive focusing" would induce time variations in the apparent structure and size of the scattered image, and since this effect will tend to conserve surface brightness, rather than total flux density, the latter quantity would be modulated producing the apparent LFV. This theory can in principle be tested observationally, but the effect scales inversely with frequency, and at the low frequencies ground-based VLBI has inadequate resolution. ***In contrast, QUASAT at 327 MHz will be ideally suited to make the necessary observations.*** This

will not only constrain the physics of compact cores, but also tell us about physical conditions in our galactic interstellar medium.

Brightness Temperature

Energetics places an upper limit of $\simeq 10^{12}$ K (the "inverse Compton limit") on the brightness temperature (T_B) of incoherent synchrotron emission, in the frame of the emitting plasma. Above this value the radiating electrons quickly lose their energy by inverse Compton interactions with the photons of the radiation field. This interaction should quench the the radio source effectively; observations of T_B above the inverse Compton limit would imply that additional physics is involved. Possible reasons why T_B values greater than 10^{12} K, which may occur in parts of the core region, might be observed include relativistic Doppler boosting of the incoherent emission, or coherent radiation processes, as mentioned above for LFV.

The brightness temperature to which a given baseline of (geometrical) length L is sensitive goes as $T_B \propto (\text{flux}) \times L^2$. On the longest baselines, constrained by the size of the Earth, currently observed brightness temperatures are always $\leq 10^{12}$ K. Possible larger T_B values can be detected only by increasing the geometrical dimension of the baseline. The recent TDRSS space VLBI experiments (see chapter 5.2) observed T_B's a few $\times 10^{12}$ K, which could be explained as Doppler boosted (incoherent) emission with moderate values of the Lorentz factor. But TDRSS working at 13 cm was unable to resolve these components in detail and hence could not obtain direct evidence for relativistic velocities. QUASAT will not only be able to do this but will also be able to search for brightness temperatures in excess of 10^{13} K in hundreds of sources. At the other end of the scale, the lower limit on the brightness temperature in components detected by QUASAT at 22 GHz is $\sim 5 \times 10^{10}$ K and hence many sources should be detected on baselines involving large ground-based telescopes. At 5 GHz the QUASAT mission can examine cores in the few mJy range corresponding to $T_B < 10^{10}$ K and important measurements (even on the relatively weak) central engines in Seyfert, and most radio, galaxies will be possible.

Size, Location and Spectrum of the Core

The physical origin of the radio core component is uncertain. A core may represent the optically thick "nozzle" of the collimating process, near the "base" of the jet. The collimated, possibly conical jets are likely to contain shocks. The shocks cause continuum bursts, probably starting with X-ray and optical emission at the base which changes, as the magnetic fields and particle energy drop, to IR, mm, and finally to radio emission. The transition to radio emission must occur on scales $\ll 1$ pc; at least one source, 3C120, (Fig. 1.1) shows superluminally moving radio blobs on sub-pc scales, thus the collimation and acceleration have already taken place. Observations of Centaurus A with QUASAT will show if collimation has taken place at 10^{-3} pc (3×10^{15} cm).

If the core is indeed the narrow end of the relativistic beam, the structure and spectrum of the core contain a wealth of information on the formation and collimation of jets and on the acceleration of the relativistic particles in jets. If the core is a separate entity from the jet, its structure may show evidence for interaction with its surroundings or for opacity effects in the dense environment of the nucleus. The main difficulty now faced in observing the core is that the resolution of ground-based VLBI is insufficient. The cores are unresolved and their images are often blended with those of new superluminal knots which are just emerging from their parent cores. Therefore, not even the spectrum of a core can be determined reliably.

Model fitting to QUASAT data will allow component diameters to be estimated down to 1/2 to 1/3 of the "restoring beam" used for imaging. This means $\simeq 20\mu$as at 22 GHz and $< 100\mu$as at 5 GHz. With this higher resolution, it will be possible to reduce the contamination of the core spectrum by the jet. The value of the spectral slope of the core depends on the geometry of the jet, i.e. the relation between its width and its length, and on the dependence of the magnetic field

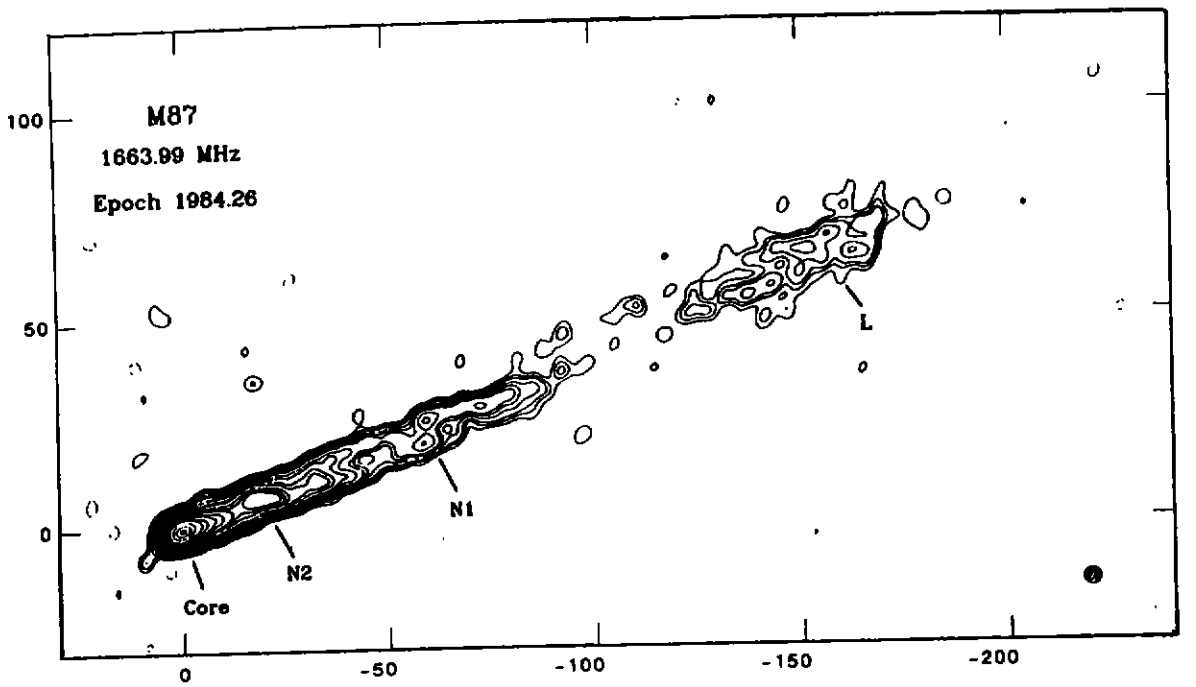

Figure 2.3: "World Array" map of M87.

Map of M87 nucleus at epoch 1984.26 made from 1.664 GHz data from 18 telescopes, the "World Array". Note that the jet is edge brightened. The peak intensity is 0.97 Jy/beam. The tick marks are in units of mas and the CLEAN restoring beam is a 4 mas FWHM Gaussian function (hatched circle shown in lower right corner); north is toward the top and east toward the left. The dynamic range is about 2200 to 1. From Reid et al: 1988 (*Astrophys. J.*, in press).

and relativistic electron energies and densities on the width of the jet. Observations of the core spectrum combined with observations of the core structure, give complementary information on the geometry and relativistic particle distribution and will lead to a better understanding of how the jet is formed and collimated. This information, in turn, should provide direct information on the nature of the central energy source. Measurement of a core size less than that deduced for the optical broad line region will provide constraints on the covering factor and geometrical disposition of the optically emitting clouds (see section 2.2.5).

2.2.4 Jet Structure and Physics

Jets, as collimated channels along which energy and momentum are transported over large distances, were first invoked to provide for the fuelling to the lobes of classical radio galaxies on scales of hundreds of kpc. It was the first case in astrophysics in which we were confronted with a process which was not intrinsically spherically symmetric; and this fact brought many new physical ideas to development However we must not forget that the evidence for outward motion in extended radio sources is still circumstantial, as the continuum spectra do not allow a direct measurement of the velocity through Doppler shifts. It is on VLBI scales only that proper motions of bright structures have been followed on times of a few years, showing that velocities are probably very close to the velocity of light. The interpretation of these data are still rather controversial, as we do not know whether we are observing a real motion or some phase velocity effect. In this sense *QUASAT will be of fundamental importance to solve the riddle of the characteristics of motions*

along jet-like structures in radio sources.

If jets are indeed characterised by collimated energy flows, these must be ***highly*** collimated suggesting the presence of stable channels of energy transport outwards from the nucleus. Dissipative processes can render the collimated flow visible over a wide range in wavelength, e.g. Cen A, M87 (Fig. 2.3) and 3C273 show radio, optical and X-ray jets. They are most easily detectable in the radio range and show structure on all size scales from pc up to Mpc. QUASAT will provided radio polarimetric images of these jets with unprecedented angular resolution.

The physics of outflows from radio cores is currently poorly understood, although numerical simulations on accretion of magnetized plasma from a torus near a black hole has suggested that this can generate a $\gamma \sim 10$ jet. Other mechanisms can generate $\gamma \sim 50 - 100$ jets of $e^+ - e^-$ plasma from accretion disks. In the former case, shocks near the base of the jet could provide the radio core and variable X-ray continuum; in the latter case these probably occur where the jet shocks and slows to $\gamma \sim 5 - 10$, with considerable particle heating due to the shock. As the jet progresses, shocks and shears caused by interaction with a possibly inhomogeneous surrounding medium or magnetic or fluid instability can give rise to knots and hot spots. As shown by time-dependent calculations, not all shocks are stationary: depending on boundary conditions, they move up- or downstream with various time scales, and can obviously be associated with transient structures and variability in AGNs.

The superluminal knots (see next sub-section) are considered to be shocks, yet the knots are poorly resolved with current earth-based arrays and there is no direct observational evidence for shock-like structures. ***QUASAT should resolve the knots and show whether they contain shocks.*** It has been suggested that shocks in the jet might cause the pattern and fluid speeds to differ, which would alter the statistical properties of relativistic jets. If indeed this is the case, we would expect to see that different shocks move with different speeds. The geometry of shocks and other features in the knots can also tell us what processes are important in the jet dynamics. For example, shocks aligned across the jet would suggest unsteady flow, whereas limb-brightening would suggest interaction with the external medium (see Fig. 2.3).

Continuum outbursts at mm and IR wavelengths are currently understood to be due to synchrotron emission from shocks near the base of a relativistic expanding jet. There is thus an intrinsic connection between these continuum outbursts and the subsequent appearance of moving knots in VLBI images. Observation and theory suggests that the radio emission from these knots is most intense at $\simeq 20$ GHz on scales of $\simeq 100\mu$as and they are thus ideally suited for observation with QUASAT. ***The VLBI images provide the crucial element for interpreting continuum outbursts*** and will lead to jet models of increased sophistication. The complementary information from these different wavelength regimes will place very firm constraints on the jet on scales smaller than that currently observable.

In regimes other than the radio: (i) much of the continuum of other frequencies may also be synchrotron radiation, and (ii) much of the X-ray radiation is likely to be self-Compton emission from the jet. (iii) Dissipation near the shocks results in considerable emission at other wavelengths. (iv) Much of the jet structure may be caused by feedback from the surrounding medium. VLBI observations plus jet modelling is required to determine the structure of both the jet and its surroundings. Because it offers the possibility of resolving the jets and their knots, QUASAT is an indispensable tool for probing nuclear jet structure, and, combined with numerical modelling and continuum observations in other wavebands, the central engine itself.

Superluminal motion – evidence for relativistic bulk motion

The observed systematic angular motion of steep-spectrum brightness enhancements ("blobs" or "knots") away from a flat-spectrum "core", which when translated into linear motion exceeds

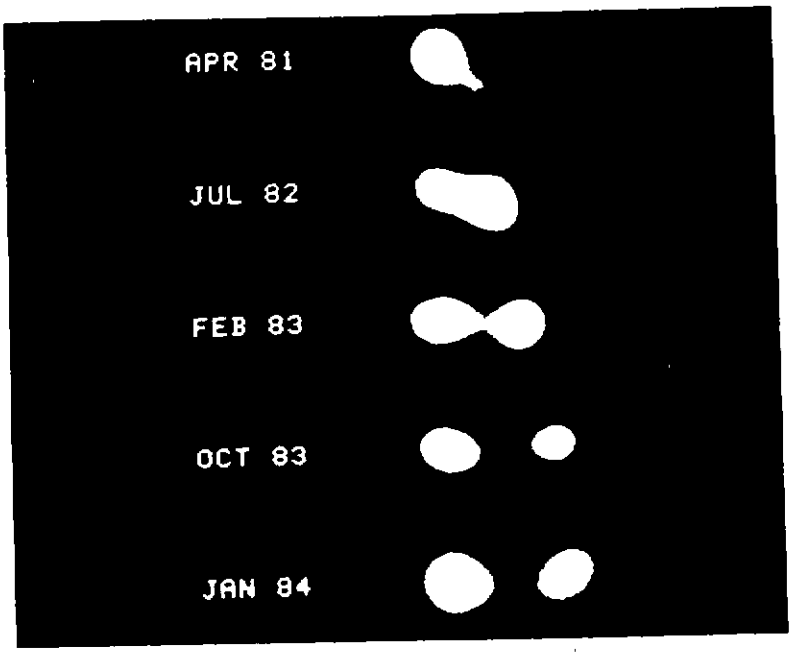

Figure 2.4: Sequence of maps of 3C345.

Sequence of maps of 3C345 ($z = 0.595$) showing acceleration and change of position angle of the superluminally moving component. The component separation in January 1984 is 0.84 mas or 4.9 pc (for $H_o = 65$ $kms^{-1}Mpc^{-1}$). At each epoch the left hand component is the "core" and the moving component is at right. This new component changed position angle and was observed to accelerate from an apparent transverse speed of 3c to 5.9c as it moved away from the core. It also caused the largest flux outburst ever seen in this object between 7 and 300 GHz. After Biretta: 1985 (Ph.D. Diss., California Inst. of Technology).

the speed of light in vacuum (c), is termed superluminal motion. The derived velocities fall in the range a few to many times c. At least 20 superluminal sources are known, including $\geq 80\%$ of the compact radio sources which have been carefully studied over a period of some years, indicating that a large fraction of the compact sources is superluminal. Surveys which select for extended radio structure, rather than compact structure, also find an appreciable fraction of superluminal objects. Thus, ***superluminal motion is a widespread phenomenon among extragalactic radio sources***, and it strongly suggests that relativistic bulk motion of the emitting material is taking place. This has important implications for the physics where the acceleration and collimation of the material takes place, which is on scales smaller than where the motion itself is currently observed.

The kinematics of the superluminal knots near the core can be very complex. Components near the core have been seen to accelerate, decelerate, and change position angle. An example of this complex behaviour is one component in the quasar 3C345 (see Fig. 2.4) which accelerated from twice to six times the speed of light when it was about 2 pc from the core. It also changed position relative to the core by about 40 degrees, indicating it was following a curved path. More recent observations reveal a newer component which is following a similarly curving path. Studying the sizes and structures of these knots near the core will clarify the physics underlying this kinematic behaviour. For example, if the acceleration is due to decreasing external pressures, we would expect the superluminal components to expand rapidly as they accelerate. Another possibility is that components encounter obstacles and slow down, or are struck from behind by more rapidly moving material. If this was the case, we would expect to see shocks develop during the periods of acceleration and deceleration. These phenomena all occur in a region which is just barely resolved with present VLBI arrays. *QUASAT observations will allow the phenomenon to be observed* 5×

closer to the central engine where the superluminal component is $5\times$ *younger, and will increase, by the same factor, the length of time that it can actually be followed and its evolution studied.*

The superluminal effect is generally interpreted as a relativistic jet in the central engine which collimates and accelerates particles to a bulk Lorentz factor γ, moving at an angle to the line of sight of typically $\sim 1/\gamma$. This geometry creates an apparent transverse linear speed of γc, and boosts the brightness of approaching components by roughly γ^3. With such a large increase in brightness, it is expected that superluminal motion should be common in the brightest sources, which is in accord with observations. Typically the brightness of the superluminal components fade on a timescale only slightly longer than the time needed to measure changes in relative separation. With QUASAT the time between successive epochs of observation can be shortened. *The higher angular resolution of QUASAT will allow us to measure superluminal motion in high redshift objects* (see 2.6) and to measure short-lived changes in apparent velocity as the knots move out.

The improved resolution of QUASAT will also permit new a new test of relativistic beaming which predicts that the jet opening angle should increase with increasing jet curvature, core brightness, and (for most sources) apparent speed. This test cannot be made with current VLBI because the widths of the jets are barely, or not at all, resolved. Increasing the observation frequency to the mm region will not help, since the knots have steep spectra and are too weak to observe; this measurement can only be made by increasing the baseline length. Besides explaining the superluminal effect, relativistic beaming also explains the one-sided appearance of jets, and accounts for the weakness of the X-ray emission from many superluminal sources. Both of these effects occur because radiation from a relativistically moving emitter is strongly beamed in the direction of motion. The relativistic jet hypothesis seems very attractive in that it explains many seemingly different phenomena in a "unifying scheme", where the observed variety is reduced to a difference in viewing angle. If indeed relativistic bulk motion plays a major role in AGNs then the appearance of the radio sky is in effect largely dominated by relativistic effects. The origin of the relativistic bulk motion itself puts important constraints on the physics of these objects on the very smallest scales.

Magnetic Fields in Jets

The high resolution of QUASAT will also permit us to study the physical parameters of jets and how they vary with distance along a jet. For example, the magnetic field strength for a knot may be derived from its flux density, synchrotron self-absorption turnover frequency, and diameter at that frequency. If several knots are present, the functional form of the magnetic field fall-off along the jet may be deduced. Uncertainties are large since the diameters are poorly known. QUASAT should give much better values for the diameters around the turnover frequency.

Linear polarization measurements with QUASAT will enable measurements of magnetic fields in the compact cores as well as in the blobs in the jets (see Fig. 2.5). It will be possible to map the topology of the magnetic field in the jets, and to study how the topology changes as "knots" propagate out from the nucleus. Is the magnetic field the same at a given point of the jet, or does it "travel with the knots" ? How homogeneous is the magnetic field; does this change with position in the jet ? Faraday rotation and/or Faraday depolarization can be used to learn more about the magnetic field and thermal particles on the scale of parsecs. This has implications for how the pc-scale jets interact with the gas in the broad- and narrow-line regions. *QUASAT will yield polarization data on scales not accessible to any other instrument.*

Inverse Compton emission – radio to X-ray

QUASAT will also address the problem of the origin of the X-ray emission in blazars, a class of compact higly variable sources believed to be oriented very close to the line of sight. The X-ray fluxes of blazars are highly correlated with the radio flux densities of compact components,

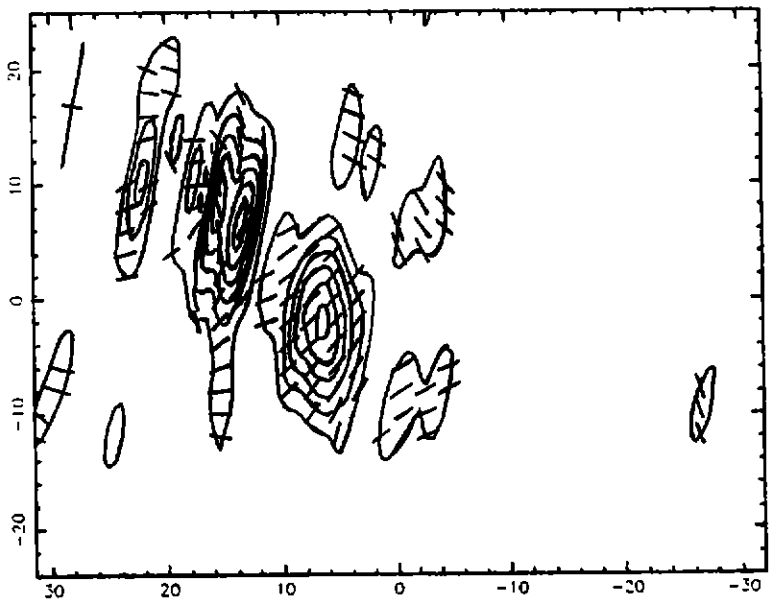

Figure 2.5: Map of polarized intensity for 3C273.

Map in polarized intensity of 3C273 at epoch 1984 October, made with a 6-antenna trans-Atlantic array. The polarized intensity is given by the contours at 15, 30, 45, 50, 75 and 90 % of the peak intensity of 113.8 mJy/beam, and the electric field direction by the sticks. The tick marks are in units of mas; north is toward the top and east toward the left in the figure. From Roberts et al.: 1988 (in preparation).

suggesting that the X-ray emission is due to self-Compton scattering within either the core or the knots. Multifrequency VLBI observations can determine all the physical parameters needed to calculate the expected level of self-Compton scattering. One of the crucial observational parameters is the angular size of the components at or near the turnover frequency. This cannot be achieved with Earth-based arrays. *The much better resolution offered by QUASAT will allow a direct measurement of the angular sizes and other parameters at or near the turnover frequency; this will allow an accurate calculation of the predicted self-Compton flux to be made.* Beyond that, coordinated monitoring of both the X-ray flux and the structure of a radio component, will enable one to determine whether variations in X-ray flux correspond to changes in the radio emission in the manner expected. There is potentially a wealth of information about the physics of blazars to be obtained from QUASAT observations contemporaneous with multi-wavelength total flux density observations in the mm/submm, IR and X-ray (ROSAT, XMM).

2.2.5 Optical-Radio Connections

During the last few years it has been shown that radio sources *do* interact with the ambient medium on the scale of a kiloparsec and above. There is every reason to believe that on the much smaller scales probed by QUASAT similar interactions will also take place. Combination of optical line data with direct images of, and measurement of (polarized) opacity effects on, the radio continuum can provide a unique set of diagnostics of the physical conditions in the line emitting region. Optical line emission from AGN's is emitted on a variety of linear scales; the inferred scale of the BLR matches the resolution of QUASAT at 6 cm for many objects, both nearby and distant.

The BLR is generally thought to have a multi-component structure of which part may be in the form of a rotating disk; claims have been made to have detected a disk signature in the line profiles. From the characteristic size inferred for the BLR from variability measurements and the

line luminosity, one can deduce that the BLR is very inhomogeneous with filling factors of order 10^{-4} or less. There is very little known about the fragmentation but it is generally assumed that the BLR consists of a vast number of cloudlets. Optical modelling and X-ray absorption data suggest that cloud column densities are of the order of $10^{22} - 10^{23}$ electrons per cm^2. Both the number of clouds and the covering factor depend on the assumed electron density. A column density of 10^{22} electrons per cm^2 will produce a free-free optical depth at 5 GHz of order one million which implies that BLR clouds are impenetrable to radio emission. If the covering factor of the BLR clouds is of order unity, very little radio emission will be able to escape from or through it. In low luminosity objects like NGC4151 the covering factor may in fact be as high as 0.9, but, in luminous objects the covering factor is generally taken to be 0.1–0.2. This difference is open to observational test. *The mere detection by QUASAT of compact high turnover-frequency radio components in objects like NGC4151 would strongly constrain BLR models.*

The disposition of the dense ($> 10^9$ cm^{-3}), fast moving (> 10000 kms^{-1}) cloudlets around the nucleus is uncertain. Unless confined, either statically or dynamically, the clouds evaporate in times much smaller than the crossing time in the BLR. It is often assumed that the confining agent is a hot (10^8 K) medium with a density about four orders of magnitude less than the clouds, but the confinement may also be partly effected by ram pressure, relativistic particles and magnetic fields. The properties of the intercloud medium may determine what one sees at QUASAT resolutions rather than the BLR clouds themselves. If the radio jets have to blast through a hot, dense, medium *the overall shape of the jet may look very different* (e.g. collimated and edge-brightened) from one that propagates through a near-vacuum between unconfined clouds (e.g. constant opening angle). In Seyfert galaxies, the jet may even be disrupted by the intercloud medium; this could explain the lack of double radio sources in these objects. If some of the BLR gas has a disk-like configuration which is optically thick at radio wavelengths then, depending on the size of the disk, part of the receding radio jet may be obscured.

The polarization properties of the jet will also be strongly affected by the properties of the surrounding medium. QUASAT images will strongly constrain its density and magnetic field content. This information cannot be obtained directly by any other means. From X-ray data it can be deduced that the column density of the BLR gas with temperatures less than about $10^{7.5}$ K is generally less than $10^{21} - 10^{22}$ atoms per cm^2 toward the X-ray source which we know lies in the heart of the BLR. For a path length of 10^{17} cm, the inferred electron density must be at most $10^4 - 10^5$ cm^{-3}. But even such a density would cause a rotation measure (RM) in the radio of order 10^6. VLA radio polarimetry of quasars suggests that for radio components at distances of about 10 pc from the nucleus the excess RM (compared to the arcsec/kpc structure) is only 100. This could imply that the outflowing gas and the intercloud medium in the BLR are contained in a cone not intersected by the line-of-sight to the radio jet. QUASAT polarization images would greatly help in interpreting this apparent discrepancy.

2.3 Masers

2.3.1 Introduction

Among the most dramatic of stellar phenomena are the beacon-like emissions generated by hydroxyl (OH) and water vapour (H_2O) masers. *The H_2O masers are capable of emitting nearly 1 $L_\odot$ in a single spectral line only 50 kHz (0.7 km s^{-1}) wide.* The OH and H_2O maser hot spots are amongst the smallest (~0.1 to a few A.U.) and brightest ($T_B \sim 10^{12} - 10^{15}$ K) radio sources known and are naturally main target objects for the QUASAT mission. This provides, for the first time, the opportunity to resolve the maser spots and provide more definitive information on their physics

and detailed astrophysical associations, neither of which are well understood.

In addition, the H_2O masers can be used as tools to measure both galactic and extragalactic distances through studies of the motion of the individual features in a cluster, see Figure 2.8.

OH and H_2O masers are associated with two extreme phases of stellar evolution. They are seen in the dusty envelopes around: (i) evolved stars that are losing mass with very high rates (up to $10^{-4} - 10^{-5}$ $M_\odot$ /year for the stars in the latest stages of evolution). and (ii) newly formed stars, still embedded in the cocoon of gas and dust out of which they were formed. *Thus, these masers provide powerful tools to probe the physical conditions (density, structure of flows or of expanding shells, velocity field, turbulence, magnetic field) in the early and late stages of stellar evolution on very small spatial scales not accessible to other techniques.*

The OH emission from long period variable stars is strongest at 1612 MHz and has a characteristic signature, occuring in two velocity intervals spaced by 7-50 km/s, see Figure 2.6. The velocity difference between the emission peaks gives the expansion velocity of the spherically expanding

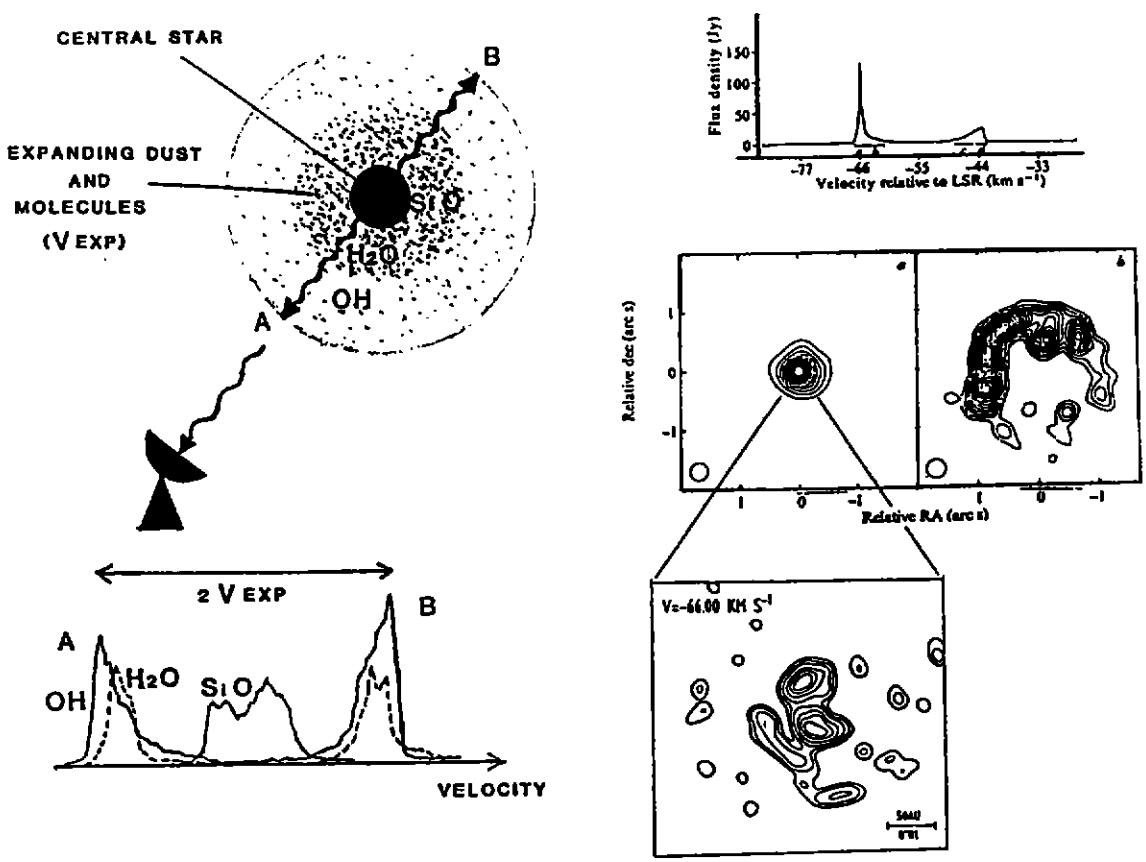

Figure 2.6: OH emission from circumstellar shells

On the left hand side is a schematic representation of a shell of dust and molecules expanding around an evolved central star. The upper part shows the geometry of the shell. The resulting spectra of the OH, H_2O and SiO molecular line emission indicate their relative location as is shown in the upper part; the distance between the two OH peaks gives an estimate of the expansion velocity. The right hand side presents the 1612 MHz OH spectrum of OH127.8 (on top) and the spatial distribution obtained with MERLIN (below) for the bracketed velocity intervals a and b. (Spectrum and MERLIN map from Booth, et al.: 1981, *Nature* **290**, p 382). The lowest panel shows a magnification of component a at -66 km s^{-1} obtained from VLBI observations; it suggests that OH127.8 might be a binary star (figure from Diamond et al., in preparation, 1988)

Table 2.1: Maser Transitions of Importance for QUASAT

Molecule	Transition	Frequency (MHz)
OH, ground state	$^2\Pi_{3/2}, J = 3/2, F = 1 \rightarrow 2$	1612.231
	$^2\Pi_{3/2}, J = 3/2, F = 1 \rightarrow 1$	1665.402
	$^2\Pi_{3/2}, J = 3/2, F = 2 \rightarrow 2$	1667.359
	$^2\Pi_{3/2}, J = 3/2, F = 2 \rightarrow 1$	1720.530
OH, excited state	$^2\Pi_{1/2}, J = 1/2, F = 1 \rightarrow 0$	4765.562
H_2O	$6_{16} \rightarrow 5_{23}$	22235.080

shell. The lag between changes in the blue- and redshifted peaks can be interpreted as light travel time across the shell giving the size and hence distance to the star when the angular extent is known. The weaker 1665/1667 MHz lines, also present in many late type stars, are not yet well explained.

The structure of the maser sources in star forming regions is often very complex (see Figure 2.7). Typically there are hundreds of bright spots with diameters in the range $< 10^{13}$cm to 10^{14}cm clustering on scales of $\leq 10^{16}$cm. These spots come from cloudlets of roughly planetary masses embedded in the very energetic outflows surrounding the newly formed star. The spectra are characterized by multiple strong and narrow features, often $> 10^3$ Jy; in the case of H_2O masers, as strong as 10^6 Jy.

Maser sources are also observed towards some Herbig-Haro objects, which are optical emission nebulae near early type stars or T Tauri stars. Herbig-Haro objects and H_2O masers are both manifestations of the outflowing material in the envelopes of young stars, and H_2O observations will trace the motions in the base of the stellar wind ejected by the central star. OH and H_2O are ubiquitous and, since they are intense masers, can be used to probe very distant invisible objects such as the IR stars in the bulge of our Galaxy. OH and H_2O are even observable in the arms of some nearby galaxies thus extending the detailed study of stellar evolution to these systems. More than 300 masers have, so far, been found in star-forming regions, more than 1000 near late type stars (including OH/IR stars), and about 30 in other galaxies (including megamasers).

The spectral lines observable by QUASAT include the four hyperfine transitions in the $2\Pi_{3/2}, J = 3/2$ ground state λ-quartet of OH at 18 cm, an excited state transition at 6 cm, and the $6_{16} - 5_{23}$ rotational transition of H_2O at 1.35 cm wavelength (see Table 2.1). ***It is important to note that, for line emission, since the frequency is fixed, higher angular resolution can only be achieved by longer baselines, in this case ground-space baselines.***

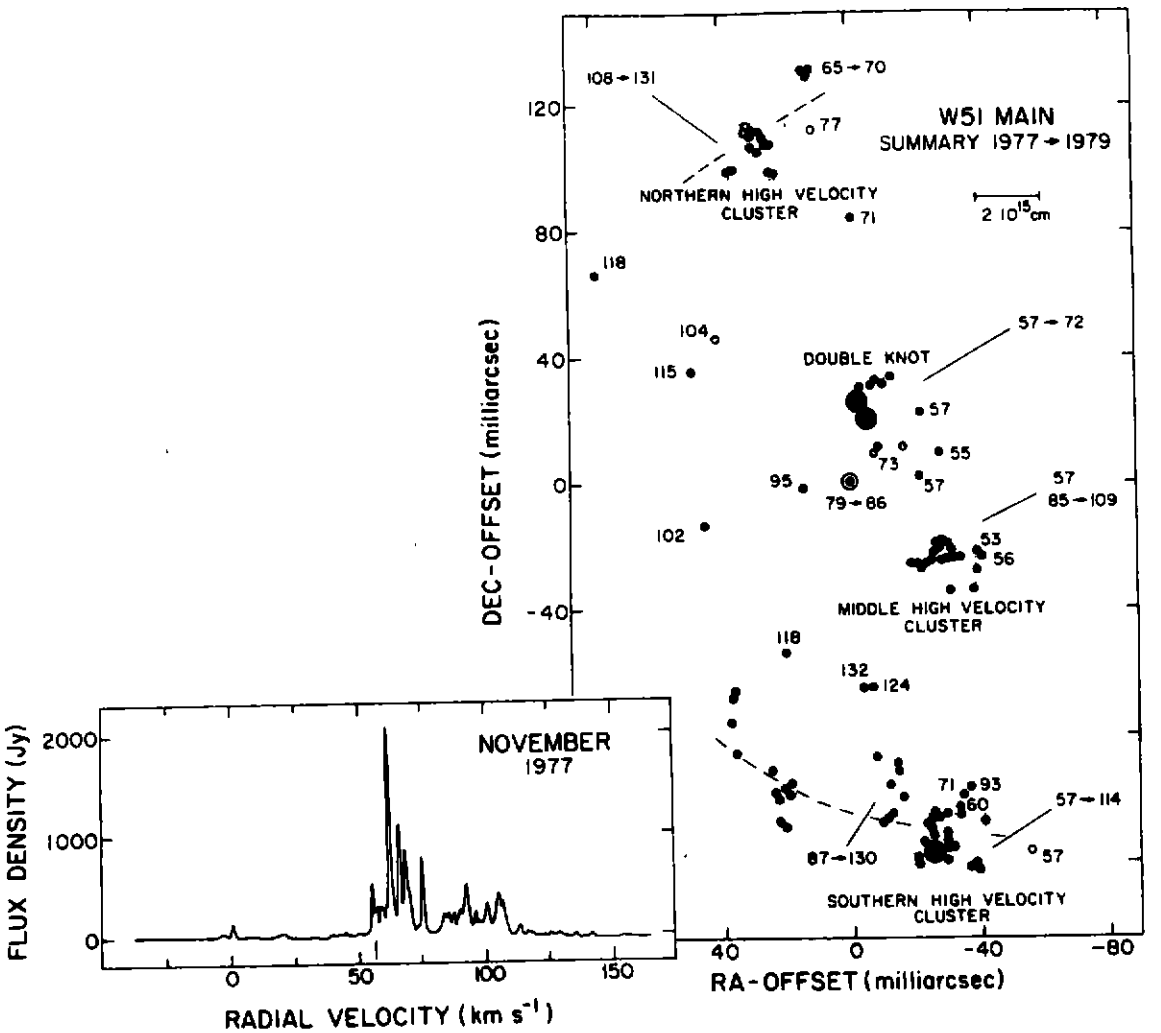

Figure 2.7: W51 Main

H_2O maser emission from W51 Main (Genzel et al.: 1981, *Astrophys. J.* **247**, 1039) The upper figure shows a map of the relative positions of the maser components; the numbers give radial velocities. The total power spectrum of the H_2O emission is shown in the lower part.

2.3.2 Masers Near Evolved Stars

MERLIN and VLA observations of OH masers near evolved stars clearly demonstrate that the molecules are in circumstellar shells (Figure 2.6). VLBI 1612 MHz observations of OH 104.9+2.4 and OH 127.8+0.0 have shown that compact OH features exist in these two strong OH/IR stars. The compact features are on the near side of the shell while there is no corresponding emission features on the far side. Transatlantic VLBI observations seem to confirm the suggestion that these are small ($\sim 10^{14}$ cm) blue shifted features which are the result of stellar radiation either from the star itself or from a flare amplified by maser action (Figure 2.6). The map in the lower right corner may even indicate a binary star. QUASAT observations both in OH and H_2O are needed to investigate these compact features. Searches and maps made at different epochs will help discover the components whose centroids and diameters are directly related to the stellar photosphere and may amplify the stellar radiation. Furthermore, because of their intimate relationship to stars

the masers are of major importance to *link the radio and fundamental optical position reference systems.*

In S Per and VX SGR the OH main line and the H_2O emission regions are distributed along two nearly orthogonal directions. The elongation of the OH region could be influenced by the circumstellar magnetic field since the OH main lines are polarized. *Measurement of the magnetic field with very high spatial resolution is vital to understand the coupling of the gas with the circumstellar flow.*

The velocity spread in H_2O is less than the velocity range of OH masers and the H_2O emission occurs in regions smaller than the OH regions (5-100 AU and 300-700 AU in Miras and Supergiants respectively, compared to $500 - 10^4$ AU for the OH emission line regions). This suggests that the H_2O masers lie inside the OH circumstellar shell as shown in Figure 2.6 and that the H_2O has not reached its terminal velocity.

Improvement of the knowledge of the actual structure of the inner circumstellar shell requires very high spatial resolution. Density inhomogeneities, turbulent motions and double expanding geometry are suggested in moderately low resolution VLA observations; disk-like structures have also been observed in VY CMa and elongated structures are present in IK Tau, R Aql, U Her, RX Boo, S CrB, VX Sgr and S Per. Stars have been detected in H_2O with VLBI, 5 regular or semi-regular variables and one supergiant. Even more complex structures may be revealed by QUASAT.

2.3.3 Masers in Star-Forming Regions

In star-forming regions, the OH masers appear to lie in the main mass concentration, typically at distances of $\sim 10^{16}$ cm from the new stars. The required H_2 densities are $\sim 10^7 cm^{-3}$. The OH masers seem to delineate the remnants of protostellar envelopes and discs, or perhaps they mark, as suggested by recent MERLIN observations, the sources of the bipolar outflows. The OH masers may show a high percentage of circular polarization that, interpreted in terms of the Zeeman splitting, gives magnetic field strengths of several milliGauss. In order to interpret the polarized OH masers in terms of Zeeman pairs, one must first identify the spatially coincident pairs. The resolution of QUASAT is ideal for this type of work. *Measurement of the magnetic field will allow us to test various theories of field compression. Comparison with groundbased observations at 4765 MHz will indicate whether the coherence properties of the OH masers are influenced by the magnetic field.* (The 4765 MHz transition is insensitive to the magnetic field).

Repeated OH maps with QUASAT will tell us whether the remnant envelope (or torus) model is general or whether the OH masers are accelerated in a stellar wind. Measurement of the motions of the OH spots may show directly, for the nearest sources, if the gas is in expansion or accretion. It is conceivable that, in the environment of massive stars, QUASAT will show, as is known for P Cygni stars, simultaneous infall and outflow of matter traced either by OH masers in different regions of the same source or by various OH and H_2O features.

H_2O masers mostly appear in outflow zones some time after a star has been formed and nuclear burning has started. Since theory predicts that the densities required in H_2O masers are $n(H_2) \simeq 10^8 - 10^{11} cm^{-3}$, the H_2O sources are either dense clumps ejected by the wind or condensations formed in the region where the wind interacts with the ambient, quiescent material.

QUASAT will be able to resolve the structure of tight clusters of H_2O masers and to chart any systematic motion or any asymmetry of the gas in the star-forming region with unprecedented precision. From repeated mappings of H_2O masers in HII regions, FIR sources or regions containing HH objects, it will be possible to derive the masses and the mass loss rates of the outflow zones. The H_2O probes a region closer to the origin of the flows than the millimeter CO lines that sample

the extended bipolar flow structure.

The *uv* plane coverage and long baselines provided by QUASAT will make it possible to construct images of H_2O masers that have high dynamic range and resolution. This capability *will make it possible to determine the actual shapes of the H_2O masers,* which may provide crucial information about these sources. For, example, if masers are freely accelerated by a stellar wind from a central star, the clumps of gas from which the maser emission arises should have tear-drop shapes with bow shocks forming on the edge facing the star. On the other hand, if maser emission occurs as clumps which are compressed when they collide with ambient gas, then the dominant bow shocks will occur on the edge away from the star. Although the systematic motions of H_2O masers observed so far always indicate outflow, the precise positions obtainable with QUASAT could reveal if some objects are at an earlier stage, that of a contracting protostar approaching the main sequence.

2.3.4 Extragalactic Masers

In 1982 a new class of extragalactic OH maser was discovered in the peculiar galaxy IC4553. It was immediately dubbed a "megamaser" since its intrinsic strength was about 7×10^7 that of the W3(OH) masers in our Galaxy. Following the initial excitement of the discovery, telescopes all over the world began searching for new megamasers until, at the time of writing, 15 are known. In addition, H_2O masers with luminosities comparable to the strongest Galactic masers ($\leq 1L_\odot$) were detected in external galaxies as long as 10 years ago. Much more luminous H_2O masers with luminosities up to $500L_\odot$ have since been found and to date 6 H_2O megamasers are known.

The powerful extragalactic masers so far discovered are all believed to be associated in some way with nuclear activity or a burst of star formation. It has been suggested that in fact all OH megamaser galaxies represent the very early stages of Seyfert activity and that this activity is triggered by the merger of two galaxies.

Interferometric observations

IC4553 is the only extragalactic OH megamaser whose structure is at all well determined. In VLA maps the source is only slightly resolved but two interesting facts emerge; a) the nuclear continuum source and the OH line emission region appear to be perfectly superposed, and b) the velocity structure of the OH emission is consistent with solid body rotation of a molecular disc. In higher resolution maps made with MERLIN the nucleus is found to be a core-dominated double similar to those seen in other active galactic nuclei. In VLBI the eastern component breaks up further into two smaller masers (the size of the maser components is $\leq$ 3.5pc). Five other OH megamasers have been observed with the VLA; Mrk 273, NGC3690, IIIZw35, IRAS 17208-0014 and IRAS 11506-3851. As expected the OH emission from each is superposed on the continuum emission but none of the sources were resolved.

VLA observations of NGC 4258, 1068 and 3079 have revealed the surprising result that the extragalactic H_2O masers are confined to very small regions ($\leq$ 4 pc) and *are coincident with compact sources of radio emission in the nuclei of the galaxies.* VLBI observations suggest that most of the line flux in NGC3079 is confined to a region of 0.02 pc in size. In addition the masers have luminosities two orders of magnitude greater than the Galactic H_2O masers in W49. It is evident that standard pumping schemes (which have difficulty explaining the Galactic H_2O masers) cannot explain the extragalactic masers.

A model for megamaser galaxies

No detailed model exists for the megamasers but several common links are evident in all cases. First, most appear to be superimposed on the continuum radio emission originating in the nucleus

of the host galaxy, implying amplification of that continuum. Secondly, OH megamaser galaxies are extremely strong IR sources found in the IRAS bright galaxy survey having far IR luminosities $> 10^{11}$ $L_\odot$; the H_2O megamaser galaxies form a different population and tend to exhibit different IR properties. The OH galaxies are usually rich in molecular gas, as shown from CO observations at mm wavelengths, and most are interacting systems. Optical spectra suggest a mixture of starburst and AGN energy sources both of which are fueled by the enormous reservoir of molecular gas. It has been proposed that *the ultraluminous IR galaxies represent the initial, dust enshrouded stages of quasars triggered by the strong interaction/merger of two gas-rich spiral galaxies.* On shedding their dust, allowing the AGN to dominate visually, they become optically selected quasars.

If this intriguing scenario is correct, the megamasers provide a probe of this fascinating evolutionary stage of quasars and detailed observations may yield important data on the molecular clouds as well as the 'imaged' galactic nuclei.

QUASAT observations

The prominent OH and H_2O megamasers all appear in galaxies with very compact radio nuclei; little extended emission line and/or continuum emission is detected in the available VLA and ground-based VLBI observations. The number of megamasers with very strong line and continuum sources is however rather small (≈ 20). But because the gains of the H_2O sources are larger, these *megamasers are good probes of the physics of molecules in the nuclear regions of active galaxies.* Furthermore, the higher gains in relatively small pockets of gas are rather susceptible to variations. For NGC3079, the 100 AU thick amplifying layer moves $\sim 40\%$ of its thickness in one year ($V = 180$ km s^{-1}). Variability of the H_2O lines is expected and is observed for the powerful megamasers. *QUASAT high angular resolution observations are required to study the source structure and the physical conditions of the masing regions for the powerful OH and H_2O megamasers.* They will help to understand the physics of this unusual example of interstellar image amplification of a nuclear radio source.

2.3.5 Distance measurements

The measurement of distance is a problem of fundamental importance in astronomy. QUASAT measurements of statistical parallaxes of H_2O maser sources within our galaxy, and in other *galaxies to a distance of 1 or 2 Mpc, will provide an important* **independent** *method of calibrating the distance scale.*

By the time QUASAT is launched, Hipparcos will have put the distance scale in the galaxy on a firmer footing with annual parallax measurements, with 10% uncertainty, of distances out to 100 pc. To go further than 100 pc will require a complex and hierarchical calibration sequence. Typically the sequence starts with a direct measurement of distance to a star that has a recognizable spectral appearance or periodic light variation. This fixes the intrinsic luminosity of the star and allows a distance to be determined to a star of similar appearance or variation by measurement of its apparent luminosity. Stars for which "luminosity distances" are known form secondary distance indicators. The scale of the Milky Way is largely determined from such stars. Some secondary distance indicators can be seen in nearby galaxies, thereby forming the basis of the even more complex extragalactic distance scale which then uses tertiary indicators.

Because of the complexity in the galactic and extragalactic distance scale, it is prone to serious systematic errors. Secondary distance indicators require a luminosity calibration and a knowledge of extinction toward the source. Thus they suffer not only from measurement errors, but also from systematic effects which are difficult to assess.

The measurement of the proper motions of H_2O maser complexes yield a direct estimate of the distance to a source, independent of absolute luminosity and extinction, and therefore this method

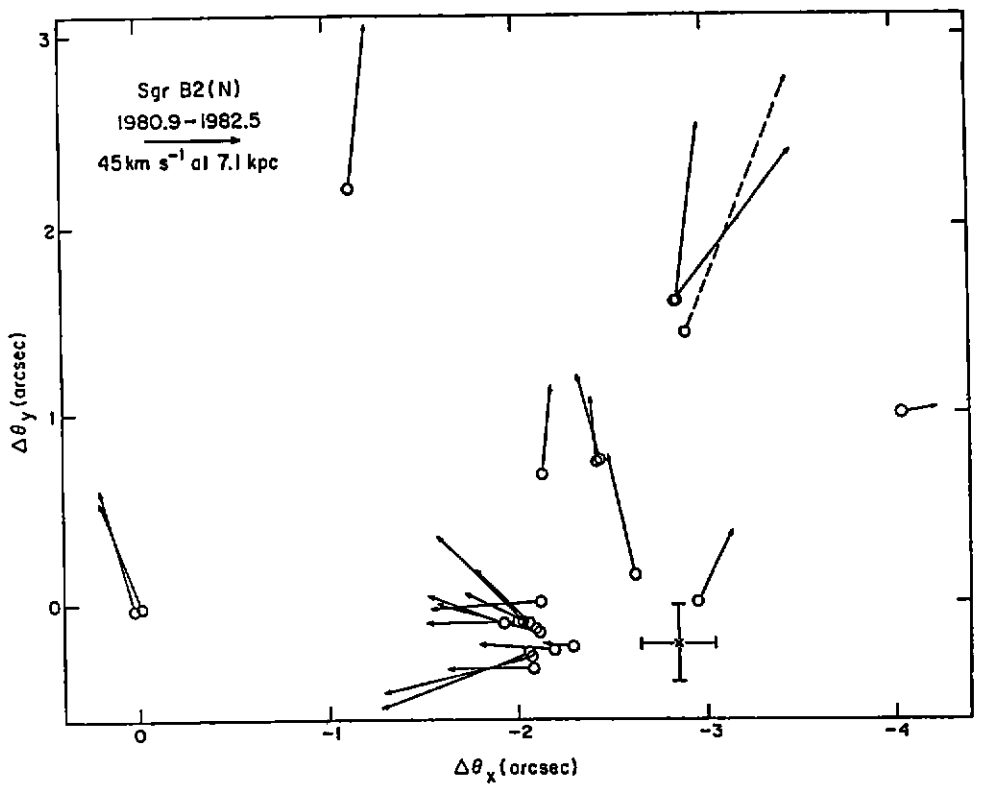

Figure 2.8: Sgr B2(N) 1980.9-1982.5

This diagram shows the proper motions of the H_2O maser spots. The maser spots appear to be expanding outward from the position indicated by the cross. A least squares fit of a uniformly expanding spherical source resulted in an estimate of the distance to the source (within 0.3 kpc to the Galactic Center) of 7.1 ± 1.5 kpc. The distance determinations are further discussed in section 2.3.5. (Figure from Reid et al.: 1988, *Astrophys. J.* **330**, 809)

shares none of the usual sources of systematic error. *Thus, obtaining a distance to even one galaxy would provide a crucial check on the calibration of Cepheids and of other distance indicators,* and hence could remove significant sources of error in the determination of the extragalactic distance scale and thereby the Hubble constant.

Distances to galactic objects using statistical parallax of H_2O masers can be estimated by measuring the internal motions within one source in an analogous way to the traditional method of statistical parallax. The line-of-sight velocity dispersion of the spots in the maser cluster (as determined from Doppler shifts of the maser lines) is compared to the relative angular velocities of the spots (determined by relative astrometry over a time baseline of about a year); their ratio is proportional to the distance of the source.

The distances to three sources in the Milky Way (Orion KL, W51 (north and main) and Sgr B2(2)) have now been measured with H_2O maser proper motions using statistical parallax methods. The distance to Orion is estimated as 480 ± 80 pc, *showing good agreement between the maser technique and optical methods for determining distances* (which range between 400 and 500 pc). The distance to W51(Main) has been found to be 7.0 ± 1.5 kpc and to W51 (North) 7 ± 2 kpc.

No optical distances are available for the W51 region due to high extinction; however, kinematic distances of between 3.5 and 7.5 kpc are indicated.

VLBI studies of the water masers towards Sgr-B2 were conducted during the period 1980.9 - 1982.5. in order to determine the distance to the galactic centre. Repeated measurements of the relative positions of the maser features show them to be expanding, see Figure 2.8. The maser spots appear to be expanding outward from a central position and a least squares fit of a uniformly expanding spherical source resulted in an estimate of the distance to the source of 7.1 ± 1.5 kpc.

Since Sgr B2 is almost certainly within 0.3 kpc of the Galactic Centre, the distance measurement can be directly used as an estimate of R_0, the distance between the Sun and the Galactic Centre. The H_2O maser distance estimate of 7.1 kpc to the center of the Galaxy is significantly lower than the standard value of 10 kpc and in better agreement with the newly revised IAU value of 8.5 kpc. *The decrease in the value of R_0 has a widespread impact on astrophysics.* Some examples are:

1. all kinematic distances would be decreased
2. the mass of the Galaxy and the Galactic Centre would also be decreased
3. recent revisions of the absolute magnitudes of RR Lyrae variables are supported by the result, affecting distances to the local cluster and hence the extragalactic distance scale
4. the missing mass problem is compounded since the estimated luminous mass of the Milky Way is decreased and the "dark matter" content is increased in the Local Group.

Distances to extragalactic objects using statistical parallax of H_2O maser complexes

Galactic H_2O maser sources have internal motions with a dispersion of about 30 km s^{-1}. At the Galactic Centre, this corresponds to transverse angular velocities of 800 mas/year or 16 QUASAT beams/year. At a distance of 1 Mpc, such motions correspond to transverse angular velocities of 6 mas/yr. To achieve a single-epoch measurement precision of 1μas with a 50μas beam would require a signal to noise ratio (SNR) $\simeq 100$. Two or more such observations are needed over a time base of about one year to determine the proper motion. For example, three 48-hour integrations, spanning one year, of the strongest maser source in the galaxy M33 (5 Jy), made with QUASAT in conjunction with a ground array would be sufficient to determine the proper motions of the dozen strongest features to the required value of SNR. *The formal fractional distance uncertainty would be 20 percent.* Observations spanning a longer time period would result in an improvement on this figure.

The higher angular resolution provided by space VLBI will be crucial in resolving the structure of distant H_2O maser clusters, as well as allowing motions to be determined over a shorter time base. This is a clear case where the full two-dimensional resolution advantage of the interferometer beam is vital. Note also that for a spectral line the observing frequency cannot be changed, and the only way to achieve higher angular resolution is to extend the baselines beyond those attainable from earth.

Initial observations of galactic maser sources indicated that typical maser spots brightened and faded on a time scale of less than a year. However results which now span a five year period indicate that many spots re-brighten while still following straight-line trajectories on the sky. Thus maser clouds retain their physical integrity while moving a distance greater than their diameters. This development suggests that observations over the full five year of the QUASAT mission will be useful for proper motion studies, significantly relaxing the signal-to-noise requirements discussed above which are based on a one year study.

Although the number of extragalactic masers which can be studied with QUASAT is small we note that not one single galaxy has yet been searched completely for H_2O masers. A major

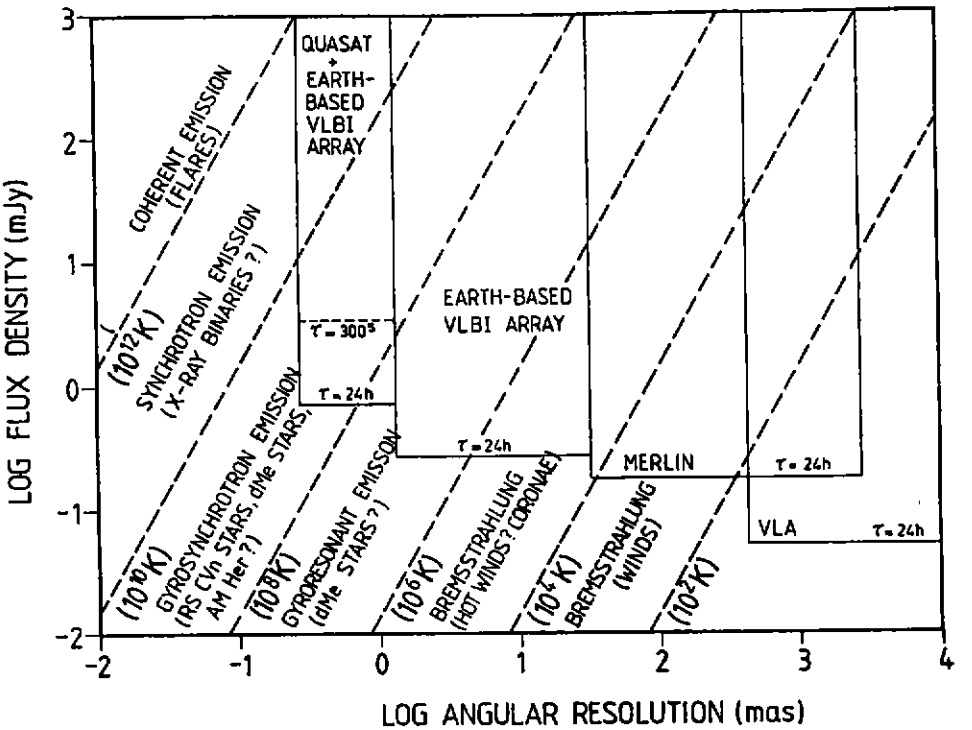

Figure 2.9: Stellar flux density versus angular resolution

The flux density as a function of angular resolution for various stellar radiation mechanisms and types of observing instrument.

ground-based program to find the best candidate galaxies for proper motion studies needs to be carried out.

2.4 Stars

2.4.1 Radio Stars

Radio emission has been detected from active regions in several different types of stars. Radio emitters include coronae of M-dwarfs (dMe type), various main sequence stars (types O, B, B_p, and A_p), pre-main sequence T-Tauri stars, from thermal winds of Wolf-Rayet stars and novae, from jets of X-ray binaries, from magnetospheres of white dwarfs (AM Her and dwarf novae binaries), detached (RS CVn) and semi-detached (Algol) close binaries. The emission can arise from a variety of physical processes such as Bremsstrahlung, gyromagnetic radiation, inverse-Compton scattering, and various kinds of coherent plasma radiation including plasma masers.

Figure 2.9 shows flux density vs. angular resolution for the various radiation mechanisms and types of observing instrument. At milli-arcsec resolution, detectable radio emission arises from the gyration of electrons in magnetic fields. Hence it provides unique information on the magnetic field and its role in the atmosphere and outer envelope of stars, as well as on the densities of high temperature plasma or non-thermal electrons. *Only VLBI measurements can determine the brightness temperature, which is vital in establishing the nature of the radio emission.* Figure 2.9 indicates the characteristics of the pertinent mechanisms.

Emission from radio stars is generally weak, and will require QUASAT observations of maximum

sensitivity utilising a ground array including at least one large diameter telescope. Several tens of objects can be studied with 300 seconds integration time (as would be needed for time variability and flare studies) and 100 or more objects if phase referencing techniques are used to synthesise a map over a 24 hour observation (see Figure 2.9). The emission is also very compact (with the exception of Bremsstrahlung emission from the outer regions of stellar winds); the apparent diameter of a star with $D_* = D_\theta$ at a distance of 10 pc is 960 micro-arcsec. *Only QUASAT can provide sufficient angular resolution to determine the morphology of the emission.*

Flaring Emission

QUASAT will not only study the quiescent radio emission from stars but also the dramatic radio flares of individual stars and interacting binaries. It is well known that the largest flares are at least a factor 1000 more energetic (in both luminosity and total energy) than those on the Sun. A clue to this activity may lie in the rather high rotational velocities observed in flaring stars ($\geq 5\ kms^{-1}$, periods of a few days) which can cause a stellar dynamo effect in a convective mantle and provide enough magnetic activity to generate a flare.

Although the majority of stars probably undergo a flaring phase after their T-Tauri (formation) phase, the theory of stellar evolution cannot yet explain this important phenomenon.

M-dwarfs

M stars comprise 80% of the galactic population; 5% of this group are dMe stars of which 25% show flaring activity. Radio outbursts from M-dwarf stars have been studied for many years. Flare durations vary from milliseconds as in AD Leo (at 20 cm wavelength) up to tens of minutes. Flaring emission of this intensity seems to be confined to the M stars rather than earlier types (F to K).

M-dwarf radio flare characteristics are very similar to solar flares, although of much greater luminosity, and it is thought that similar mechanisms are at work. Brightness temperatures may exceed 10^{15} K for the short duration flares, implying a coherent mechanism such as electron cyclotron maser action. The longer duration flares are thought to arise from gyro-synchrotron radiation and here simple measurements of size of the emission region plus flux density variations will clarify ideas on the emission process and facilitate estimates of magnetic field and electron density in the stellar corona.

QUASAT is highly suited for study of these flare sources since it will have sufficient resolution to study active regions on some nearby M-dwarfs in detail. It should be possible to follow the development of a flare and hence derive much information on the stellar atmosphere. QUASAT observations give more *uv* coverage in short periods of time than the ground VLBI arrays alone and therefore is better suited to these observations.

Interacting Binaries

Binaries with orbital periods of a few days or less utilize mass exchange between the stars as a source of gravitational energy for high energy phenomena. The active, non-thermal emission objects relevant to QUASAT are:

1. RS CVn and Algol Type Binaries

These consist of a pair of relatively normal main sequence stars in a close binary system with separations of around 10^{12} cm. They are the most common kind of radio star, with radio flux densities reaching 1 Jy in cases such as Algol and the RS CVn type star HR1099. The radio emission of Algol varies on timescales of tens of minutes to months, with many flares having durations of a few hours. VLBI observations have shown the presence of core-halo type structures in UX Ari (Figure 2.10). The assumption of gyro-synchrotron radiation leads to magnetic field estimates varying from 10 to 50 gauss in active regions and brightness temperatures of 10^8 to a few

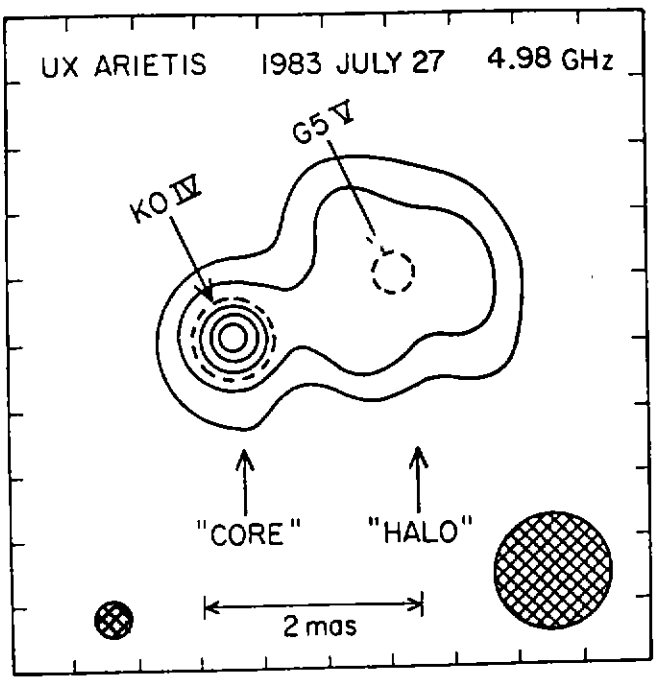

Figure 2.10: UX Arietis

VLBI hybrid map of UX Arietis at 4.98 GHz. The restoring beam (shown in lower right corner) is a circularly symmetric Gaussian of FWHM = 1.0 mas. (N-S structure is somewhat overresolved.) The QUASAT beam is showed in the lower left corner. The contour levels are at 25%, 35%, 50% and 90% of the peak brightness. The dashed circles show the stellar system at phase 0.2. Note that the alignment of the radio and optical images is conjectural. (After Mutel et al.:1985, *Astrophys. J.* **289**, 262).

times 10^{10} K. Angular sizes of 0.5 to 2 mas have been found, comparable with the sizes of stellar coronae and binary separation.

The detection of a cyclotron maser with 100% circular polarisation in Algol during a 10 minute burst is clear evidence for even stronger magnetic fields in the energy release region. We expect that the site of the radio emission will move and grow as a flare progresses and thus can only be investigated when the resolution is adequate. QUASAT gives us the opportunity to follow the development of flares in detail.

2. X-Ray Binaries

There are at least fifteen radio emitting stellar X-ray sources known, of which at least four have unresolved components (< 1 milliarcsec) on Earth baselines. In the radio domain they are characterised by strong variable synchrotron emission, and by variable X-ray emission. SS433 and Cyg X-3 are particularly interesting examples of radio X-ray binaries, both exhibiting strongly variable radio emission and mildly relativistic motion in their radio structures.

VLBI observations have "zoomed-in" on the compact central component in SS433 and, with an angular resolution of 10 milliarcsec, have brought the detailed motion of the emitting material into focus. This has shown that the radio emission is in the form of blobs moving outwards ballistically with an angular velocity of $\sim$ 9 mas/day, and that the radio emission flares at an angular distance of between 50 and 100 milliarcsec from the stellar system (4 to 8 $\times 10^{15}$ cm).

SS433 has been resolved on scales of 1 or 2 milliarcsec on Earth baselines at 5 GHz, so QUASAT's contribution to its study will be at the longer wavelengths, where the angular resolution is not sufficient on Earth and the flux density is higher.

2.4.2 Radio Supernovae and their Remnants

Recently it has become clear that the emission from extragalactic supernovae and their remnants can rise to extreme power levels at radio wavelengths, reaching up to several thousand times the current luminosity of Cassiopeia A. Most radio bright supernovae belong to the optical class II although a few shortlived events associated with type I have also been detected. Interestingly, several of the brightest radio supernova remnants have been discovered via radio studies of nearby galaxies; their optical types are unknown. Most of the ten or so extragalactic radio supernovae have been detected with VLBI techniques. A few of them have been or are being mapped. Two objects, SN1986j in NGC891 and 41.9+58 in M82, reached peak flux densities at 6 and 21 cm above 100 mJy and would have been easy targets for QUASAT. Several others reached flux densities in the tens of mJy at peak brightness. SN1987a, which peaked above 100 mJy for a short period is a special case because it is very sub-luminous in the radio.

There is a variety of astrophysical questions posed by the studies conducted so far which could be answered via a combination of high resolution mapping and multi-wavelength light-curve monitoring. These include:

1. What is the electron acceleration process in supernovae and supernova remnants?
2. Are there neutron stars inside and do they create mini Crab Nebulae?
3. How much mass is ejected in the explosion, when does it break up in filaments and is it axially symmetric?
4. What is the history of the pre-supernova mass outflow?
5. Can supernova expansion measurements lead to a direct value for the Hubble constant?

The improved resolution afforded by QUASAT is crucial to most of these questions. In the first five years following the supernova event there are a variety of spectral effects containing important physical information. In that period a typical radio supernova appears to be about 1-2 milliarcseconds in size. For the very rapidly evolving (1-3 months) type I supernovae sub-milliarcsecond resolution is required before the source fades too much.

Some of the flavour of radio supernovae studies is already contained in the few objects under investigation right now, two of which are described below:

SN1979c

The supernova SN1979c in the galaxy M100 in the Virgo cluster had a peak total flux density of $\sim$ 12 mJy at 1.4 GHz and is presently the most distant of all radio supernovae discovered. Although the supernova was too compact at the time of its peak flux density for ground based VLBI and later too weak for an image of it to be made, its diameter has been measured at four epochs and its rate of expansion determined (Figure 2.11). If the angular diameter, θ, is given as $\theta \propto t^m$, with t being the time since explosion, then $m = 1.03 \pm 0.15$. This determination is the first one for any supernova or young supernova remnant that is consistent with free expansion.

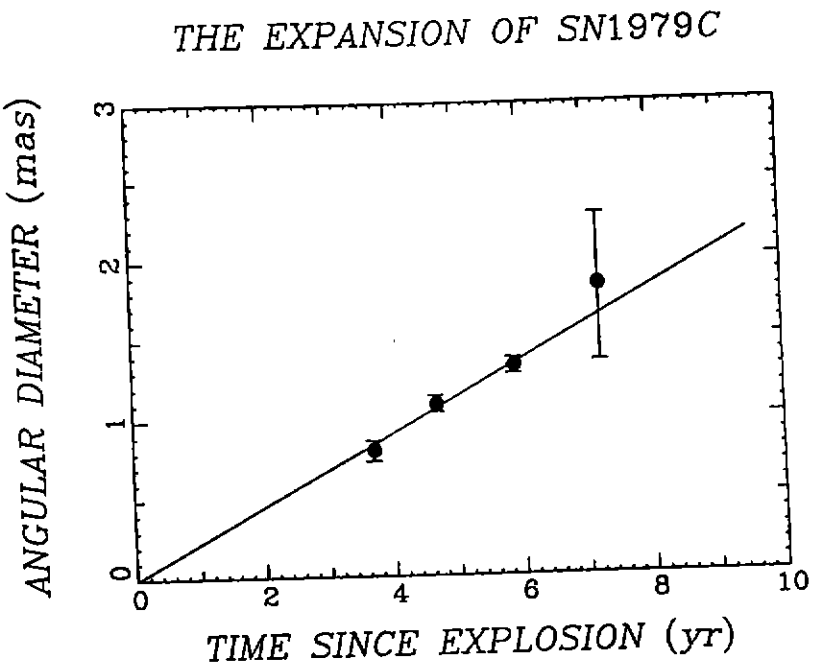

Figure 2.11: The expansion of SN1979c

The angular diameter determinations for a shell model. For a ring and a uniform sphere, the ordinate scale has to be multiplied by 0.8 and 1.3, respectively. The solid line represents free expansion. From Bartel: 1988 (*IAU Symp. No. 129*, ed. M. J. Reid and J. M. Moran, Reidel, Dordrecht, p. 175).

SN1986j in NGC891

This is the most recent and most powerful supernova. It was discovered at radio wavelengths several years after the estimated explosion date (about 1983) and is currently at its peak flux density of 110 mJy at 21 cm. It is only 2-3 milliarcsecond in diameter and in great need of more resolution. Although no optical supernova has been discovered there is a slowly expanding source of very bright optical line emission, probably internal to the radio remnant. It will still be around in five to ten years.

Assuming QUASAT will have a lifetime of about 5 years, there will be several new supernovae flaring up and bright enough to be studied in their first eventful years during the QUASAT era. In addition there will be remnants a few years old, and a few bright middle-aged supernova remnants going through turbulent phases of interaction with pre-supernova mass outflow and swept-up interstellar matter.

2.5 Scattering by the Interstellar Medium

Fluctuations in the density of ionized gas of the interstellar medium introduce excess phase changes in signals propagating through it and broaden the observed angular size of the source, as well as fluctuations in signal amplitude at low frequencies. At high galactic latitudes, the angular broadening of the extragalactic sources is approximately $\theta_s(\text{mas}) \sim 1.3\nu^{-\frac{1}{2}}|b|$, where b is the latitude and ν is the frequency in Gigahertz. *Hence at frequencies of 1.5 GHz and above and at high galactic latitudes, QUASAT observations will not be affected by interstellar scattering.*

While unobservable at higher frequencies, interstellar scattering at 0.3 GHz is extremely useful as a probe of the ISM on scales that would otherwise be unobservable. In the plane of the galaxy the scattering is highly variable with direction, and the angular sizes of galactic sources are on the order of $\theta_s(\text{mas}) \sim \theta_0 L^{1/2}\nu^{-2}$, where $\theta_0 \simeq (1 \sim 100)$ mas and L is the distance to the source in kiloparsecs. Analysis of interstellar scattering yields information about the electron density

fluctuations on scales of typically 10^{11} cm; the clumpiness of the interstellar scattering near the galactic plane varies significantly on angular scales less than 5°. *Pulsars and masers, which have very small intrinsic sizes and are preferentially located near the plane of the galaxy, can be used by QUASAT to study interstellar scattering. In addition, at 0.3 GHz, QUASAT observations of pulsars will make it possible to probe the scattering law at much higher galactic latitudes than can be done with ground based VLBI.* See also the section on Low Frequency Variables in the section on AGNs on page 13.

2.6 Cosmology

Ever since the demonstration that Cygnus A was an extragalactic radio source of unprecedented power, it has been clear that the methods of radio astronomy offered a new way of exploring the far reaches of the universe. The active galaxies are such luminous objects in the radio part of the spectrum that they can be detected easily at redshifts close to, or beyond, the reach of conventional optical techniques.

An even more dramatic development, the discovery of quasars in 1963, highlighted the way in which radio methods have led the way in discovery so often in the last few decades. These most distant and most luminous known objects in the universe have proven to be visible at enormous distances, and the optical follow-up has shown that they were in all probability far more numerous at an earlier epoch in the history of the universe, as were active galaxies in general. The radio quasars, generally speaking, represent the most luminous examples among the quasars, and nearly all the quasars with redshifts greater than 4 originated from the radio source lists.

The seat of the activity for both quasars and radio galaxies lies at their nuclei, and this has been the prime discovery area for VLBI studies. The cosmological relevance of the superluminal expansion studies was demonstrated by Cohen et al. (1988, *Astropys. J.* **239**, 1) in their study of 32 superluminal sources. These studies make sharp cosmological tests as the redshifts of the sources being studied increase beyond unity; the Einstein-deSitter universe is a familiar example in which angular sizes of standard measuring rods become larger when the redshift exceeds five-fourths. The measurement of proper motion with VLBI involves transformations in both space and time; an assemblage of superluminal sources in an Einstein-deSitter universe exhibit a proper motion that diminishes as z increases, but the proper motion asymptotically approaches a limiting value (0.2 mas/y for the parameters given by Cohen et al.) Their sources give proper motion results that are consistent with the standard cosmology, but their angular resolution limits the sharpness of this cosmological test. *With the angular resolution advances given by QUASAT the limits could be pressed to higher redshifts and smaller proper motions. With this capability, the large-scale geometry of the universe can be probed in a way that is totally different from the conventional optical approaches.* This follows because it is angular-size distance, not luminosity distance, that is the relevant geometrical quantity.

These are the classes of object in which the conventional syncrotron models have failed their first critical test. The advance in angular resolution given by the first VLBI experiment in space, the TDRSS demonstration described in chapter 5.2, showed that the high fringe visibilities observed on the longest baselines were inconsistent with present self-absorbed radiation models. The sources are far too compact, and most probably bulk relativistic motions must be present. The new QUASAT data should permit the construction of more realistic physical models.

There is a more general class of results that can be anticipated with the addition of QUASAT to the ground-based VLBI arrays. All the known quasars having a redshift in excess of 3 show flat spectra, and this means that one is dealing with a class of active nuclei that have strong, self-absorbed synchrotron emission. This has direct relevance for cosmology, for if one wants to use the

quasars as cosmological probes in any part of the electromagnetic spectrum, physical understanding of the sources gives far greater certainty to the cosmological interpretation.

An obvious example is provided by the larger-scale radio structures associated with active nuclei. The most compact structures are probably influenced most strongly by the immediate surroundings of the nucleus. As the relativistic, superluminal plasma proceeds into the interstellar medium of the host galaxy, it can be measurably deflected by that medium, and as the jet proceeds further it interacts, in turn, with the intracluster and intergalactic medium. At a redshift of 3, for example, the Universe was presumably 64 times denser than it is today; the interstellar medium in the early radio galaxies and quasars was almost certainly very different from its constitution in our nearest neighbours. It is hard to see how this potentially valuable probe, however, can become a quantitative cosmological tool until the sources themselves are better understood, and the physical understanding will proceed from the QUASAT studies. A contribution will be made by QUASAT to the study of cosmological evolution in quasar properties by observing the compact structure of objects with redshifts > 3 and comparing the results with a sample of objects with redshifts less than 1. The bending and brightening effects on the jets in the lower redshift sample are already being studied by using earth-based arrays, but many of the highest-redshift quasars, beyond a redshift of 3, are still unresolved on the longest earth baselines. QUASAT will provide that structural information.

2.7 Gravitational Lenses

All space is warped by the gravitational fields of the matter in the universe, and the phenomenon of gravitational lensing is a direct expression of these effects. All matter, whether it is luminous and stellar, or in the form of dark matter, contributes to the lensing. The background object is usually a quasar, and since the quasar luminosity generally varies with time, and since the path lengths to the observer usually differ from image to image, there can be a differential time delay that provides a completely new class of cosmological tool. The study of gravitational lenses, has deep implications, both for the large-scale geometry of the universe and for the distribution and nature of matter on the scale of galaxies and clusters of galaxies.

Observations by QUASAT address the three main aspects of the gravitational lens problem: the establishment of the lensed character of a given source, the measurement of detailed lens properties, and the determination of relative time delay.

The original twin quasar, 0957+561, can be used as an illustration. The 6 cm radio map (Figure 2.12) shows the A and B condensations corresponding to the optical quasars; the insets to the right show the nuclear structures of A and B at the milliarcsecond level, found by VLBI. The opposite parities of the jets show clearly, and are exactly as the lens models require. The nuclei show evidence of barely resolved structure. The magnification matrices are not identical, since the jet of A appears elongated with respect to B, but the differences in magnification are not large. Even if optical observations of the redshift equality had not been available, the radio data alone would have been sufficient to show that this is an example of lensing.

The capacity of QUASAT to improve our knowledge of lens images is illustrated by the nuclei of A and B. They have what seem to be small jets on a scale of 1 milliarcsecond, but these are barely resolved. Inferring the mapping detail to 225 microarcseconds with QUASAT at 6 cm is only part of the story; the lens itself magnifies the quasar images by a factor of 5 or 6 in linear dimension. Thus one is effectively looking with an angular resolution of 3×10^{17} cm at the quasar itself, and one can start to probe the radio structure on scales of the broad-line region of extremely distant quasars.

Measurements of changes in the flux density of components A and B in 0957 + 561 indicate a

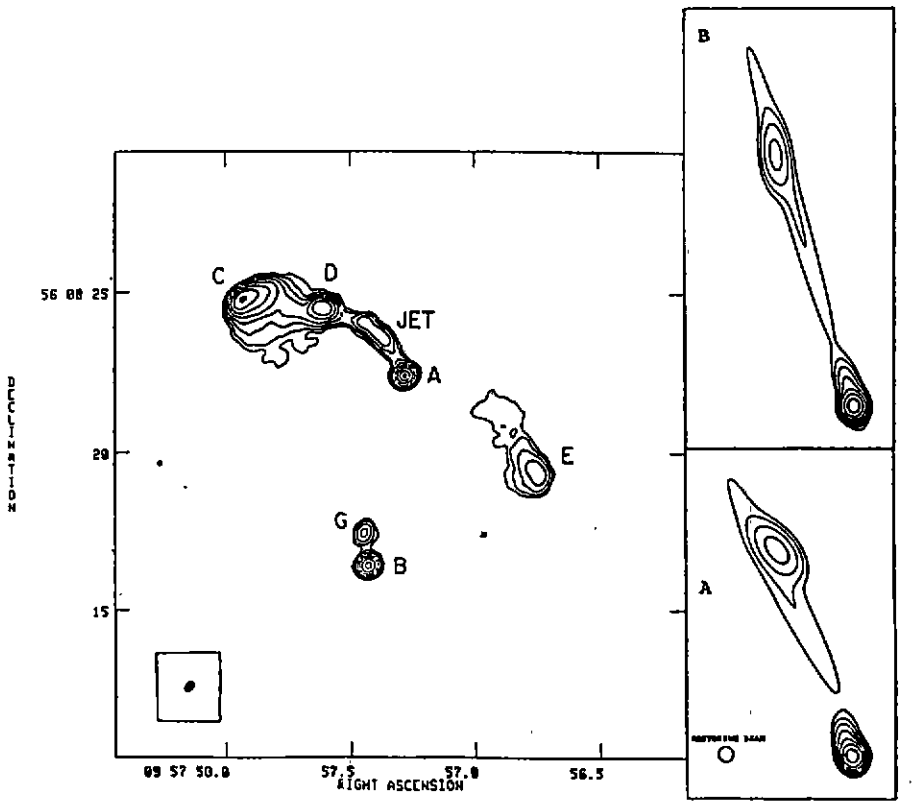

Figure 2.12: The double Quasar 0957+561

To the left a 6 cm map from the VLA at 0.3 arcsec resolution. To the right, 3.5 milliarcsec resolution VLBI maps (from Gorenstein et al.: 1988 *IAU Symp. No. 129* eds. M. J. Reid and J. M. Moran, Reidel, Dordrecht, p. 201). The scale is ×135 the VLA map.

relative time delay of approximately 500 days. A value of the Hubble constant of $H_o \leq 66 \pm 15$ can be derived; the uncertainty quoted allows for various lens models. One major problem that QUASAT helps solve with its high resolution and detailed map-making ability is the isolation of the time-varying part of the nuclear source. As a result, far more accurate measurements of the time delay can be made.

Two other radio candidates are known with sufficient flux density for QUASAT's sensitivity. The discovery rate at this flux level appears to be about one per year, so that one can expect the sample for QUASAT observations to be of order 10 by the mid-1990's.

Chapter 3

Science, Mission and System Requirements

3.1 Science Requirements

3.1.1 General Requirements

The principal mission requirements are to produce high resolution, high dynamic range maps of celestial objects over a broad range of radio frequencies.

Sky Coverage

QUASAT must be capable of providing data leading to good quality maps of northern hemisphere sources when operated in concert with either, or both of, the European VLBI Network and the US VLB Array. It must be capable of producing good quality maps of southern hemisphere sources when operating with the southern hemisphere antennas.

Sensitivity

The QUASAT design should maximize the instrument sensitivity, within the bounds of technological constraints and mission costs. The higher the sensitivity, the more sources can be observed and the better the image quality. Antenna size, system temperature, and bandwidth must be chosen to give a SNR of at least 6 to 1, within an integration time of 300 s for sources of flux densities of 100 mJy, on baselines involving ground-based radio telescopes of 25m diameter with typical system temperatures in the range of 25 K (L band) to 100 K (K band).

Frequencies

Observation frequencies are at K-band (22 GHz), C-Band (5 GHz), L-Band (1.7 GHz), and P-Band (0.33 GHz). These frequencies correspond to wavelengths of 1.35 cm, 6 cm, 18 cm, and 92 cm respectively. Simultaneous observation at any two chosen frequencies with both hands of polarization is desirable. All frequencies should operate for the entire mission.

Polarisation

The QUASAT receivers must detect both hands of circular polarisation at all frequencies.

3.1.2 Mission Lifetime

Operational lifetime must be at least two years. Mission design must allow at least five years lifetime.

3.1.3 Orbit Requirements

The choice of orbital parameters is based on a requirement to achieve the highest angular resolution possible consistent with good image quality and high dynamic range. It was therefore thought that the mission required two phases with different orbits: the first orbit giving high angular resolution while maintaining acceptable image quality and the second orbit providing better coverage in the uv plane at reduced resolution. Following a study on the image quality in different orbits, see section 5.3, it was decided that the baseline would be a single orbit. The orbit selected was the higher apogee one (higher resolution). This is a geostationary transfer orbit with modified inclination ($\geq 30°$) and perigee altitude ($\sim$ 5000 km). This orbit gives an image quality equal to the best currently achieved on the ground.

Apoapsis

The orbit semi-major axis must be large enough to provide space-ground baselines which are sufficiently long to significantly improve mapping resolution obtainable from earth, but not so high that unacceptable holes in the (u-v) plane coverage result. A reasonable goal is to provide baselines of at least $\approx$ 35 000 km. The height of apoapsis should be great enough to achieve this goal.

Periapsis

The periapsis of the orbit must be low enough to provide intermediate length space-ground baselines down to intercontinental distances. Thus the height of periapsis should be less than about 7000 km.

Inclination

The orbit inclination should be chosen to maximise the north-south interferometer baselines between QUASAT and the ground, while maintaining a reasonably circular interferometer beam. Inclinations $\geq 30°$ are acceptable.

3.1.4 Mapping Sequence Requirements

Mapping Time

QUASAT should provide a capability for full mapping of a source within 48 hours. The typical mapping period should be 24 hours. Depending on the scientific goal, some observations will last only a few hours.

3.1.5 Spacecraft Navigation Requirements

Orbit Control

Requirements on the achievement of the desired orbit are quite loose, about 1-2% of the targeted orbital parameters. This allows a positional control tolerance of a few tens to a few hundred km.

Orbit Reconstitution

The VLBI correlator requires that the position, velocity and acceleration shall be determined with an accuracy of 300 m, 0.01 m s^{-1} and 2×10^{-7}m s^{-2}, respectively. In addition, the modeling of the trajectory must be accurate enough that positional deviations from an estimated smooth trajectory over the observation integration time (300 s) do not accumulate to greater than $\lambda/16$ (0.8 mm at 22 GHz).

3.1.6 Space Systems Requirements

The expression for signal-to-noise ratio (SNR) on a single baseline linking two antennas is given by

$$\mathrm{SNR} = KS_c D_1 D_2 [g_1 g_2 \frac{e_1 e_2}{T_1 T_2} B\tau]^{1/2}$$

where $K \simeq 1.8 \times 10^{-4}$, and
S_c = correlated flux of the observed radio source in Janskys
$e_{1,2}$ = antenna efficiencies
$D_{1,2}$ = antenna aperture in meters
$T_{1,2}$ = receiver system temperatures in K
B = bandwidth in Hz
τ = integration time in seconds
$g_{1,2}$ = mispointing coefficient (typically 1 for ground-based antennas)

Assuming realistic values for the different parameters the QUASAT antenna aperture shall be at least 10 meters.

3.1.7 Instrument Requirements

The science instrument should consist of a microwave antenna, a dual polarisation 4-frequency receiver at the feed point consisting of low-noise amplifiers and phase stable frequency down converters to produce IF signals, and data digitisation equipment. The tunable range should be:

- 500 MHz (between 22.0 GHz and 22.5 GHz) at K-band
- 300 MHz (between 4.72 GHz and 5.02 GHz) at C-band
- 130 MHz (between 1.6 GHz and 1.73 GHz) at L-band
- 4 MHz (between 0.324 GHz and 0.328 GHz) at P-band

On-board facilities to verify the system noise and phase performance should be available.

Receiving Bandwidth

The instantaneous receiver bandwidth should be at least 64 MHz, 32 MHz per polarisation, except for P-band. A dual channel IF system is required in order to obtain both hands of polarization.

System Temperature

The receiver should be cooled so that the system temperature are less than 200 K when operating at K-band, 75 K at C-band, and 40 K at L-band and P-band.

Antenna Microwave Performance

The microwave performance of the antenna must be sufficient to meet requirements associated with frequency reception up to 22 GHz (K-band). A single antenna beam is necessary, with on-axis aperture efficiency as high as possible. Sidelobe levels are of secondary importance. The RMS surface error should be 0.8 mm or better. The desired on-axis polarisation purity should be better than 30 dB.

Antenna Pointing Accuracy

The electrical axis of the antenna must be pointed to within one eigth of the beamwidth of the target source if useful VLBI data are to be obtained. This corresponds in the worst case to 30 seconds of arc at 22 GHz. Near continuous knowledge of the pointing history is required to an accuracy of 5 arcseconds.

Observing Direction

The spacecraft design must permit pointing the antenna and observing a radio object in any direction. If necessary for thermal reasons a zone of 30° around the sundirection may be excluded.

3.2 Spacecraft Requirements

The spacecraft may be attitude stabilized about the electrical axis of the VLBI antenna. The spacecraft must provide a system for antenna pointing and slewing, power for the instrument, RF equipment for communication with the earth, a computer to regulate the observing program, and cabling to link the RF equipment. It is desired that the spacecraft attitude control be provided by non-consumable techniques like torque rods or momentum wheels.

The major system requirements imposed by the QUASAT mission concept are:

Launch and Mission requirements:

- QUASAT will be launched by Ariane 4 in a dual launch configuration and injected into a Geostationary Transfer Orbit (GTO).
- Insertion into the first operational orbit will take place after a few revolutions in the GTO. *The requirement for the spacecraft study was that after a period to be determined (1-2 years), the spacecraft would enter the lower apogee orbit. Thus, Chapter 7 describes the two orbit option.*
- The mission lifetime shall be 2 years minimum with consumables budgetted for 5 years.
- Science measurements may last from 3 to up to 48 hours with operation in eclipses up to a maximum duration of 1 hour.

Spacecraft and Payload requirements:

- The spacecraft shall be 3-axis stabilized and accommodate the radio astronomy payload for interferometer observations in conjunction with a ground-based VLBI network.
- The payload must consists of a deployable radio astronomy antenna of at least 10 m diameter, feed assembly, low noise receivers including the down-converter IF section and a local oscillator driven by a ground-based reference signal.
- The K-and C-band preamplifiers need to be actively cooled to a desired temperature of 80 K. The required system temperature for the L-band preamplifier is 250 K. In addition, part of the feed corresponding to the highest frequency shall be kept as cool as possible.
- The required overall antenna efficiency at 22 GHz must be at least 0.25.
- A feed adjustment mechanism to position the feed with respect to the focus of the best-fit paraboloid is required.

- The spacecraft shall have an on-board propulsion system for injection into the operational orbits and for attitude control.
- The spacecraft shall have mechanisms for antenna and boom deployment and for communication antenna steering.
- The absolute pointing requirement of the radio astronomy antenna boresight axis must be 30 arcsec or better.
- The attitude reconstitution accuracy of this axis shall be 5 arcsec.
- The absolute orientation in roll shall be 0.5°.
- A capability for offset pointing of up to 2° shall be provided (for phase referencing). Movement to this offset pointing including settling time shall take less than 180 sec.

3.3 Ground Segment Requirements

The ground system operating with QUASAT must be capable of nearly-continuous communication with the spacecraft via both the uplink and downlink signals. The uplink must provide for commanding the observational sequence and slewing/pointing parameters, and transfering the receiver reference frequency, and the downlink must carry the VLBI signal in an analogue or digital form.

The VLBI data correlation function is taken to be part of the science data processing, and is not included in the mission ground system. The principale products of the mission ground system are therefore recorded tapes or files of the digitized VLBI data.

The major requirements on the ground system are:

- Scientific mission management.
- Mission control through a suitable network of ground stations and mission control centre.
- Satellite science data acquisition through a suitable network of ground stations.
- Provision of a stable phase/frequency signal to drive the local oscillator on-board the spacecraft. For a signal decorrelation of less than 1 % due to phase transfer errors, the required maximum r.m.s. phase error about the best fitting phase error rate over 300 sec is 0.14 rads at 22 GHz.
- High precision spacecraft tracking. Position, velocity and acceleration shall be determined with an accuracy of 300 m, 0.01 m s^{-1} and 2×10^{-7} m s^{-2}, respectively.
- Ground science data acquisition through a suitable VLBI network.
- Science data processing at a VLBI correlation facility.

3.3.1 Frequency Standards

The ground system must be capable of supplying, via a two-way link, a stable radio tone that will allow a signal decorrelation loss due to phase transfer error of no more than 1% at 22 GHz for a 300 second integration time. This performance corresponds to an RMS phase error of 8° at 22 GHz (phase slope removed). If the link is dominated by white phase noise, the required square root Allan variance is 3.3×10^{-15} in 300 seconds.

3.3.2 Signal Recording

The ground system must provide the recording facilities to record the signal in real time consistent with VLBA format and digitization rates (at least 128 Mbits/sec).

3.3.3 Doppler Data

The ground system must provide the facilities for reception, recording, and processing of doppler data for orbit determination and phase reconstruction.

Chapter 4

Mission Concept and Design

4.1 Introduction

The primary instrumental goal of QUASAT is to achieve substantially higher angular resolution than is possible at centimetre wavelengths on the ground while maintaining the ability to construct high quality images of the radio sources. Image quality is characterised by the term dynamic range which is the ratio of the brightest to the faintest reliable features. In the case of current ground-based images, dynamic range has reached 1000 to 2000 to 1 as a result of increasing the uniformity of aperture or uv plane coverage and improved image construction algorithms. In space VLBI, image quality and increased angular resolution are not necessarily compatible, since lengthening the baselines to only one element will, in general, result in a poorer uv coverage. A modified geostationary orbit has been chosen as the operational orbit for QUASAT (see Section 5.3) in order to provide 5 times higher resolution, and images with the same quality as the best now achieved on the ground. A second orbit with a smaller apogee height was also studied in order to determine if any significant improvements in image quality would result.

These ideas are best understood in terms of the basic concepts of VLBI which are developed in the next section.

4.2 Basic concepts of space-VLBI

A VLBI system is essentially a radio analogue of the Michelson stellar interferometer. Because the radio technique employs the heterodyne principle, successful VLBI depends upon the ability to maintain coherence, at widely separated telescopes, of the local oscillators required to mix the received radio frequency signals down to manageable intermediate frequencies for correlation. This is normally achieved by the use of local atomic frequency standards (hydrogen masers). The converted signals from each telescope are recorded on magnetic tape and cross correlated later at a central location. A combination of several telescopes tracking a radio source as the Earth rotates can be used in this way to synthesize a telescope whose aperture has been limited by the size of the Earth.

The operating principles of VLBI are illustrated in Figure 4.1. A pair of antennas form a Michelson interferometer when their phase-coherent outputs are combined vectorially, either in real time (as in conventional radio interferometry) or in post-real time (as in VLBI). The antennas in Figure 4.1 are observing the same source, and if it is effectively pointlike (unresolved), the correlated output or interferometer fringe will vary sinusoidally in time. The fringe is characterized by an amplitude and a phase, which can be combined in a single complex number, the source

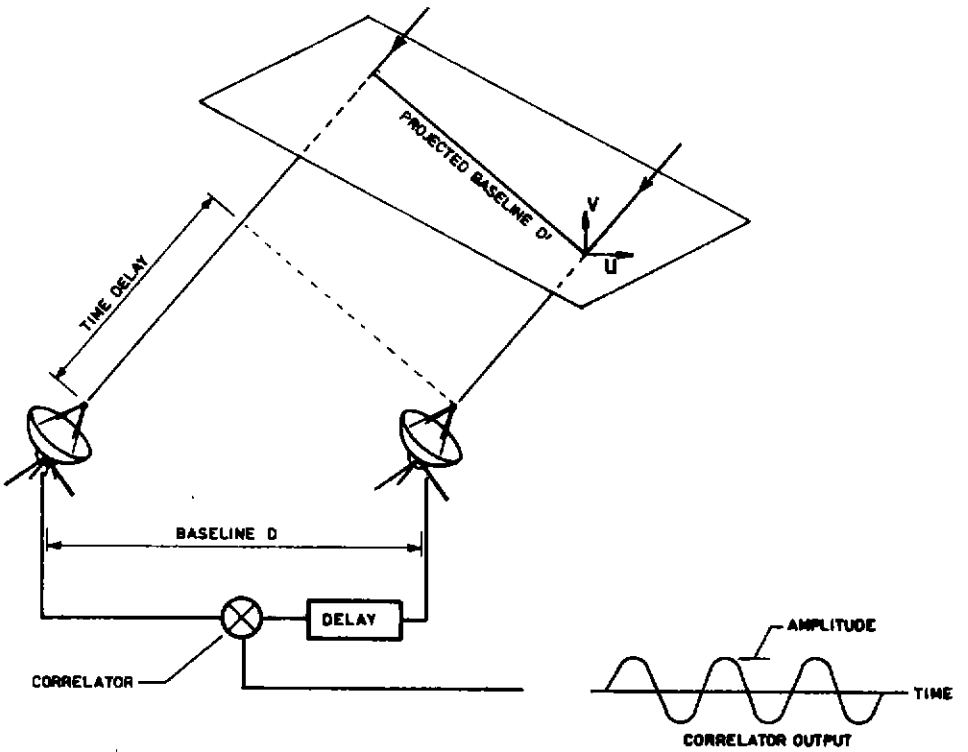

Figure 4.1: Operating principles of interferometry

visibility.

If the radio source is extended, the resulting visibility will change in amplitude and phase as the Earth rotates, due to the changing mutual interference of the various parts of the source. In effect, the visibility as a function of baseline is proportional to the Fourier transform of the source angular brightness distribution. A simple geometrical interpretation can be given for this process. The source brightness distribution B_{xy}, is a function of the two angular coordinates, x, y which are the Right Ascension and declination. A two-dimensional Fourier transform yields the Fourier conjugate V_{uv},

$$V_{uv} = \int\int B_{xy} e^{2\pi i(ux+vy)} dxdy$$

where u, v are coordinates determined by the following process. Construct a plane perpendicular to the line of sight to the source, as shown in Figure 4.1; let the u and v axes be east-west and north-south in this plane, respectively. Then take the physical baseline vector D joining the antennas, measured in wavelengths of the observation, and project it into the uv plane to give a vector D'. At each instant the interferometer pair measures the value of the Fourier transform V_{uv} of the brightness distribution B_{xy} for the current values of u and v determined by D'.

The complete Fourier transformation V is built up by the technique of earth-rotation aperture synthesis. As the Earth rotates, the projected baseline D' moves in an elliptical locus, permitting measurement of V for a family of values of u, v. When many different antennas are available, each antenna pair corresponds to a different physical baseline, and each traces out a different elliptical locus in the uv plane. If the baselines are well-chosen, a good sampling of V is obtained. A Fourier inversion of the visibility thus collected yields its Fourier conjugate, the source brightness

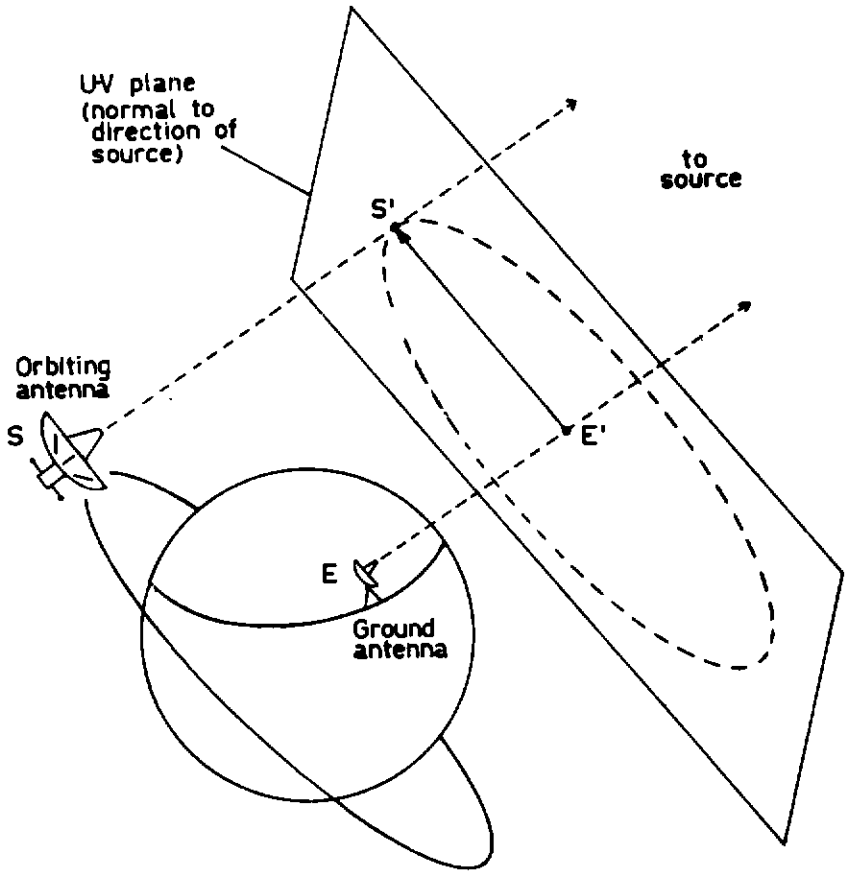

Figure 4.2: Simple illustration of space VLBI

distribution B_{xy}, convolved with a finite angular spreading function (the "beam") imposed by the lack of measurement of V_{uv} on baselines longer than those available in the observation. The angular resolution improves with increasing physical baseline and/or observing wavelength, that is the width of the beam decreases.

There is no difference conceptually between space-based VLBI and ground-based VLBI; a space VLBI observatory can be considered an outlying antenna of a ground-based array. To illustrate space VLBI, we consider the simplest system of a single station in orbit observing in conjunction with a single ground station, as shown in Figure 4.2. The uv plane is constructed in the same way as discussed above and a single orbit of the space antenna results in the uv locus shown schematically in Figure 4.3.

Figure 4.4 shows schematically the uv coverage after a number of orbits. The plot consists of a series of loops. Each individual loop is due to the rapid satellite motion during one orbit; it is slightly displaced from its adjacent loop by earth rotation which causes slightly different east-west baseline projections on each orbital pass.

In practice, a network of ground antennas will be used to effect more rapid filling of the uv plane and to allow antenna-based calibration via the closure amplitudes and phases obtained in the various quadrilaterals and triangles of baselines in the system. The density of uv coverage will also be increased by observing through successive orbits. The use of a range of frequencies within each band can further improve uv coverage. The potential image quality effect that this has on has been demonstrated by extensive simulations of imaging with QUASAT combined with the ground VLBI arrays (see section 5.3).

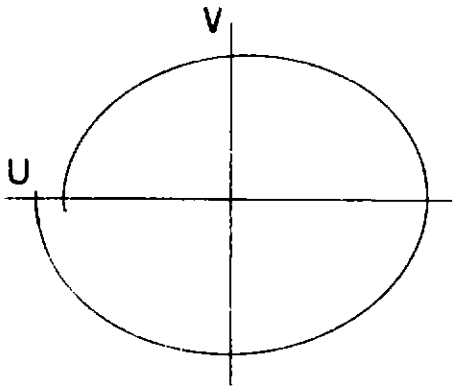

Figure 4.3: Single Orbit

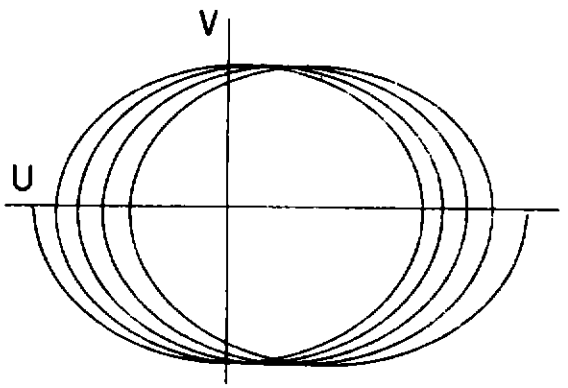

Figure 4.4: Successive Orbits

4.3 Operational Orbit

In order to reduce launch cost a dual launch with a geostationary companion has been adopted. This imposes a Geostationary Transfer Orbit (GTO) as the initial injection orbit. The perigee of this orbit (200 km) is too low since the QUASAT to Earth baselines overlap too much with those of the ground-based arrays alone and the inclination gives very bad uv plane coverage for low declination sources. Hence, this orbit will be modified with the on-board propulsion system with a minimum practical delta-v. An optimisation study has selected a perigee altitude of 5000 km and an inclination of 30°. Two possible operational orbits have been studied. The parameters of these two orbits are shown in Table 4.1. The higher apogee orbit was chosen to give maximum resolution and acceptable image quality; the lower apogee orbit was chosen to give better uv coverage and hence give higher image quality at the expense of some loss of resolution. We have selected the higher apogee orbit for the reasons given in section 5.3. The GTO and orbits considered for QUASAT are shown in Figure 4.5.

Table 4.1: Orbit parameters studied for QUASAT

Orbit parameter	higher apogee orbit		lower apogee orbit	
semi major axis	26771.1	km	19943.0	km
eccentricity	0.5749		0.4229	
inclination	30.0°		29.1°	
right ascension of asc. node	348.7°		253.4°	(depending on epoch)
argument of perigee	180.0°		331.7°	
perigee height	5,000.0	km	5,130.0	km
apogee height	35,786.0	km	22,000.0	km
period	12.1088	hrs	7.7857	hrs
velocity at perigee	7.43	km s^{-1}	7.07	km s^{-1}

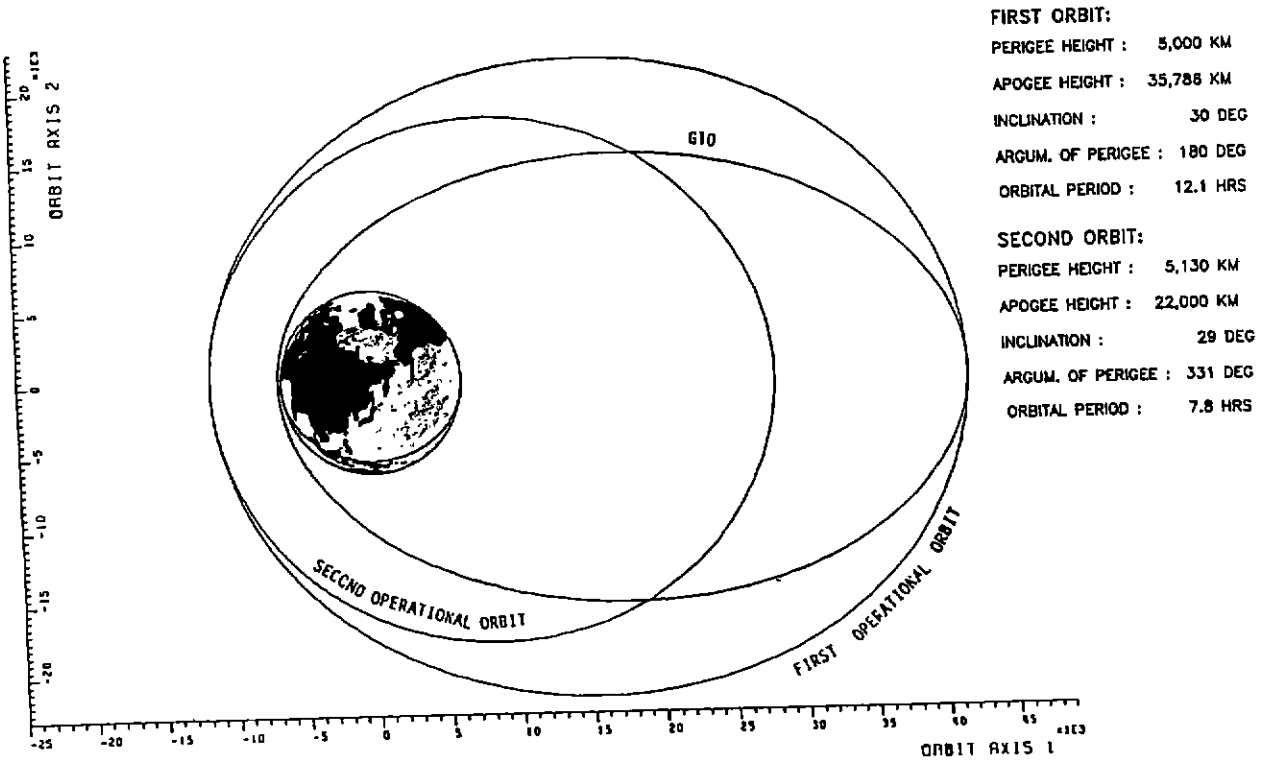

Figure 4.5: QUASAT Geostationary Transfer Orbit (GTO) and the possible Operational Orbits The higher apogee orbit is the one selected for QUASAT.

4.4 Launch and Injection

QUASAT will be launched by an Ariane 4 launch vehicle in dual-launch configuration into a standard Geostationary Transfer Orbit (GTO). The maximum lift capability of Ariane 4 into this orbit is 4200 kg. A few revolutions in GTO are required before a perigee raising maneuver can be performed at apogee to lift the perigee altitude from 200 km to 5,000 km, with a change of inclination from 7° to 30°. This maneuver will require an impulsive velocity increase of 821 m s^{-1}, and results in an orbit with a period of 12.1 hrs. For an initial spacecraft mass of 1214 kg in GTO this orbit change requires 454 kg of hydrazine leading to a spacecraft mass of 760 kg.

4.5 Launch Window

The launch window is driven mainly by the geostationary companion which requires a launch around midnight. A nominal Ariane launch window of 2 hours around midnight leads to acceptable solar aspect angles for QUASAT assuming injection at the 4th apogee. This launch window will be open during the whole year; however, if specific right ascensions of the ascending node have to be avoided (because of uv plane coverage requirements of specific objects/targets) the launch window would open during certain seasonal periods only.

4.6 Eclipses

During operation eclipses of up to 105 minutes can be expected within some 25 day periods. However, there will also be eclipse-free periods of 3 to 4 months.

4.7 Ground Station Coverage

The visibility of the satellite from the various ground telemetry stations has been determined for both possible orbits. The average percentage coverage for (elevation angle > 5°) is given in the following table:

Table 4.2: Ground station coverage percentages

Ground Station(s)	Higher apogee orbit	Lower apogee orbit
a. Kourou, Malindi and Perth	82.4	80.6
b. Goldstone, Madrid and Canberra	88.3	78.4
c. Goldstone, Madrid, Canberra and Malindi	95.5	89.9

4.8 Orbit Determination

The 1σ accuracy of the orbit determination is required to be not greater than 300 m in spacecraft position, 0.01 m s^{-1} in spacecraft velocity and 2×10^{-7} m s^{-2} in spacecraft acceleration, so that the residual fringe rates and delays on QUASAT baselines can be brought within standard windows in the VLBI correlators.

The achievable orbit determination accuracy is mainly influenced by the accuracy of modelling solar pressure effects, but also by AOCS maneuvers and the on-board transponder characteristics. An analysis has been performed which revealed that the requirements cannot be met using one or multiple S-band ground stations. However, using Doppler measurements derived from the phase transfer signal in K_u-band (see subsections 7.3.4 and 7.4.10, the required orbit determination accuracy could be achieved for more than 80% of the operational duration using multiple (2 to 3) Ku-band ground stations (only one station at a time). The analysis assumed an error model (e.g. radiation pressure error: 5%, station location error: 2 to 5 m, delta V maneuver error: 2 to 5%, Doppler noise/bias error: 1mm s^{-1}, unbalanced 8 thruster configuration) and took into account a potential scenario for AOCS momentum wheels off-loading once per orbit, as well as the availability of a continuous orbit reconstitution (post event). For potential contingency situations it has been assumed that 2 AOCS maneuvers per orbit are required. In this case the requirements could still be met, except for some perigee passages where the spacecraft velocity can only be determined to within 18-20 mm s^{-1}. If also the radio astronomy signal is used then both velocity and position can be determined with 2 to 3 times better accuracy.

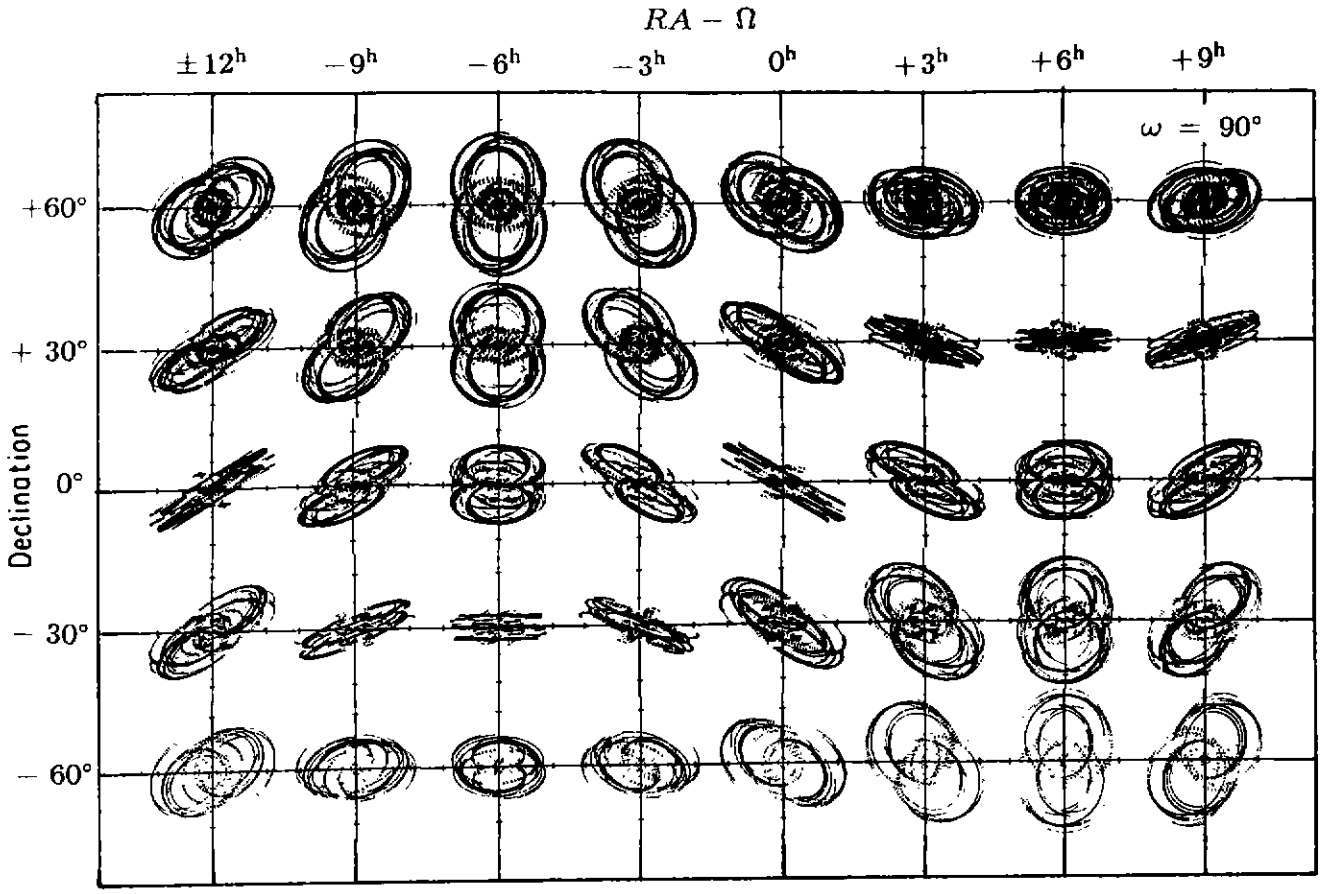

Figure 4.6: An example of uv plane coverage as a function of sky direction for a ground array and a telescope in space.

4.9 Celestial Viewing Constraints and uv Plane Coverage

The mission requires that the following minimum aspect angles are maintained:

(a) Sun 30°
(b) Earth 10°
(c) Moon 5°

Following a detailed coverage analysis at ESOC it has been demonstrated that these constraints do not restrict the scientific mission objectives. In fact, during the operational phase, most of the sky can be observed at any time and any currently unobservable regions can be observed at other times during the mission.

An example of uv plane coverage has been plotted in Figure 4.6. The area where the uv plane coverage collapses to one dimension corresponds to the projection of the orbital plane onto the sky. The precession rate of the right ascension of the ascending node ($\dot{\Omega}$) is -3^h6^m ($-46.5°$) per year. The argument of perigee changes at a rate ($\dot{\omega}$) of 74° per year.

Figure 4.7 is a uv diagram for the selected orbit with the observing direction $RA - \Omega = 18^h$, $\delta = 45°$ and a ground array of 17 telescopes.

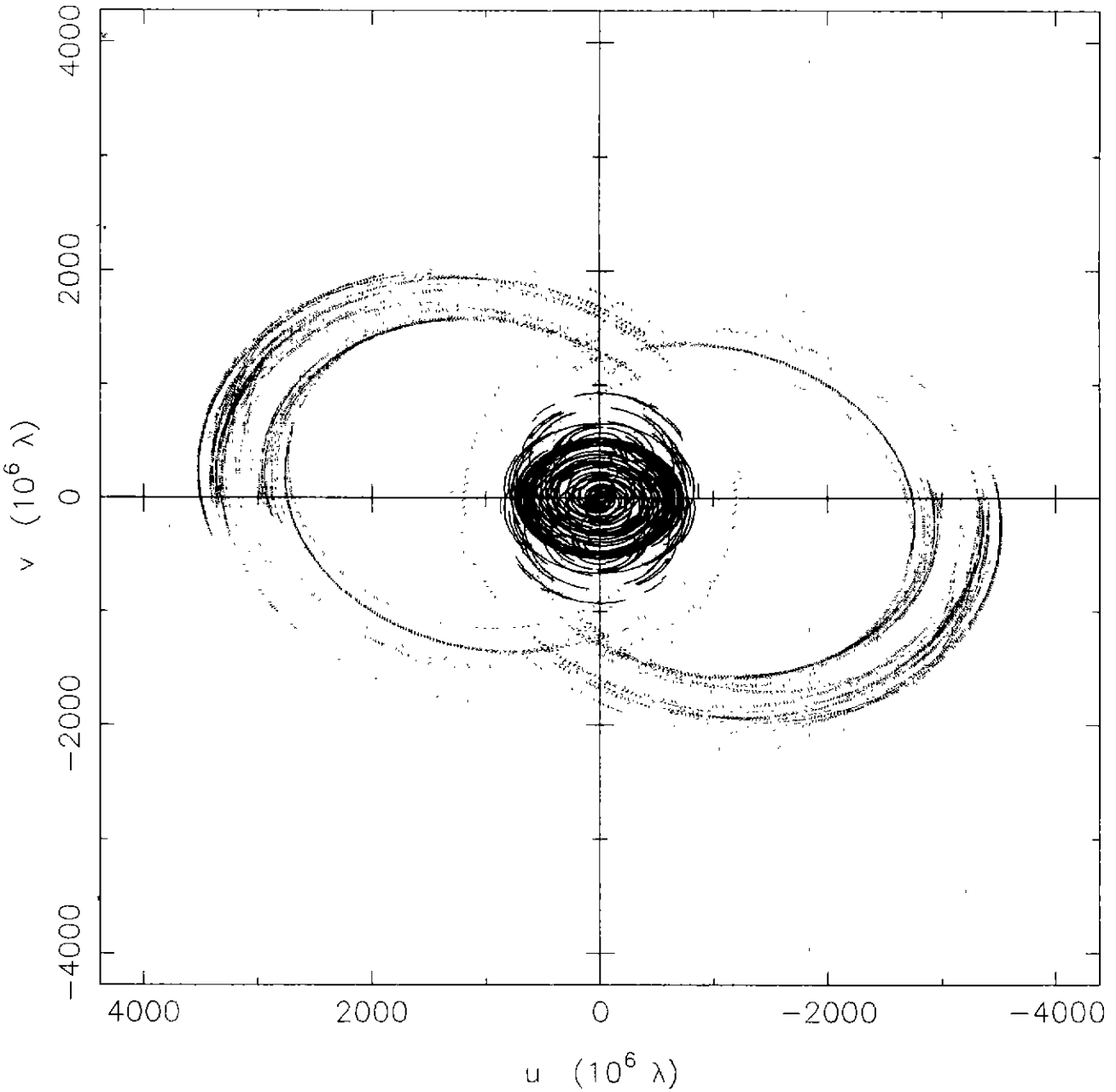

Figure 4.7: The *uv* coverage at a declination of 45° in the operational orbit

Chapter 5

Demonstration of Space VLBI

5.1 Introduction

QUASAT is unlike most scientific space missions in that the science payload performs functions identical to those of, and in conjunction with, well-proven ground equipment, and thus the space element has little scientific value in itself. QUASAT needs to be in space solely because the Earth is not big enough to accommodate the physical baselines that are necessary.

The principles and practice of VLBI have been developed over the past twenty years and VLBI is now a routine activity at many observatories. The new features of VLBI using QUASAT are, a) higher angular resolution, b) the high velocity of the QUASAT astronomy antenna with respect to the ground-based astronomical array, c) the need for a phase-transfer radio link to convey a reference frequency from a ground-based frequency standard to the spacecraft and d) the need to receive a broad-band downlink science signal. The high angular resolution comes at a cost, namely that there are larger gaps in the synthesized aperture plane than are desirable for the highest image fidelity.

The effect on the image-making process of QUASAT and the gaps in coverage have been tested by extensive simulations of QUASAT plus ground-array data.

The high velocity of QUASAT might affect both the correlation of data and the image-making process. The current generation of VLBI correlators can barely cope with the high velocity and acceleration of QUASAT but the next generation to be constructed in the next few years are designed so that, with minor additions, they will. Also the effect of the QUASAT motion on the imaging process has been simulated.

The extension of the VLBI technique to space has been anticipated by experiments that have demonstrated phase transfer between ground stations via satellite radio links, and a proof-of-concept of VLBI in space has been convincingly given by the TDRSS experiments. These experiments and the simulations clearly demonstrate the viability of QUASAT. They are covered in the remainder of this chapter.

5.2 The TDRSS Experience

One of the major premises of the QUASAT proposal is that space VLBI is based upon presently existing techniques. It was realized that a demonstration of space VLBI with an existing spacecraft designed for a completely different task could verify this premise.

The Tracking and Data Relay Satellite System (TDRSS), a communications system employing a geosynchronous satellite for communicating with low-earth satellites, had a configuration which

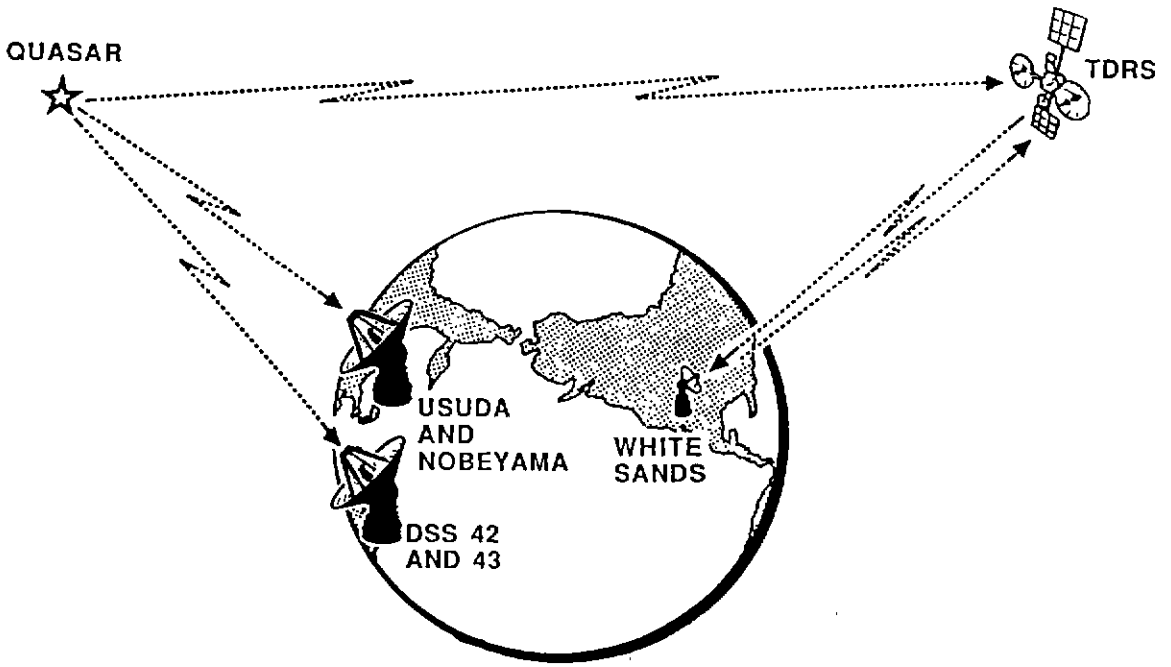

Figure 5.1: The geometry of the TDRSS experiment

appeared to have the characteristics required for a space VLBI demonstration. The spacecraft has the following capabilities making such observations possible:

1. Two 5-metre unfurlable high gain antennas which are independently steerable over a limited field of view.

2. Parametric amplifier receivers at both 2 and 13 cm for each high gain antenna.

3. Coherent local oscillators referenced to a ground frequency standard by a microwave uplink channel.

4. Wideband downlinks which transmitted a coherently frequency translated version of the received astronomical radio frequency signals.

5. Precise spacecraft tracking capabilities.

Characteristics 1 and 2 were required for sensitivity, 3 and 4 provided phase integrity, and 5 permitted accurate spacecraft orbit determination (necessary for data correlation).

In December 1985, phase stability tests showed that by using an appropriate configuration it would be possible to operate the TDRSS as an orbiting element of a VLBI array. In July and August 1986, space VLBI observations were conducted using TDRSS in conjunction with the Deep Space Network (DSN) 64-metre antenna near Tidbinbilla, Australia and the Institute of Space and Astronautical Science 64-metre antenna near Usuda, Japan. The geometry of the observation is illustrated in Figure 5.1. The tapes were brought to the Haystack Observatory for correlation. Minor software modifications were made to the correlator to handle the dynamic baselines introduced by the orbit errors. Provisions were made to use the spacecraft orbital parameters in the correlation process. Interferometric fringes were obtained from the sources 1720–130, 1510–089 and 1741–038 at a wavelength of 13 cm.

In January 1987, a series of seven observations totalling 25 hours were performed, again using a wavelength of 13 cm. Twenty three of the twenty four sources were detected on space-ground baselines as large as 2.15 earth diameters. These baselines gave the interferometer much better sensitivity to high brightness temperatures than any earth-based observations. Brightness temperatures of 1 to 4 times the 10^{12}K inverse Compton limit were measured for 12 sources, suggesting bulk relativistic motion in these sources. Coherence values of approximately 85% for integration times of 360 seconds were obtained.

The success at 13 cm made observations at 2 cm appear feasible. In February and March 1988, a series of 7 observations were made at an observing wavelength of 2 cm using the 45-m Nobeyama telescope of the Tokyo Astrophysical Observatory as well as the Tidbinbilla DSN facility. Successful detections have been obtained at 2 cm from approximately half of the quasars observed.

The observations at both 2 and 13 cm have shown that space VLBI is feasible with existing technology, and that:

1. A ground-based frequency reference can be accurately transferred to an orbiting radio telescope.
2. The radio astronomical signals can be acquired by a spacecraft, coherently amplified and transmitted to a ground station for recording on a wide bandwidth VLBI terminal.
3. Adequate orbit determination measurements can be made with existing systems and used for data correlation.
4. An existing VLBI correlator with minor software modifications can be used for space VLBI data.

Although the TDRSS was an excellent spacecraft to demonstrate the feasibility of the space VLBI technique, its limitations as an astronomical observatory must be realized. The geosynchronous orbit combined with the very restricted nadir-centred elliptical field of view ($\pm$ 31 N-S by $\pm$ 21 E-W) produced very limited uv coverage. This limited uv coverage made it impossible to produce significant maps. QUASAT's orbit will be optimized for high dynamic range image formation. The 5-metre antennas and ambient temperature parametric amplifiers yielded sensitivities over an order of magnitude less than is anticipated for the QUASAT. The TDRSS antenna pointing system was designed to track cooperating spacecraft rather than at an absolute celestial coordinate, as will be the case in QUASAT.

The TDRSS observations demonstrated the technical feasibility of the space VLBI concept, but only provided a tantalizing glimpse of the astronomical capabilities that a QUASAT mission optimized for the task would provide.

5.3 Image Simulations

The TDRSS experiment has shown that it is technically feasible with space VLBI to obtain fringes from radio sources on baselines exceeding the earth's diameter. However the restricted field of view and orbit of the TDRSS satellite made it impossible to produce images of radio sources. As the production of radio images is the prime goal of the QUASAT mission, extensive simulations on the imaging capability of QUASAT have been undertaken to compare the imaging potental of the two orbits under study. With all VLBI imaging there is a trade-off between resolution and image fidelity. The final compromise depends on the goals to be achieved and our simulations have shown that the higher apogee orbit provides a better compromise than the lower apogee one. The desirable higher resolution obtainable with the higher apogee orbit is not accompanied by a significant image

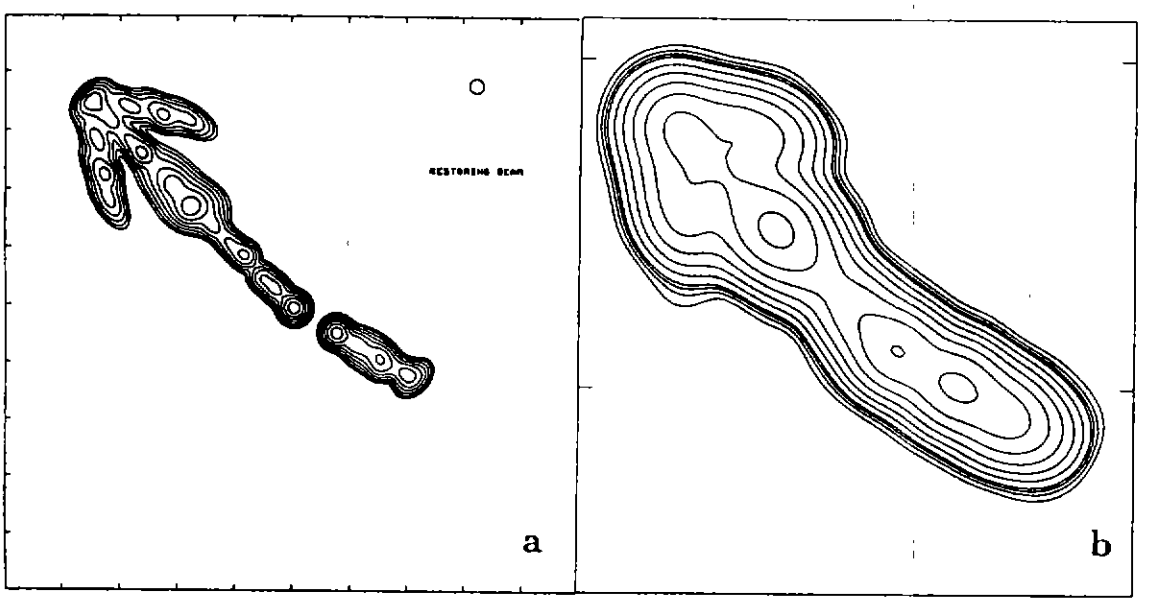

Figure 5.2: Source model and simulated Earth only image
The SOURCE1 model is seen to left (1.94 Jy at 22 GHz). To the right the image obtained with a 48^h observation at 22 GHz using a ground array of 17 telescopes. Source at $\Delta R.A. = 18h, \delta = 45°$.

degradation compared with the lower apogee orbit. The disadvantage of the higher apogee orbit is a slower rate of precession of RA of the ascending node compared to the lower apogee orbit. However, within the predicted mission lifetime good *uv* coverage will obtained for sources in all parts of the sky.

Image fidelity is a complex function of *uv*-coverage, source complexity and the errors present in the visibility data. *uv*-coverage is a strong function of the orientation of the source relative to the QUASAT orbital plane, the orbital parameters, number and distribution of the radio telescopes in the ground array, and the number of telemetry stations used to receive scientific data from QUASAT. Figure 4.6 illustrates how source orientation affects *uv*-coverage. The large holes in the *uv*-plane at certain values of R.A. cannot be reduced by using a larger number of telescopes in the ground array but are an inevitable consequence of selecting orbits in which the apogee heights exceed the diameter of the earth. The existence of the *uv*-holes means that we do not sample all the Fourier components which make up the structure of the source. This puts the onus on the deconvolution algorithms to interpolate into the *uv*-holes; the quality of this interpolation has been studied during the phase A. The size of such holes can be reduced by observing the source at a different value of of the RA of the ascending node and this will be possible in practice due to the precession of the ascending node.

To demonstrate the success of the deconvolution algorithms and to illustrate the increased resolution obtainable in the two orbits compared with that obtainable with ground arrays alone, we simulated a 48 hr observation of a ficticious source, SOURCE1, with a 17 telescope ground array operating on its own and then with QUASAT in the higher and lower apogee orbits. The model, SOURCE1, is shown in Figure 5.2a and the resulting images are shown in Figures 5.2b and

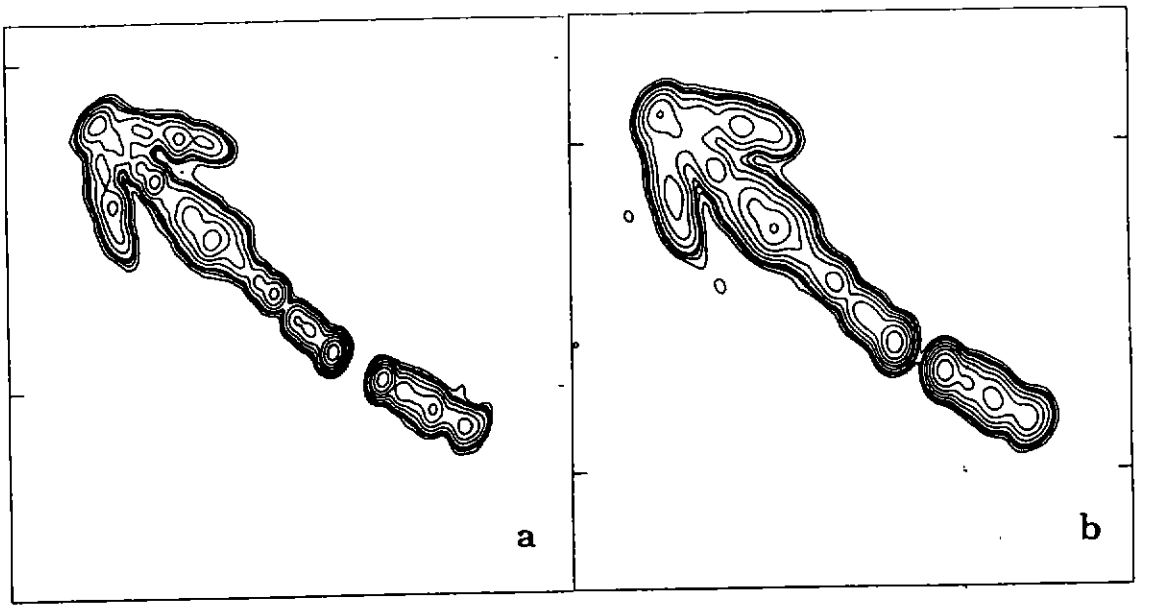

Figure 5.3: Simulated QUASAT observations for high and low apogee orbits
The images show two SOURCE1 images obtained with simulated 48^h observations at 22 GHz. 17 telescope ground array and source at $\Delta R.A. = 18h, \delta = 45°$. On the left hand side the image when QUASAT is in the higher apogee orbit, on the right hand QUASAT was assumed to be in the lower apogee orbit.

5.3 respectively. For this simulation SOURCE1 was assumed to lie at a declination of 45 degrees with a 18 hour difference in R.A. between the source position and the ascending node of the orbits. The QUASAT images reveal features that cannot be seen from VLBI observations at the same frequency on the ground alone. As also can be seen, there is no substantial difference in image quality between the two orbits, but the image from the higher apogee orbit has increased angular resolution.

Our simulations have also examined whether the size of the uv-holes provides an unacceptable limitation on the image quality that can be obtained when using QUASAT in the face of realistic data errors. In order to simulate interferometric data realistically, for any given pair of telescopes i and j, we relate the true visibility data, V_{ij}^T to the simulated 'observed' visibility data, V_{ij}^O, as follows:

$$V_{ij}^O(t) = g_i(t)g_j^*(t)V_{ij}^T(u,v) + \epsilon_{ij}(t) \tag{5.1}$$

where g_i and g_j are the antenna-based complex gains of the telescopes i and j respectively. For these simulations we assume that there are 360° phase errors, that is at each integration the phase of the complex gain for any telescope is a random number between 0° and 360°. This random phase simulates the situation of real VLBI data where typically absolute phase information is lost. Thermal noise, ϵ_{ij}, which is an easily calculated function of antenna size, aperture efficiency, system temperature, observing bandwidth and integration period, is also added to the simulated data. Furthermore amplitude errors that simulate calibration , atmospheric attenuation as well as

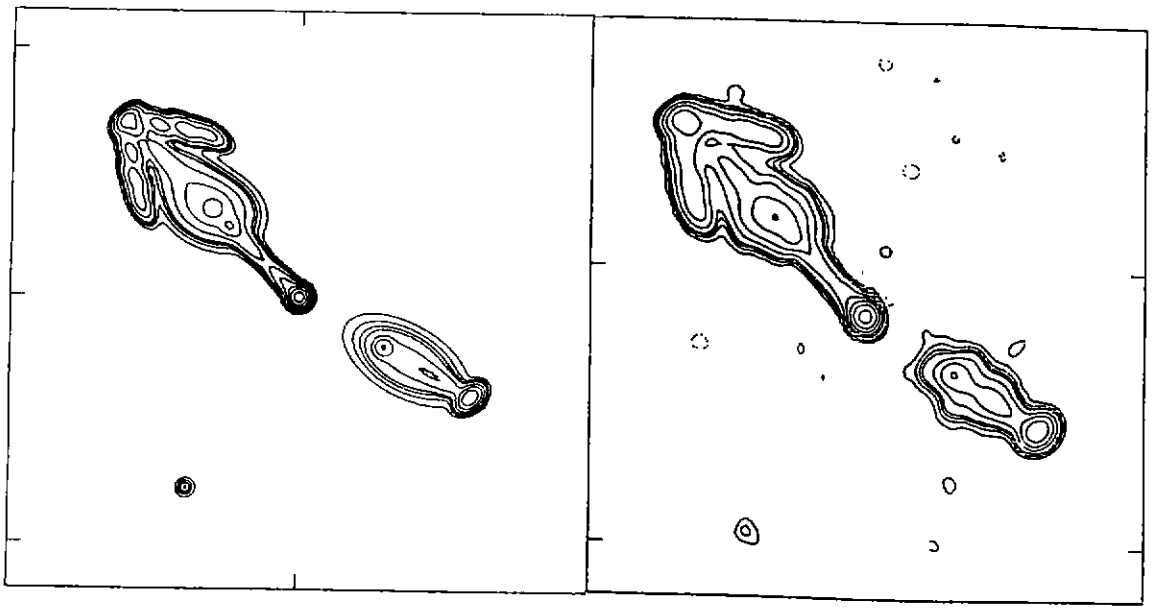

Figure 5.4: The model SOURCE2 and a detailed simulation
The SOURCE2 model (1.64 Jy at 22 GHz) is shown to the left. On the right hand side is a SOURCE2 image, obtained from visibility data that contains amplitude and phase errors as well as thermal noise. 48^h observation at 22 GHz with QUASAT in the higher apogee orbit, 13 telescope ground array and source at $\Delta R.A. = 18h, \delta = 40°$.

antenna pointing errors can also be added to the simulated data.

If we simply Fourier invert a set of visibility data with large phase errors we obtain an image with radio emission scattered at random over the image. In order to proceed we need to use some starting model for $V^T_{ij}(u,v)$, so that we can self-calibrate the observed visibilities. The usual starting model is simply a point source, which can have the undesirable tendency to 'spuriously symmetrise' the image, unless care is taken in manipulating the data. This problem is most severe for sparse arrays with an 'outrigger' telescope and was first recognised by Linfield (1986,*Ap.J.*,**92**,213) in a space VLBI context. We should expect from first principles that establishing source symmetry near a compact nucleus will be more difficult with the large orbits we are proposing to use compared with the smaller orbit proposed in the QUASAT Assessment Study (SCI(85) 5). The advantage of the new orbit is its increased resolution but the disadvantage is the larger uv-holes.

In order to be confident that the uv-holes do not prevent useful imaging of extended structures, a series of "blind" tests at 22 GHz has been carried out. In these tests a set of visibility data, with realistic errors, is presented to the image analyst, who is unaware of the true structure of the source. He then has to produce an image of the source, which can then be compared with the true source structure. In Figure 5.4 we show the model of the source SOURCE2, which is similar to but different from SOURCE1. The "blind" reconstruction of this source, when QUASAT is in the higher apogee orbit, is shown in Figure 5.4. This image was produced with a uv-coverage that had

the largest uv-holes for the source's declination (δ=40°) — it is a worst case example. In order to produce this image a new technique had to be developed to overcome the 'spurious symmetrisation' problem and involved systematic application of uv constraints in the self-calibration stages of the imaging process. This method has proven to be highly successful in combating the self-calibration problems presented by the new orbits. This simulated data as well as having phase errors also include amplitude errors which we know will be present in observations at 22 GHz but which will not be a problem at 1.6 GHz or 5 GHz. 10% amplitude errors are present in the data set used in the data set to create the image shown in Figure 5.4. The excellent reconstruction has shown that amplitude errors have not seriously limited our ability to image extended structure.

To summarize: the results of the study into the imaging potential of QUASAT have shown that a comparison of the imaging potential of the two orbits under study leads us to prefer the higher apogee orbit with its increased angular resolution compared to the lower apogee orbit. The images will be at least as good as the best current VLBI images but with much better resolution. Note also that the figures for the sensitivity and angular resolution quoted throughout the report were obtained from the results of these computer simulations.

5.4 Phase Transfer

Radio astronomers have examined satellite systems for two VLBI applications other than extending the baseline length. One application is to use a communications satellite to relay astronomical data from observatories to the correlator facility and thus allow correlation to be performed in real time. The savings in time and in data recording costs are, however, inadequate compensation for the extra costs of such a system. The other application is to transfer phase from a single, hydrogen maser frequency standard to each observatory and thus achieve array coherence without the need for a multiplicity of frequency standards. This application is economically attractive.

Tests of phase transfer between ground stations via satellites have been performed by many investigators. For example, van Ardenne et al (IEEE Trans. IM-32, pp370-376, 1983) used OTS-2 and Knowles et al (Radio Science 17, pp1661-1670, 1982) used ANIK-B for this purpose. In both cases existing frequency-translating transponders were used, necessitating the use of a carrier-difference method of phase transfer i.e. the difference in phase between two carriers is transferred. The separation in frequency between the carriers is limited by the bandwidth of the transponders so that differences of 20 MHz and 60 MHz respectively were used. Further tests of this technique are about to be performed by CSIRO using AUSSAT 3 with a view to transferring phase between the elements of the long-baseline array of the Australia Telescope.

Although these experiments have demonstrated the viability of the technique, they did not demonstrate phase transfer in the same way as planned for QUASAT primarily because the carrier-difference method places a very high premium on link signal-to-noise ratio, amplitude-to-phase conversion and overall stability. However they do provide a clear indication that a purpose-built coherent transponder can meet the phase-transfer requirements of QUASAT.

Chapter 6

Science Payload

6.1 Introduction

The Science Instrument (SI) of QUASAT consists essentially of a large reflecting antenna, a multi-frequency feed for the antenna, and a set of sensitive radio receivers which operate in wavebands K, C, L and P. The receivers are super-heterodynes which select, translate in frequency, digitise, format and relay the astronomical signals to the ground where they are recorded on magnetic tape. The tapes are shipped to a data-processing centre for correlation with similar tapes recorded at the ground-based telescopes of the array.

The SI is functionally identical to the radio equipment located at a ground VLBI telescope. Since the functions are broadly similar to those performed on almost all spacecraft, there can be no doubt as to the feasibility of the SI. Indeed, the experiments by Levy et al., see section 5.2, using the TDRSS satellite have already demonstrated space VLBI using equipment designed for other purposes. The SI study needs therefore to show that the superior requirements of QUASAT in terms of sensitivity and performance can be met in the space environment.

The major requirements on the SI are that QUASAT data are compatible with, and phase coherent with respect to, data from the ground network, and that the sensitivity targets are attained. The SI allows the same selection of waveband, polarisation mode, bandwidth, band centre frequency, and of precision of digitisation as at a ground VLBI facility and the format on tape is the same.

The coherence of the signals from the ground telescopes is partly assured by using receiving systems running from extremely-stable frequency standards. Such a frequency standard needs to be located at each telescope. QUASAT differs from a typical ground telescope in that the frequency standards are located at tracking stations and the reference frequency is transmitted to the spacecraft over phase-stable and phase-compensated radio links. All the local oscillators for the SI are generated coherently from the phase-transfer link. The phase-transfer link has been the subject of part of the QUASAT Phase A study. It is necessary to ensure that the SI matches or betters the phase stability of the transfer link. The other critical area is the electromagnetic compatibility of the SI with the rest of the spacecraft.

6.2 The Science Instrument

The specification of the SI is given in the Science Requirements (section 3.1). Figures 6.1 and 6.2 are schematic diagrams of the electronic portions of the SI that perform the processing operations, and Figure 6.4 shows the local oscillators required for the receivers. The sections that follow discuss

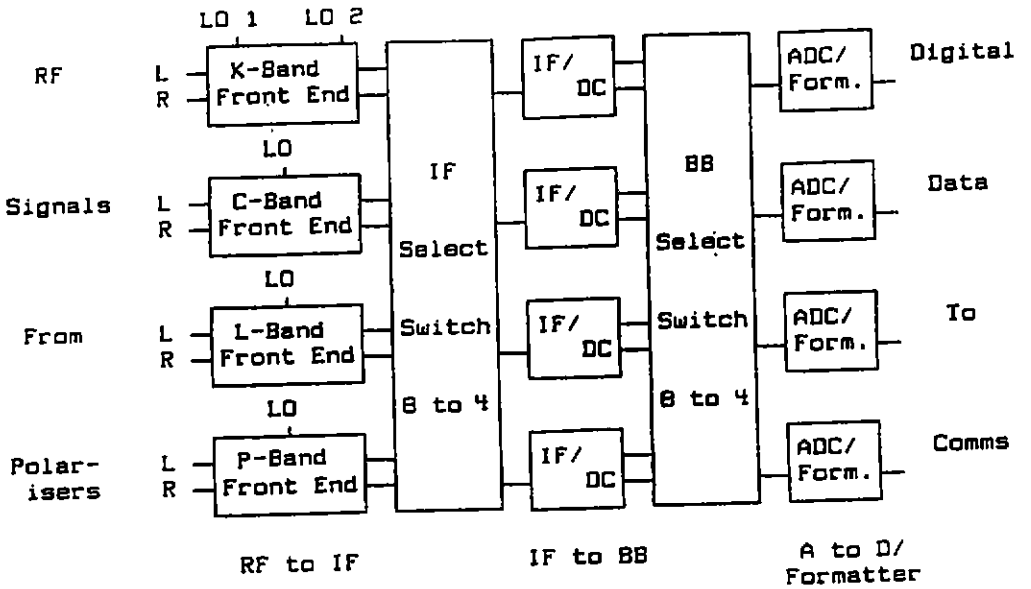

Figure 6.1: The Quasat astronomical receiver system

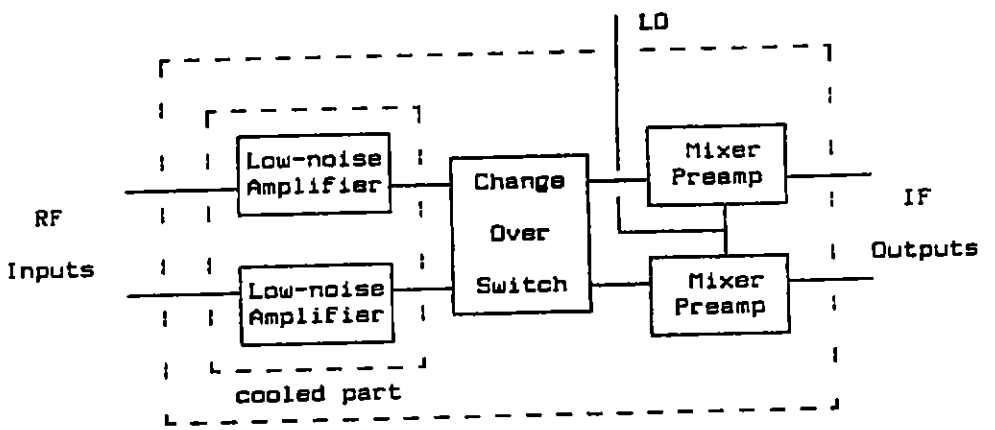

Figure 6.2: A schematic diagram of a front end

in more detail the functions performed by the circuit blocks in these figures and also the preferred methods of implementing them. Fuller accounts can be found in the QUASAT Science Package Report.

6.2.1 The Antenna Feed

The function of the antenna feed is to collect as efficiently as possible the radiation from the antenna in the four wavebands of interest whilst minimising the pickup of extraneous radiation. The polarisers separate the left and right-hand circularly-polarised signals. The feeds can only be assessed as integral parts of the complete antenna system for which many different configurations exist. The optimisation of the antenna system has been considered as part of the industrial Phase A Study. It is concluded that the best performance overall is offered by a centre-fed antenna operated at prime focus with an F/D ratio of 0.39.

A coaxial feed for the three shortest wavebands has been the subject of an ESA development

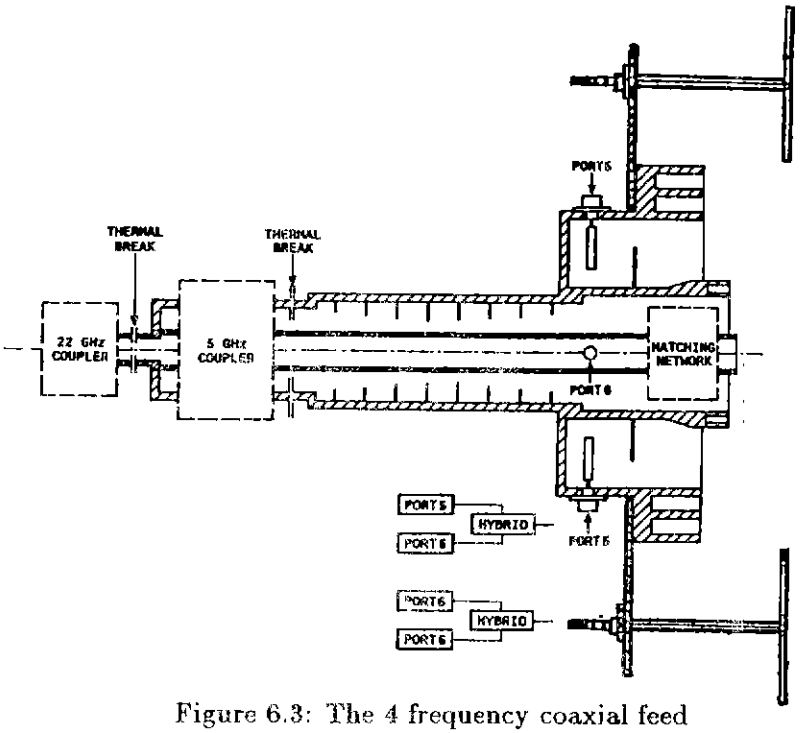

Figure 6.3: The 4 frequency coaxial feed

contract with CSELT. Figure 6.3 is a cross-sectional diagram of the feed that has been developed, with four dipoles spaced around it to support the fourth waveband. Measurements on this feed show that it combines good radiation characteristics with good matches to free space over large bandwidths. Table 6.1 shows the expected antenna performance in the four wavebands.

The polarisers for the two shortest wavebands are integrated into the feeds whereas the longest wavebands use external components. The estimated losses in these polarisers are included in Table 6.1, and the effects on noise performance are shown in Table 6.2.

6.2.2 The Low-Noise Front Ends

The purpose of the RF amplifiers is to amplify the very weak signals coming from the astronomy antenna whilst adding the minimum amount of noise. Four front ends are employed to receive the four wavebands and each front end handles both hands of polarisation. The front ends also translate the frequencies of the signals to intermediate frequencies in the range 540 to 780 MHz. There are great similarities between the implementations in the four wavebands so what follows may be taken to apply to all wavebands unless a specific exception is made. For example, the K-band front end uses an extra step of frequency translation to simply the filtering requirements.

The only practical low-noise amplifiers in microwave applications where high reliability is essential are based on GaAs FETs (GASFETs) or high-electron-mobility GaAs transistors (HEMTs). The HEMTs are particularly advantageous in applications in the two shortest wavebands of interest to QUASAT where their lower noise and higher gains are important. These advantages are marginal in the two longest wavebands

The noise added to a signal comes from processes inside devices such as transistors or as a consequence of resistive (absorptive) loss in transmission media or in circuit components. Since both sources of noise depend upon the physical temperature of the device/medium, they can be reduced by cooling. For best sensitivity, all lossy components prior to significant amplification should be cooled.

Table 6.1: Antenna efficiencies and polariser losses

Waveband	Antenna Efficiencies %	Polariser Loss dB
K-band	31	< 0.2
C-band	62	< 0.2
L-band	66	< 0.2
P-band	59	< 0.5

Table 6.2: The effective noise and physical temperatures of the receivers.

	Effective noise/ Physical temperatures [K]				
	Cooler sets operating				
	A	B	C	D	E
K-band	95/75	110/95	130/140	140/150	220/300
C-band	45/110	50/150	70/300	50/150	70/700
L-band	–	–	–	–	60/300
P-band	–	–	–	–	135/300

A corresponds to both sets of coolers operating

B corresponds to 1 set operating

C corresponds to a K band cooler operating with no shroud cooling

D corresponds to only a shroud cooler operating

E corresponds to no coolers operating

The noise-performance goals for QUASAT in the two longer wavebands can be met without resorting to active cooling. The performance target at K-band can only be met by using active cooling of the Low Noise Amplifiers (LNA) and as much as possible of the transmission lines and the polariser . The C-band system also needs some cooling assistance to meet the performance goals. Active cooling of the K and C-band receivers has been examined as part of the industrial Phase A Study. The conclusion of the study is that, even with the limited heat-pumping capability of available space-qualified coolers, it is possible to achieve acceptable noise targets. Increased pumping capability would further improve the sensitivity.

The LNAs can operate over a very wide range of physical temperature. Failure of the active cooling system, partial or complete, does not cause a failure of the astronomical systems but only reduces the sensitivity. Table 6.2 summarises the expected noise temperatures of the receivers for various assumptions about the status of the cooling system.

6.2.3 The Cooling System

The function of the cooling system is to lower the temperatures of the critical components in the early stages of the K and C-band receivers.

It is not possible to achieve the temperature targets by passive means but a viable system can be made using mechanical coolers of the type developed for the ISAM Spacecraft. The heat-

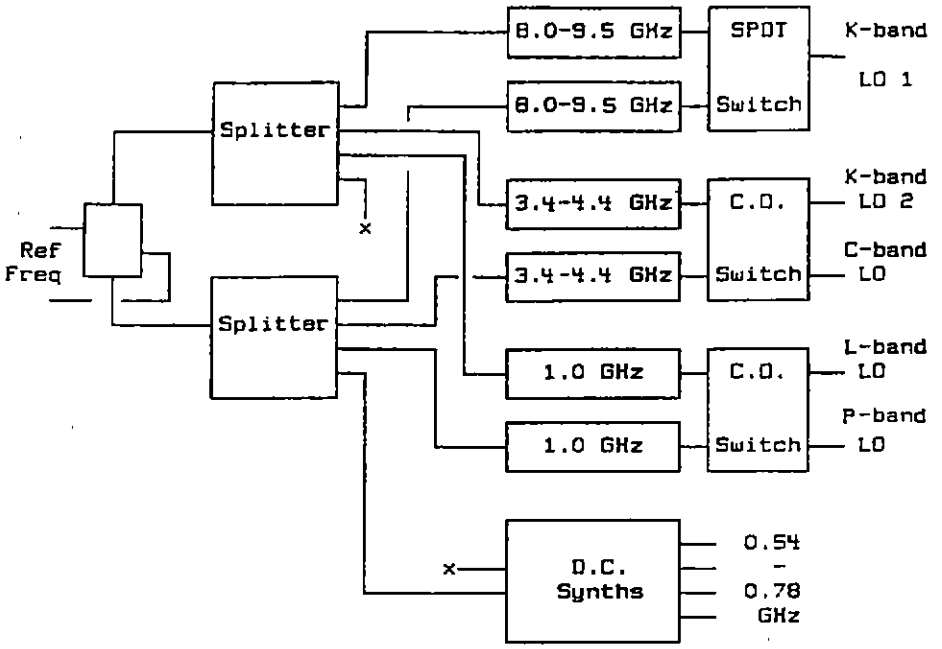

Figure 6.4: The frequency synthesis system

lift capacity of these small coolers is not sufficient to permit both K and C-band LNAs to be cooled to less than 100K. A cooler is used to cool a shroud to 150K, and a second cooler lowers the temperature of the K-band LNAs to 95K. The C-band LNAs and the K-band polariser are thermally in contact with the shroud. Thermal breaks are used extensively in transmission lines, the feeds and the polarisers to minimise the heat flows, and thermal switches are used to isolate a redundant set of coolers.

The SI is mounted centrally in the spacecraft with heat pipes to carry heat to an external radiator. The physical temperatures of the LNA's are shown in Table 6.2, along with the expected receiver noise temperatures.

6.2.4 The Local Oscillator System

The function of the LO system is to generate coherent LOs for the receivers, each locked to the reference frequency from the phase-transfer link. The net LOs need to be settable to a fraction of the narrowest bandwidth of the astronomical receivers i.e. to 100KHz in the QUASAT implementation. This allows spectral-line features to be positioned within the receiver bands and allows some of the high Doppler shifts to be compensated on board.

The first LOs are implemented using voltage-controlled oscillators which are phase locked using harmonic mixers to lower reference frequencies. The final downconversion LOs use digital dividers and VCOs to allow the fine steps in frequency to be obtained. Second-order phase-locked loops are used with the bandwidths chosen to achieve the phase-noise specifications and good phase stability. Where necessary, pretuning of the VCOs is employed to ensure that the correct lock is achieved.

6.2.5 The IF Select Switch

The IF Select Switch is an 8-input, 4-output device which allows any of the IF signals in the band 540 to 780 MHz from the front ends to be routed to any of the outputs. In the normal mode of operation, two of the IF signals are selected so the other channels are spare. Cross-talk between channels in the switch needs to be less than -40dB but the insertion loss is not critical.

The preferred solution uses dual-gate FETs as the switching elements in a cross-point arrangement. The high input and output impedances of the FETs provide low disturbance taps and good isolation between channels.

6.2.6 The IF/Downconverters

An IF/Downconverter (IF/DC) unit takes an IF input signal and a local oscillator signal (variable in 100 KHz steps), both in the range 540-780 MHz, and produces 2 baseband signals in the range 1 KHz to 16 MHz. The 2 baseband signals are independent of one another having been generated in image-reject mixers: one of the basebands comes from IF frequencies higher than the LO, the other from IF frequencies lower than the LO. The overall gain of an IF/DC, IF to baseband, is switchable to allow for changes in signal strength and for gain changes in the electronics. There are no exceptional requirements on this unit.

6.2.7 The Baseband Switch

The BB Select Switch is a 8-input, 4-output device which allows any of the BB signals in the band 1 KHz to 16 MHz from the IF/DC units to be routed to any of the outputs. In the normal mode of operation, two of the BB inputs are selected so the third and fourth channels are spares. The requirements on the baseband select switch are almost identical to those on the IF Select Switch and it is proposed to implement them in the same way, but with suitable changes in component values.

6.2.8 The Analogue-to-Digital Converter/Formatters

An analogue-to-digital converter/formatter unit (ADC/F) takes an input signal of bandwidth 16 MHz, amplifies it, filters it if necessary, samples and digitises it and then converts it to a standard format for the data downlink to transmit to the ground. The power level of the signal into the sampler/digitiser is monitored and controlled automatically.

The major requirement on the ADC/F unit is to process the signals in a way that is compatible with the VLBA standard. The implementation on the spacecraft is partial — only the 4 wider signal bandwidths are selectable. The 5 narrower bands are left to be implemented in digital filter units at the telemetry stations. This relaxes the specification for settability of the on-board LO from 10KHz to 100KHz and reduces the number of filters that need to be implemented in the SI.

The penalty for this simplification is that the data need to be digitised to greater precision than otherwise in order to avoid a signal-to-noise penalty from the digital filtering operation. The narrowest physical bandwidths on QUASAT are digitised to 5 or 6-bits rather than the 1 or 2-bits finally required. The data rate is still within the link capacity because the sampling rate is reduced to 4 Msamples/sec.

It is preferable to employ a single, multibit ADC for all modes of operation but there do not appear to be any high-speed ADCs that have space qualification. The ADC/F units have been sized to allow parallel 2-bit, high-speed, and 6-bit, low-speed ADCs to be implemented from existing space-qualified devices.

6.2.9 The Power Control Unit

The Power Control Unit (PCU) controls the provision of power to the various front-ends, coolers, synthesisers, and IF/BB processing units in the SI so that the SI can be configured to the desired mode. Switching of the raw 42.5 volt spacecraft-bus supply is employed for the RF, LO and cooler units, and via low-voltage regulators for the IF/BB units. All functions are controlled by latching on/off or change-over relays. There are no difficulties in building such a unit.

6.2.10 Performance Verification

The noise performances of the receivers of the SI, and the pointing of the astronomy antenna are verified by a noise-adding radiometer system. A switching noise source injects noise into the receiver front ends. The receiver outputs are detected and the mean and switching levels are averaged for 1 second, digitised and relayed to the ground. These data enable the system noise temperatures to be determined relative to the noises added from the noise sources. Since the system noises depend on what the astronomy antenna is pointing at, raster scans of strong radio sources by the antenna allow pointing to be calibrated.

The internal coherence of the SI, the relative phases of the receivers for the two hands of polarisation and the setting of the LOs are determined, when required, by injecting a 1MHz comb of frequencies into the front ends at levels -20dB with respect to to the noise power in a bandwidth of 2MHz. The comb products in the data can be measured at the tracking stations or at the correlator.

6.2.11 Control and Monitoring

The control requirements of the SI are related to setting up the configurstion and to monitoring the status and performance of the system. The configuration of the SI requires about 172 control bits that are relatively static: typically, configuration changes are not expected more frequently than about once per orbit. The control of the monitoring system is much more dynamic with some calibration parameters required every second and other parameters required less frequently on a regular cycle.

The monitoring requirements of the SI can be divided into two categories: one category is concerned with the high-priority information that is required by the investigator for calibration or verification of system health, and the other category is concerned with low-priority, diagnostic monitoring of parameters within, and the status of, the SI. About 128 analogue signals from 8 sub-assemblies need to be digitised to 12-bit precision at a rate of one per second and a cycle time of 128 seconds. It is proposed that each sub-assembly is equipped with a 16-to-1 multiplexer, 12-bit ADC and a serial interface unit to the SI controller in order to digitise and communicate these parameters.

There are about 14 parameters to be monitored every second: up to 16 lock-status bits from the LO synthesisers, noise-on/noise-off signal levels and Automatic Voltage Control (AVC) levels from up to four operating ADCFs, and the selected low-priority parameter. The total monitoring requirement is thus about 42 bytes per second if each parameter is padded out to 3 bytes with identifying bits.

6.3 Critical Areas

Since VLBI using an orbiting telescope has already been successfully demonstrated by the TDRSS experiments of Levy et al., QUASAT is technically viable. However, there are a few areas where

the performance of the SI and other spacecraft sub-systems are critical to the mission. These areas are examined in this section.

6.3.1 Coherence

The SI needs to achieve a phase performance commensurate with that of the phase-transfer system, see subsection 3.3.1.

The design of the SI follows the practices established for ground-based VLBI to ensure good phase stability. The factor most likely to influence the phase stability on the time scales of interest is the effect of temperature fluctuations during and shortly after eclipse acting on the most sensitive parts of the SI, the first LO synthesizers.

It is desirable that the phase stability of an LO synthesizer system as a function of temperature is measured so that the magnitude of any thermal effects can be assessed. If necessary, it is possible to employ temperature compensation and/or stabilisation of the most critical components.

6.3.2 Sensitivity

The factors that most affect the noise performances of the receivers are discussed in subsection 6.2.2. The performances of the L and P band systems are good enough. The performances in the other two bands could be improved by reducing the ohmic losses and by lowering the physical temperatures of the lossy parts. Any advance in the heat-lift capacity of the coolers would improve receiver performance.

It is also possible to improve system performance by switching on the redundant set of coolers (See Table 6.2). This can be done for limited periods without prejudice to life expectancy, but only when the power sub-system can cope with the extra load. For instance, early in the mission before the solar arrays are degraded by radiation, and for orbits without eclipses.

6.3.3 Electromagnetic Compatibility

EM interference can be conducted and radiated from other parts of the spacecraft to the SI. Since any pickup is very unlikely to be coherent with any signals received by a ground-based telescope, the end effect is that the astronomical data become uncalibrated in amplitude and may be unusable. The limits on in-band pickup are very severe and can only be guaranteed by proper design and construction practices for the spacecraft sub-systems. Out-of-band interference can cross-modulate into band or can simply affect the system gain to the desired signals.

EMC has been studied in the industrial Phase A study. The astronomical requirements can almost all be met using standard practices but with the addition of extra filtering in transmitter outputs to reduce spurious emissions. A possible exception is radiation from the solar-array power control system interfering with the astronomy P-band. This area needs further study.

6.4 Reliability

The SI is largely composed of standard electronic devices operating at relatively low power levels. The functions of most of the electronics are identical to the functions performed on almost all spacecraft. It is possible therefore to use well-proven, space-qualified devices to ensure high reliability. This is not possible for the GaAs transistors in the low-noise amplifiers, and the closed-cycle coolers which have not yet established a proven high-reliability record, although there are reasons to believe that they will.

There are no wear-out mechanisms likely to affect the performance of the SI. The radiation environment in space will not be a threat to system coherence, short of component failure. The major effect of radiation on the systems will be cumulative, with slow, small increases in noise temperature and decreases in gain. These changes will be acceptable.

The requirements on the SI of the capability for simultaneous observations in more than one RF band or with more than one hand of polarisation is used to allow the inbuilt redundancy to compensate for unit failure, albeit then with some loss of functionality. Change-over switches and redundant units are used throughout the SI to provide high reliability. The only area of the SI where this is not possible is in the LNAs. Additional switches here cause appreciable performance penalties. Table 6.3 summarises the SI capabilities for various single failures.

Table 6.3: The consequences of single failures in the SI

Failure of:	Consequence:
A cooler	loss of spare
LNA	loss of polarisation in band
RF/IF unit	polarisation by multiplexing
K-band LO	loss of spare
C-band LO	K and C-bands not possible simultaneously
L-band LO	P- and L-band not possible simultaneously
IFSW output or IF/DC	loss of spare
BBSW output or	
ADC/F or D.C. LO	loss of certain modes
PCU	loss of 1 of the units above

6.5 Science Instrument Parameters

The major parameters of the SI are summarised in Table 6.4.

Total power consumption ranges from about 30 Watts (1 long waveband, no polarisation, no coolers) to 140 Watts (2 short wavebands, with polarisation and with coolers operating).

Table 6.4: The physical parameters of the SI

	Number of Units	Each Unit			Control Bits	Monitor	
		Size (mm)	Weight (kg)	Power (W)		Bits	Voltages
Feed	1	600 × 600 × 600	5.0				
Front Ends							
K-band	1	250 × 150 × 50	3.0	2.8	3	3	16
C-band	1	250 × 150 × 100	3.0	2.8	3	3	16
L-band	1	250 × 150 × 100	2.0	2.0	3	3	16
P-band	1	250 × 150 × 100	2.0	2.0	3	3	16
Coolers							
Compressor	4	120 ⌀ ×200	3.0				
Displacer	4	75 ⌀ ×190	0.9				
Power Unit	4	225 × 230 × 150	4.5	40.0	4	4	16
Synthesisers							
K-band	2	60 × 60 × 15	0.2	3.0	5	8	8
C-band	2	60 × 60 × 15	0.2	3.0	9	12	8
L-band	2	60 × 60 × 15	0.2	3.0	1	1	8
D.C. LO	4	tbd	tbd	tbd	64	64	8
IFSW	1	165 × 76 × 25	0.4	0.2	9	9	
IF/DC	3	165 × 101 × 30	0.7	1.2	9	9	
BBSW	1	165 × 76 × 25	0.4	0.2	12	12	
ADC/F	4	165 × 110 × 30	0.8	3.2	16	16	16
PCU	1	165 × 165 × 50	1.4	5.2	32	32	6
Monitoring	1	150 × 150 × 35	2.0	2.5	tbd	tbd	

Notes: The control bits change only a few times a day. Monitoring of any function is never more frequent than once per second.

Chapter 7

Spacecraft System Description

7.1 System Requirements

The major system requirements imposed by the mission concept have been listed in section 3.2.

7.2 System Trade-offs

The major driver governing the choice of the spacecraft overall design was the low cost approach, leading to the requirement of using existing (European) hardware and technologies as much as possible. In addition, spacecraft launch mass, and to a lesser extent launch configuration, influence the total project cost through the launch cost. Below a certain threshold (1140 kg for a standard Ariane 4 GTO) launch cost is not dependent on spacecraft mass. However, above this threshold the launch cost increases with the mass of the spacecraft.Although the launch cost is not directly influenced by the spacecraft configuration, a configuration such that the spacecraft fits within the lower launch compartment (Spelda) is advantagous. This leaves more space for a second passenger which then might be found more easily.

In order to select a system baseline in accordance with the aforementioned ground rules, a number of major design trade-offs were performed during the first phase of the study. These trade-offs covered the radio astronomy antenna, the on-board propulsion system, the RF links for the science data telemetry and the phase transfer and finally the overall spacecraft configuration.

7.2.1 Radio Astronomy Antenna

The two basic reflector options were either a centre-fed reflector or an offset reflector. The offset reflector was considered because advantage could be taken of existing offset reflector designs under development in Europe for telecommunication applications (Contraves LOAD 10, MBB UMA and Aerospatiale Truss) and thus could contribute a cost saving.

However, compared to a centre-fed reflector, an offset reflector showed several decisive disadvantages:

- Due to the asymmetrical configuration, solar pressure torques as well as gravity gradient torques are much larger, requiring an extra propellant mass of approximately 50 kg for reaction wheel off-loading.
- Deployment of the offset reflector results in a centre of mass shift which is about an order of magnitude larger than would be acceptable for the attitude and orbit control system.

- The AOCS requires a relatively large separation between the control frequency and the fundamental structural frequencies. This requirement leads to a large antenna boom mass.
- A new feed design would be necessary as an offset reflector requires a much larger f/D. This also implies that the reflector is more difficult to manufacture due to the larger curvature and greater asymmetry.
- Opposite beam squint for the two circular polarizations and a higher cross-polarization

Advantages of a configuration with an offset reflector are:

- Solar array and communication antennae can be body-mounted, thus avoiding structural and dynamical complications of long booms.
- The reflector is far from the feed and yields a less severe thermal input into it.
- Gain losses due to blocking are lower.

Despite these minor advantages, the disadvantages were considered so severe that the centre-fed option was selected.

The following European and US candidate reflector designs were considered for QUASAT:

- Contraves Inflatable Space Rigidized Reflector (ISRR)
- MBB Unfurlable Mesh Antenna (UMA)
- Aerospatiale Deployable Truss
- Lockheed Wrap Rib (WR)
- Harris Hoop Column (HC)
- Solid Panel Reflectors (Dornier Daisy and TRW Sunflower)

An evaluation of these designs, taking into account such factors as mass, stowed volume, complexity, surface accuracy, dynamic behavior, design maturity, overall performance of the science system and cost led to a final selection of a 15 m Contraves ISRR with its high surface accuracy, low cost and mass, easy stowage during launch, simple mechanical design and deployment concept. An additional advantage of this design is the possibility to implement a configuration without a forward module and its supporting structure (Section 7.2.4)

7.2.2 Propulsion System

The propulsion system of QUASAT has to perform the following functions:

- Transfer from GTO to the first operational orbit (821 m s^{-1})
- Transfer from first operational orbit to second operational orbit (354 m s^{-1})
- Attitude control during the 5-year lifetime of the mission.

Three different propulsion system concepts were envisaged and analysed:

- Monopropellant hydrazine system for all maneuvers
- Bipropellant system with one 400-N thrusters for orbit changes and 10-N thruster for attitude control.
- Monopropellant hydrazine system with an additional solid motor for the first injection maneuver.

The solid motor concept was abandoned on the following grounds:

- A spin rate of about 50 rpm would be required during solid motor firing, thus increasing complexity and cost of the AOCS.
- Accommodation problem of solid motor.

The remaining bipropellant/hydrazine concepts were traded-off against each other and cost did not prove to be a decisive discriminating factor. The higher launch cost with the hydrazine option (200 kg more propellant) is approximately compensated by the higher subsystem cost for the bipropellant design. Because of higher reliability and lower complexity the monopropellant hydrazine option was tentatively selected as the best propulsion system for QUASAT.

7.2.3 RF Links

The RF links between the spacecraft and the ground station(s) perform the following functions:

uplink	downlink
telecommand phase transfer	housekeeping telemetry science data telemetry phase transfer

The main topics which required a trade-off during the initial phase of the study were:

- choice of frequency band(s) for phase transfer and science data downlink.
- science data transmission technique: analogue or digital.

The frequency bands that have been considered for the two-way phase transfer link as well as for the science data downlink are X-band (up: 7.190 - 7.235 GHz; down: 8.450 - 8.500 GHz) and Ku-band (up: 13.25 - 14.00 GHz; down: 14.00 - 15.35 GHz).

The maximum availability of 50 MHz for the downlink in X-band and a likely practical allocation of 20 MHz or less, placed severe constraints on the science data bandwidth.

Both analogue and digital transmission schemes would be forced to employ polarization multiplex to achieve a minimum desired science bandwidth of 32 MHz. For digital data transmission, a bandwidth-conserving type of modulation such as 8-PSK would be needed.

Use of Ku-band with its enormous bandwidth resources (larger than 500 MHz) will permit radio source correlation over wider bandwidths without the use of polarization multiplexing and thus increase the scientific value of the mission.

For the phase transfer, a H-maser derived frequency has to be transferred from the ground station to the spacecraft. This is achieved by the use of phase-coherent up and down links. If the up and downlink frequencies are nearly equal, reciprocity of the links can be assumed and the phase shift on-board the spacecraft is half the phase shift measured on the ground. In X-band the

two frequencies are separated by at least 1.2 GHz and an additional (coherent) spacecraft-Earth link (in S-band) would be required for correction of the ionospheric error.

Also for this application the use of Ku-band offers a considerable advantage because up and downlink frequencies can be assigned at a sufficiently small distance either side of the 14 GHz boundary and there is no need for a second coherent downlink in a different frequency band.

Concerning the choice between a digital or an analogue science data downlink, it was found that in terms of on-board complexity, mass and power consumption both options are comparable. However, the analogue option has a number of disadvantages which could result in changes in coherence. These include: effects of transmitter intermodulation distortion, small changes in relative amplitude and phase across the transmitter band, probable small non-linearities in amplitude and difficulties in calibration. For this reason a digital downlink was selected with QPSK modulation. With an on-board sampling rate slightly higher than the Nyquist rate, and the requirement for synchronization and formatting a transmission bit rate of 144 Mbps is required to transmit the observation bandwidth of 64 MHz.

The following baseline was thus established:

Phase transfer uplink	13.9 GHz
Phase transfer downlink	14.1 GHz
Digital science data downlink	14.8 - 15.0 GHz

In order to avoid simultaneous S-band transmission during the operational phases, the phase transfer links will also support the satellite TT&C (telecommand and housekeeping telemetry) during these phases.

The use of S-band frequencies is only foreseen for the support of the satellite TT&C during LEOP and Transfer Orbit Phases and in contingency situations during the operational phases.

7.2.4 Configuration

The two major configuration options can be classified in terms of the relative location of the feed and spacecraft bus.

For the dual-module configuration, the feed , the radio astronomy receivers and the cooling equipment are housed in a forward module at the paraboloid prime focus, while the spacecraft bus is located beneath the apex of the reflector. This option requires a fixed or deployable forward module support tower with a height of 5 – 6 m.

As an alternative, both the spacecraft bus and the payload could be located in a single module at the paraboloid prime focus. This single-module configuration is only suited for the inflatable reflector since it is more or less self- supporting. To increase the structural stiffness of the inflatable reflector it was necessary to provide a central cylinder between the reflector and radome membranes made of the same material as the reflector and radome and rigidized during the reflector curing process.

The main advantages of the single module configuration are:

- lower antenna RF losses
- antenna diameter not limited by forward module support structure
- accommodation inside Spelda possible
- lower launch loads on payload
- lower cost

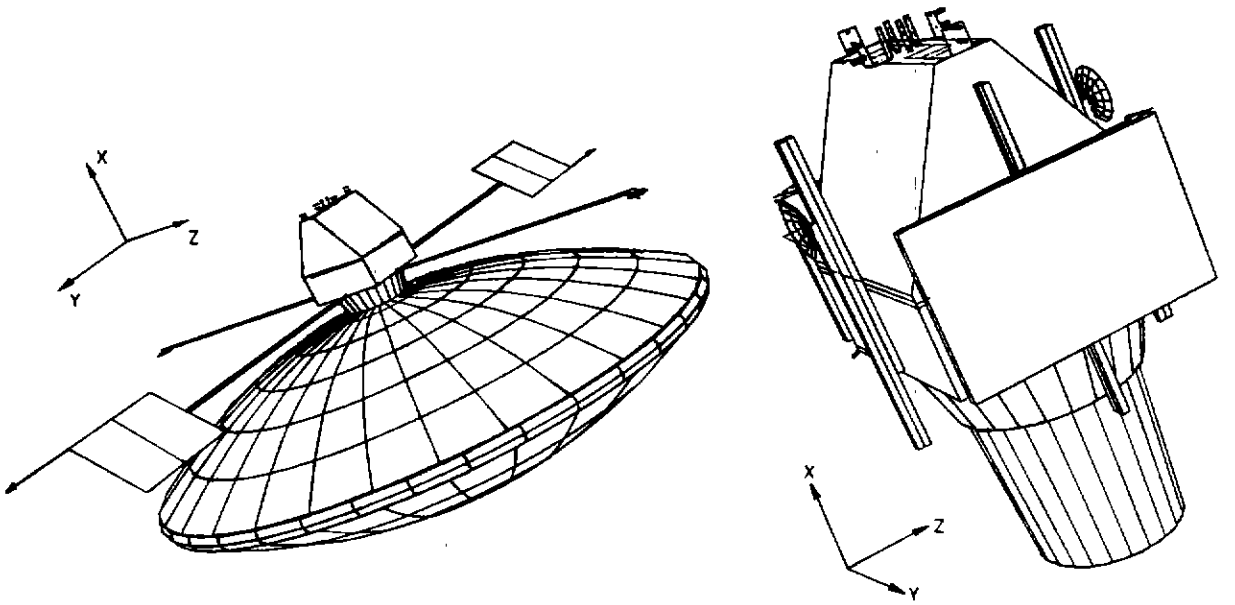

Figure 7.1: Spacecraft in operational and launch configuration

The main disadvantages found were related to the coupling (both thermal and RF) between payload and service equipment. The specification on preamplifier temperatures can not be met completely for the single module configuration and at 22 GHz an interferometer sensitivity loss of about 10 % results.

However, these temperatures are based on the present (prototype) Stirling coolers and improvement in their efficiency can be expected in the near future.

EM interference problems, although more severe than in the dual-module configuration were found solvable and the single module configuration was eventually preferred on grounds of antenna efficiency and cost.

7.3 System Design

7.3.1 Configuration description

The operational spacecraft configuration is shown in Figure 7.1a and Figure 7.1b shows the spacecraft in the launch configuration. The following main features can be distinguished:

- a 15 m aperture centre-fed radio astronomy antenna
- a spacecraft bus housing the payload package and subsystems
- 4 deployable booms, two of which carry the solar array wings while the others carry the Ku-band communication antennas.

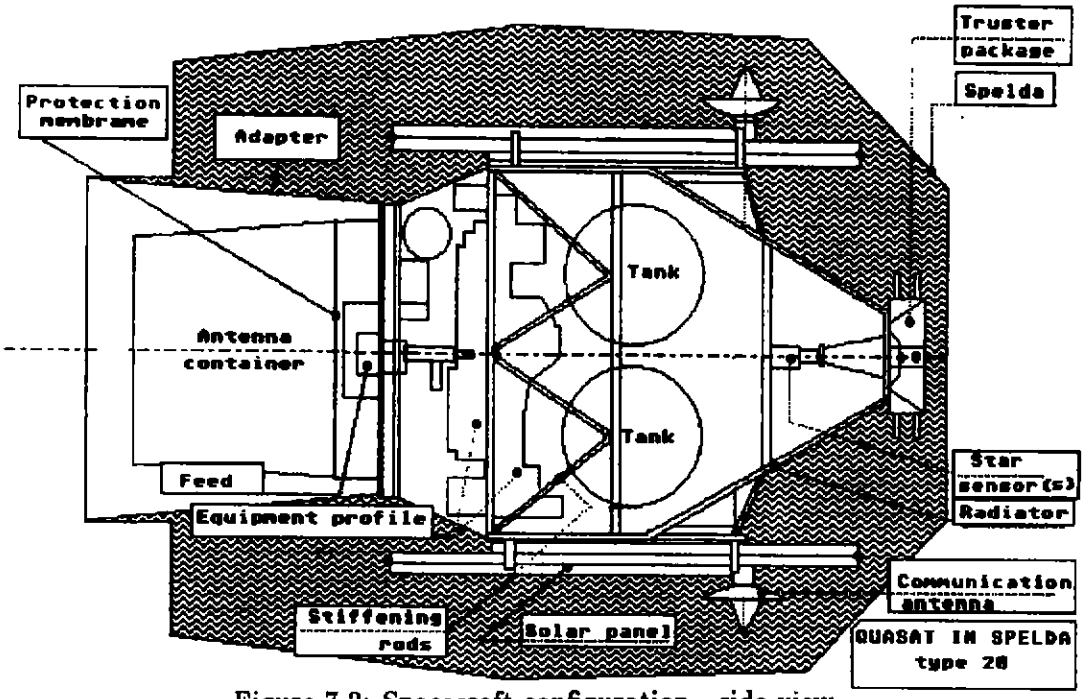

Figure 7.2: Spacecraft configuration - side view

The radio astronomy antenna is the Contraves inflatable space-rigidized antenna. It is a new development and will be described in subsection 7.4.1. The antenna is assembled and launched with the material in its flexible prepregged state to enable its folding for stowage in the container. After operational orbit insertion the antenna is deployed by inflation with nitrogen and then is cured by pointing the radome side of the antenna towards the Sun. After curing the nitrogen is evacuated.

The main features of the spacecraft bus are shown in Figure 7.2. The lower platform carries the feeds and the reflector presurization equipment. The reflector stowage container is mounted on the underside of this platform and protrudes within the special-purpose adaptor during launch.

The main equipment platform is located directly above the feed. A system of variable conductance heat pipes runs from this platform to the slanted radiator. All high dissipation equipment is mounted on the upper side of this platform for maximum heat exchange with the heat pipes. Low dissipation equipment is mounted on the underside. A vertical panel between the lower platform and the main equipment platform close to the feed supports the payload items which require active cooling and the Stirling coolers.

The upper platform carries four hydrazine tanks and orbit insertion and AOCS thrusters are mounted on the top platform. The -Z wall connecting the tank and thruster platforms is the spacecraft radiator which is tilted 30° for maximum thermal efficiency (see Figure 7.2)

An intermediate structure carries three offset star trackers, which together with a gyro package provide the attitude information during the operational phase. During initial acquisition and in emergencies sun acquisition sensors, mounted on the solar array are used.

The long (approx. 7 m) booms are required for the solar arrays and the Ku-band communication antennas in order to "view" past the radio astronomy antenna. These booms are folded in three segments to permit stowage.

The solar array wings, each consisting of two deployable panels are connected to the Y booms via BAPTA drive units.

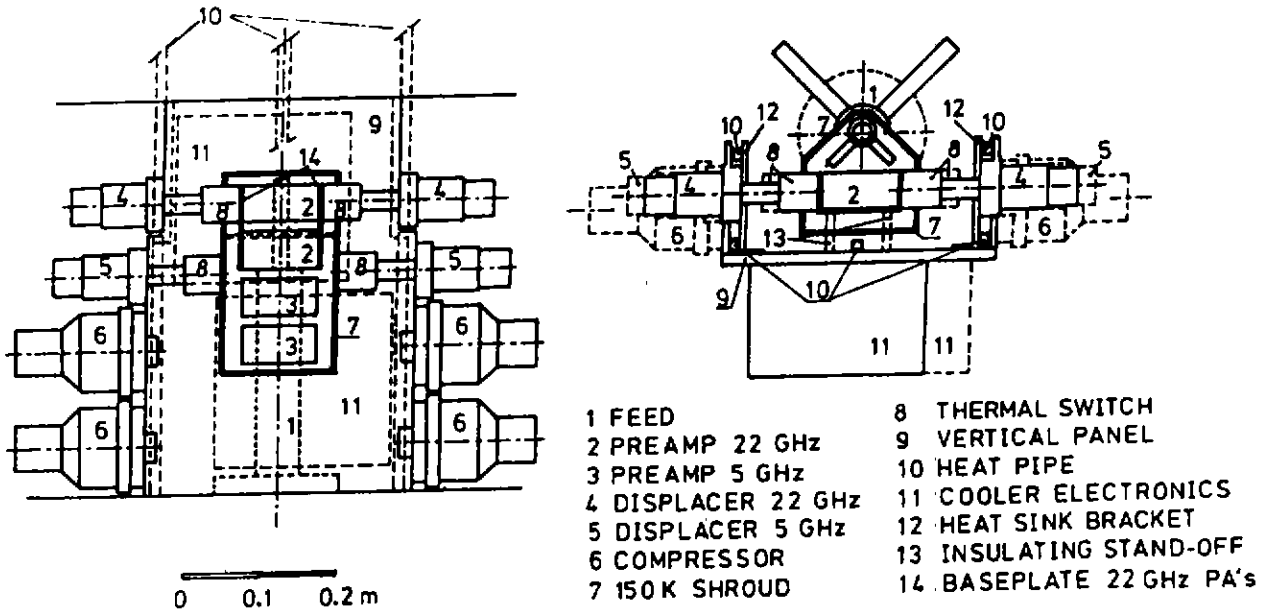

Figure 7.3: Assembly of coolers and preamplifiers, mounted near to the feed

The Z booms carry the Ku-band communication antennas with a two degree-of-freedom antenna-pointing mechanism. The RF links along the booms are obtained via silver-plated carbon fibre waveguides mounted inside the booms.

The S-band antennas are mounted on deployable booms connected to the outer rim of the solar array wings.

7.3.2 Payload Accommodation

A vertical panel alongside the feed is used for mounting the K-and C-band preamplifiers and the cryogenic cooling equipment (Fig. 7.3). One Stirling cooler is used to provide a cold shroud around the K-band preamplifiers. This shroud encloses the coaxial K-band feed output section as well. The C-band preamplifiers are mounted to this shroud so they run at shroud temperature. The K-band preamplifiers mounting plate is attached to the shroud by means of insulating stand-offs and is further cooled by another cooler.

For complete redundancy, each cooler is backed-up by a standby cooler. Passive thermal switches are inserted between each cooler and the object to be cooled to avoid excessive heat inputs from the non-operating coolers.

The remaining payload equipment and the cooler electronics are mounted on the underside of the main equipment platform.

The triple-frequency coaxial feed is mounted via a mechanism to the lower platform. This mechanism permits limited precise displacement of the feed for refocussing.

The feed, which consist of 4 dipoles, is mounted via stand-offs to a circular base plate, which in turn is mounted to the coaxial feed.

A truncated cone mounted on the underside of the lower platform supports a fixed membrane to avoid contact of the feeds with the stowed radio astronomy antenna during launch (see Figure 7.2). This cone also supports the reflector mounting flange and the ejectable reflector stowage container.

7.3.3 Functional Description

The system functional block diagram is shown in Figure 7.4. The key functions of the baseline system are provided by the following subsystems:

- *A standard S-band RF subsystem for TT&C during LEOP, TOP and emergencies, comprising:*

- two boom-mounted deployable hemispherical-coverage antennas.
- a radio frequency distribution unit (RFDU)
- two S-band transponders (1 in cold redundancy)

- *A Ku-band RF subsystem for science data transmission and phase transfer (phase transfer links also used for platform TT&C during operational phases). This subsystem consists of:*

- two boom-mounted 0.5 m Ku-band antennas
- antenna pointing mechanisms (APM) for hemispherical coverage
- a radio frequency distribution unit
- two science data transmitters (1 in cold redundancy)
- two Ku-band transponders (phase transfer)

- *The on-board data handling (OBDH) subsystem, including:*

- an internally redundant Central Data Management Unit (CDMU) for science data and telemetry formatting, command distribution, on-board time keeping and time distribution and OBDH bus control.
- two OBDH buses (one operating, one in cold redundancy)
- two Remote Terminal Units (RTU), one dedicated to the platform, the other to the payload, for command distribution and data acquisition.

- *The power subsystem which consists of:*

- two deployable boom-mounted solar array wings as the electrical power source in sunlight.
- two solar array drive mechanisms (BAPTA's) to keep the array sun-pointing.
- two 18 Ah NiCd batteries to supply power during eclipses.
- the array switching regulator (ASR), providing the regulated bus (42.5 V) and controlling the other regulating elements (BCIU and BDR)
- two Battery Control and Interface Units (BCIU) for battery management and pyro and heater control.
- five Battery Discharge Regulators (BDR) for main bus regulation during eclipses.

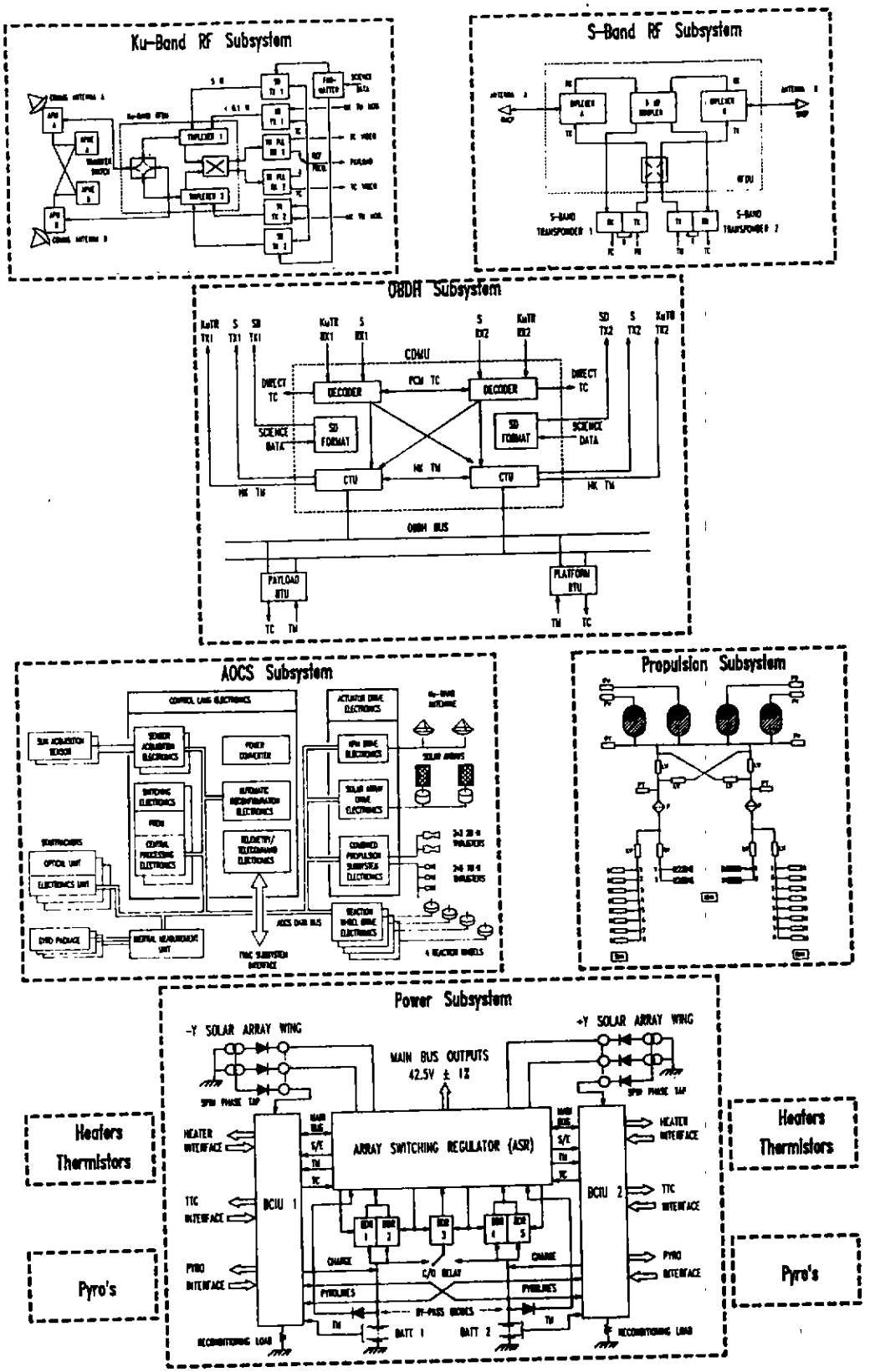

Figure 7.4: System functional block diagram

- *The Attitude and Orbit Control Subsystem (AOCS), including:*

- three offset star trackers (1 in cold redundancy) for attitude measurement during stabilized phases.
- three gyrometer units providing attitude information during slewing phases.
- two Sun acquisition sensors used during the first Sun acquisition phase and for back-up and safe modes.
- control law electronics for attitude determination from sensor data and generation of actuator commands.
- actuator drive electronics for solar array and communication antenna pointing and reaction wheel and propulsion system control.
- four skewed reaction wheels to execute the slew maneuvers and to compensate the disturbance torques during pointing.
- the AOCS data bus connecting all the equipment

- *The propulsion subsystem consisting of:*

- four 160 l hydrazine tanks for blow-down operation
- two thruster branches each containing two 20-N hydrazine thrusters for the orbit maneuvers and eight 10-N hydrazine thrusters for AOCS.

7.3.4 Phase Transfer

The radio source data are processed in non-real-time, and there are no frequency standard reference links between the various radio telescopes (including QUASAT) and the VLBI processing system. Thus, ultra-stable frequency standards are required at each telescope to reduce to acceptable levels signal crosscorrelation degradation due to drifts and noise on the frequency references.

Ground based VLBI stations use hydrogen maser frequency standards to obtain the requisite frequency stability. For QUASAT, the high- stability reference signal from which the on-board local oscillator frequencies will be derived, is obtained from the uplink phase transfer carrier, which in turn is derived from a hydrogen maser at each ground station.

However, along the transfer path there are various contamination sources which will affect the uplink signal and degrade its coherence.For QUASAT the coherence goal that the RMS phase fluctuations about the best phase rate must be less than 0.14 radians at 22.3 GHz within 300 sec integration time. Assuming a Gaussian phase noise model, this requirement results in a coherence factor of 0.99.

There is no requirement to transfer phase accurately in real time because the best phase rate is estimated and corrected during VLBI data processing. However, phase fluctuations and higher order phase rate terms are not corrected and contribute to degradation of coherence.

The phase transfer system envisaged for QUASAT consists of a two-way Ku-band link (13.9 GHz up; 14.1 Ghz down). The uplink frequency will be offset phase-continuously by the predicted Doppler shift to minimize tracking loop stress in the spacecraft receiver's phase-locked loop and to provide first order phase transfer.

The phase-coherent links are used to obtain estimates of the phase errors on-board the spacecraft. These estimates, which approximately equal half the phase difference (between uplink and

downlink) measured at the ground station, are used during VLBI processing to close the phase transfer loop. They contain the following reciprocal effects:

- residual Doppler effects
- reciprocal ionospheric and tropospheric propagation effects
- long-term instabilities in the on-board Ku-band system.

The remaining phase noise of the astronomy receiver reference frequencies to be included in the coherence evaluation is due to the following:

1. non-reciprocal propagation effects, comprising
   - tropospheric scintillation
   - ionospheric scintillation
2. receiver phase errors, due to
   - additive noise generated in antenna circuits and transponder receiver amplifiers
3. multipath effects, mainly due to
   - RF signal reflections of the back of the radio astronomy antenna into the sidelobes of the receiving Ku-band antenna.
4. mechanical instabilities, including
   - temporal changes of phase centres of Ku-band and radio astronomy antennas
   - (thermal) distortion of waveguides
5. higher-order phase rates, i.e. mainly
   - resulting Doppler rate due to uncertainties in the knowledge of the spacecraft's acceleration.

Mean coherence factors for the individual components have been established and are shown in subsection 7.5.6. The expected overall coherence (0.9784) falls below the 0.99 goal.

The effect of a 2% loss in coherence is potentially more damaging for the calibration accuracy than the corresponding loss in sensitivity. However, the simulation studies have shown that the latest data reduction algorithms can compensate for such small losses of coherence. Thus, the expected overall loss is tolerable.

7.3.5 Payload Calibration

During the commissioning phase following operational orbit injection, as well as at regular intervals during the mission, the following payload calibration tasks will have to be performed:

- antenna pointing calibration
- antenna defocussing calibration
- radiometric calibration

The purpose of antenna pointing calibration is to determine the bias between the reference X-axis of the spacecraft and the antenna boresight axis. The boresight axis (and the bias) can be identified by performing a sufficient sampling of the antenna pattern on a relatively strong H_2O line source. The estimated calibration accuracy is 20 arcsec and the calibration time is of the order of one hour. Such a calibration should be performed for several solar aspect angles (different thermal distortion).

Defocussing of the feeds can be an additional consequence of thermal distortion. The lateral defocussing is of minor importance, but axial defocussing should be compensated for by adjusting the feed position. For various solar aspect angles calibration of the feed position can be performed by pointing the antenna at a known calibration source and moving the feed to determine the gain maximum.

Finally, radiometric calibration has to be performed continuously to obtain gain and system temperature which are needed to derive properly calibrated flux data after correlation. Noise sources and couplers will be provided before each amplifier, with coupling into the feed, to permit calibration of system noise temperature. The use of a single noise source for both polarizations enables coherence and gain tests between the two IF channels.

Injection of a frequency rail with 1 MHz separation between spikes, in addition to the noise source, allows for independent phase difference and coherence tests and, more importantly, allows checking of the on-board frequency settings.

This feature and the common noise source also can be used to distinguish instrumental polarizations due to the polarimeter from the polarizations of the complete system (including feeds and antenna). For the latter case observations of astronomical radio sources must be used to complete the calibration.

7.4 Subsystem Design

7.4.1 Radio Astronomy Antenna

The design of QUASAT is based on an antenna reflector using the Inflatable Space Rigidized technology, which is being developed by Contraves under ESA contract.

The wall of the Inflatable Space Rigidized Reflector (ISRR), when chemically rigidized, consists of a thin fibre-reinforced composite lamina (Kevlar fibres impregnated with a special matrix developed by CIBA-GEIGY plus a Kapton foil). This lamina is practically black and opaque but RF transparent. The reflector is assembled and launched with the wall in its flexible prepregged state to enable folding for stowage in the reflector container.

The main elements forming the reflector are (Fig. 7.5):

- the parabolic reflector, which has a coating of vacuum deposited aluminium on the space-side acting as RF reflector and thermal insulator.
- the parabolic radome coated with Indium Tin Oxide (ITO) in order to avoid potentially dangerous electrostatic charge accumulation on the dielectric surface.
- the toroidal transition segment, also aluminized on the outside to improve curing (increase temperature).
- the central tube providing the axial stiffness.
- the stabilization torus, a light-weight plastic foil.

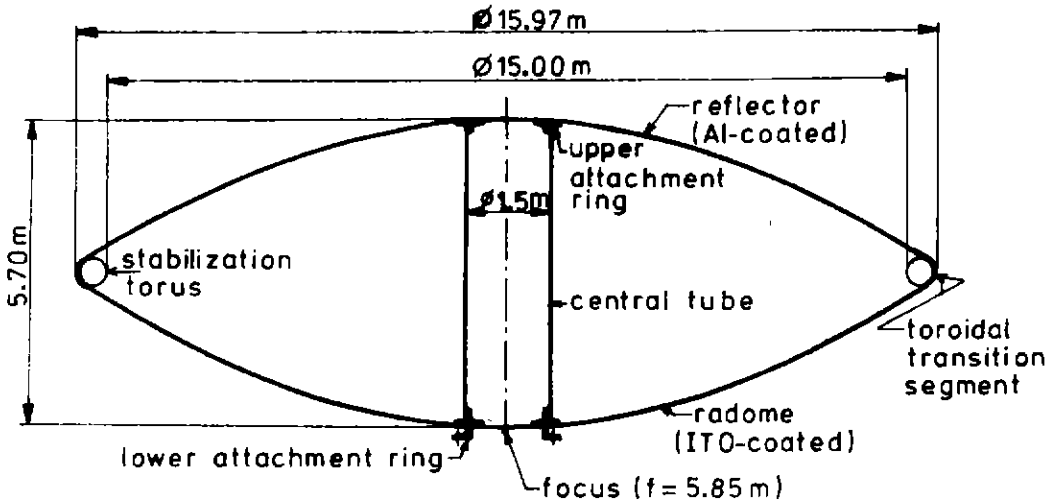

Figure 7.5: The main elements of the reflector

- two 1.5 m diameter attachment rings for connecting the central tube to reflector and radome membrane, while the radome ring is also used to mount the antenna to the spacecraft structure.

The antenna's shape is determined by appropriate gore preforming and joining. The stabilization torus is a pressure support element and does not have a critical shape function.

During launch the reflector is stowed in the reflector container which protrudes within the special purpose adaptor (Fig. 7.2). After injection in the first operational orbit, the reflector container is ejected and the reflector is deployed by inflating the torus (11.5 kPa), main chamber (10.0 Pa) and central cylinder (125.0 Pa) with nitrogen. Curing is then effected by pointing the boresight of the antenna towards the sun for about 10 h, during which the temperature of all the antenna elements will be 110° C. After curing the nitrogen is evacuated.

In its deployed state the antenna aperture (inside diameter of torus) is 15 m and the outside diameter is 15.97 m. The focal length is 5.85 m corresponding to a f/D ratio of 0.39 which is optimal for the proposed coaxial feed.

The total reflector mass, including the presurization elements (bottle with gas, valves and plumbing), the stowage elements and a 10 % contingency is 124 kg. The required volume for stowage is 1.7 m^3.

A thermal analysis was performed for various thermal load cases depending on the solar aspect angle and the temperatures obtained are between 120° C, reached when sun-pointing (cure case) and -230° C after a two-hour eclipse.

A structural analysis was performed to evaluate the eigen- frequencies and to derive the thermal distortions using the results of the thermal analysis. The lowest eigenfrequency found is 3.33 Hz corresponding to a fundamental bending mode about an axis normal to the boresight axis.

The effects of thermal distortions are essentially equivalent to a slight transverse displacement of the focus (max. 2.5 mm) and/or a small axial shift (max. 2.5 mm). The worst case occurs for lateral illumination when the defocussing leads to a gain loss of 0.20 dB. However, a feed refocussing mechanism, allowing controlled displacement of the feeds along the boresight direction, is provided to adjust the focal length of the inflatable reflector after deployment. This mechanism could also

be used to correct for the defocussing due to thermal deformations.

The overall efficiency budget for the reflector has been evaluated for the four frequencies. The results are shown in subsection 7.5.7. The following loss factors have been taken into account:

Illumination and spillover The illumination and spillover budgets have been evaluated by CSELT who developed the feed.

Blocking The major contribution comes from the central blocking, giving a shadowed area of 2.1×2.1 m, while the booms shadow about 0.8 m^2, leading to a total loss of about 6 %.

Central tube attenuation The central tube is a cylindrical rigidized membrane with a diameter of 1.5 m composed of a 114.6 micron kevlar-epoxy layer and a 25 micron kapton sheet. For normal incidences this material has very low transmission losses. However, the feed is located internally and the incidence angles of the wave on the surface are far from normal and consequently the transmission losses increase, especially for the highest frequency.

Surface error Loss of efficiency results from the deviation of the surface from the ideal paraboloid. In a first approximation the Ruze formula for gain loss can be used. The expected RMS surface error for a 15 m reflector as evaluated by Contraves is 0.8 mm yielding a 43 % loss at 22 GHz.

Dielectric losses In addition to the central cylinder, the RF waves cross three layers of about the same thickness: once the radome and twice the reflector membrane.

Reflector mismatch This is only significant when the focal distance is relatively short in terms of wavelength, as it is in the P-band.

Anti-static coating The radome should be coated with a semiconductive material like ITO to ensure sufficient electrical conductance. RF losses are only significant at K and C band.

Axial defocussing According to the specification the maximum axial defocussing shall not exceed 1 mm (feed focussing mechanism) yielding a power loss of about 1 %.

Transverse displacement of the feed. For a maximum transverse displacement of 5 mm as specified the gain loss is about 1 % at K-band and negligible at the other frequencies.

Thermal deformation This effect has been discussed before and in the worst case, with no refocussing leads to a loss of 6 % (at 22 GHz).

The overall antenna efficiency is thus 0.31 at 22 GHz and about twice as high at the lower frequencies.

7.4.2 Structure

The QUASAT structure is composed of a primary structure withstanding the high launch loads and a secondary one sustaining lighter loads. *The primary structure is composed of:*

- an aluminium corrugated cone interfacing with the adaptor via a marmon clamp system.
- an aluminium sandwich circular plate supported by the inner part of the separation plane ring. This platform sustains the feed and the reflector pressurization equipment.
- an Al sandwich square equipment platform stiffened by two orthogonal CFRP beams on the upper side.

- a sandwich square tank platform with CFRP facesheets and with two CFRP beams inside the platform.
- a CFRP truss structure joining the tank platform to the main equipment platform.

The secondary structure is composed of:

- a jettisonable reflector stowage container made of kevlar
- a shaped cover closing the satellite formed by two rectangular 30° skewed panels, two parallel trapezoidal plates and on top a rectangular plate sustaining the thruster system (all Al sandwich panels).
- a crossed reinforcing structure supporting star sensor heads and stowed booms.
- four deployable booms (to be discussed in next section)

The launch configuration requires a special purpose adaptor to allow stowage of the reflector within the adaptor. The lower ring (1920 mm) is bolted to the Ariane interface plane, while the upper ring (1666 mm) is fitted with the standard clampband. For separation, an external spring system is used.

The structure, being designed for stiffness requirements, has high strength margins of safety. In the launch configuration the first two dynamic modes are lateral modes at about 20 Hz, which is well above the 11 Hz Ariane requirement. The first axial mode is at 35 Hz leaving some margin above the 31 Hz requirement.

7.4.3 Booms and Mechanisms

Four long booms are required to carry the solar array wings and the Ku-band antennas. To reduce design, manufacturing and test cost all four booms are structurally identical. The total length is 7.2 m. In order to allow stowage inside the Spelda, the booms are segmented into three sections with inner and outer boom sections of equal length (2.2 m) and a middle section of 2.8 m.

Consideration of geometric blockage of the reflector aperture and of the pointing requirements led to a rectangular cross section with the small side parallel to the reflector aperture plane. For reasons of stiffness, thermal expansion and cost a thin-walled CFRP structure is used.

Analysis has shown that for a 30×60 mm cross section the dynamic behaviour of the booms is compatible with the requirement for sufficient separation between structural frequency and AOCS frequency and with the communication antennas pointing requirement.

Each boom joint is made up of two precisely machined parts (the boom segment extremities), two journal bearings, a pulley system and a latching device.

The solar array wings are attached to the booms via BAPTA drive units and the Ku-band communication antennas are mounted via a two-degree-of-freedom antenna pointing mechanism (TELDIX). The RF links along the booms are obtained via thin-walled silver-plated CFRP waveguides mounted inside the booms with open-choke flanges at each boom segment end.

During launch, each stowed boom is retained with an upper and a lower lock-and-release mechanism supporting the boom stack in the plane of deployment as well as in the orthogonal plane. Deployment is started by firing of a pyrotechnic cable cutter which releases both the upper and the lower lock mechanism.

Deployment is actuated by a small electric motor at the boom root. The motion is transmitted to the outer boom sections by a pulley and cable system. The cable is pre-tensioned to ensure step-by-step equilibrium and to act as a spring helping to complete deployment of the outer sections.

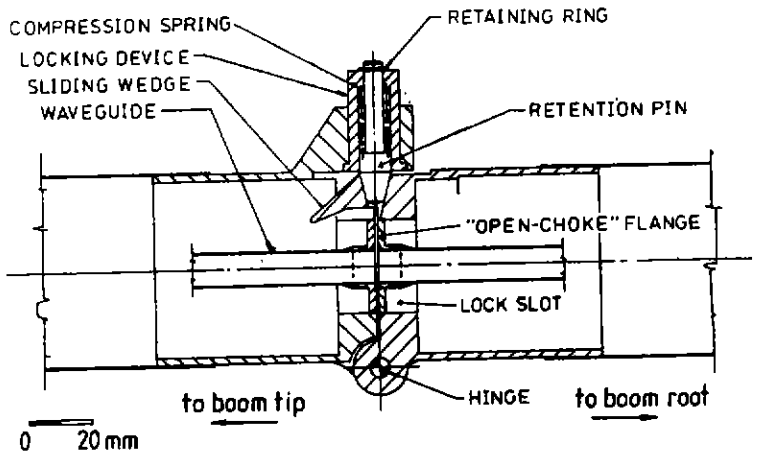

Figure 7.6: Boom Joint - Longitudional Cross section

Deployment is completed by a latching device designed such as to allow no play between the boom sections and to ensure coupling with minimal friction and without backlash. A longitudinal cross section of a communication antenna boom joint is shown in Figure 7.6.

To allow precise controlled displacement of the feed along the boresight direction for focus adjustment, a feed positioning mechanism is foreseen. This is basically a screw spindle mechanism with the spindles attached to the feed platform by means of ball bearings and nuts attached to the feed support structure.

Three spindles, separated by 120°, are used and one of the spindles is driven by a motor with planetary gearhead.

The turning of the three spindles is synchronized by a pinion-crownwheel system. Position control can be obtained by means of an encoder giving the motor position. An accuracy of 0.01 mm can be obtained this way.

7.4.4 Thermal Control

Three main tasks are performed by the thermal control subsystem:

- heat rejection of spacecraft internal dissipation from equipment and payload at the required temperature level.
- maintaining acceptable temperatures on all external parts.
- cooling of payload preamplifiers and feed.

Figure 7.7 shows the spacecraft overall thermal control configuration.

Spacecraft internal dissipation is rejected to space by a fixed radiator of 3.3 m^2. The radiator is positioned on the $-Z$ surface of the spacecraft where no direct sunlight is received. The radiator plane is inclined by 30° (minimum required solar aspect angle) in order to minimize the heat input from the radome. A coating of optical solar reflectors (OSR) is required to maintain sufficient radiator performance during the period of antenna curing and to reduce albedo heating during perigee passages.

A controlled radiator heat rejection is necessary to prevent excessive heater power during cold mission phases. A solution using variable conductance heat pipes (VCHP) which are available in Europe was preferred to louvers because of better thermal performance.

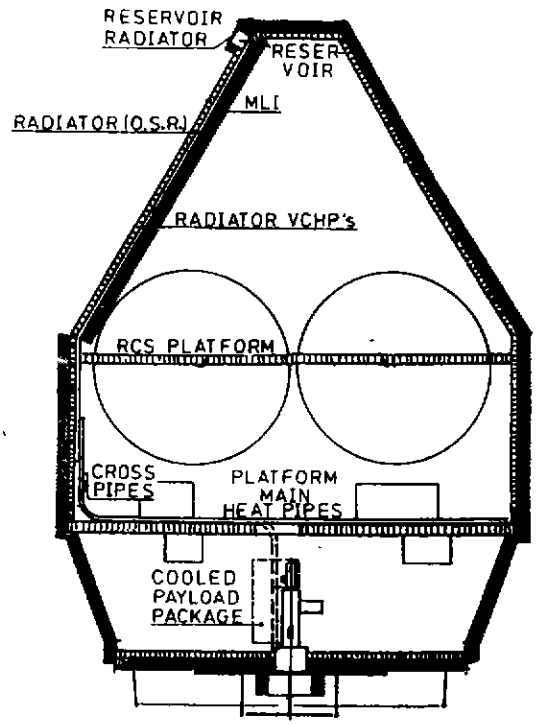

Figure 7.7: Thermal Control Subsystem equipped with VCHP's

The recommended solution consists of 28 parallel VCHP's mounted on the inner facesheet of the radiator panel. At the bottom of the radiator panel the pipes are bent over 30° and end with vertical mounting flanges. Half of the VCHP's interface with 12 equipment platform heat pipes (CCHP's) and with two heat pipes coming from the Stirling coolers. The other 14 radiator pipes are connected to cross pipes located in the vertical pipe section area. The platform pipes are mounted on top of the platform and all boxes with high dissipation equipment should also be placed on the upper side.

The spacecraft interior is insulated from the external environment by means of Multi Layer Insulation (MLI) blankets with Kapton outer layers. The usual black paint on platforms, internal radiator surface and boxes supports the function of the heat pipes.

Heater circuits are required for the batteries and the flow control valves of propulsion subsystem as well as to compensate for the missing dissipation from payload or platform equipment during transfer orbit or in survival mode.

Temperature control of external components such as solar array, BAPTA, APM, Ku-band antenna and booms is obtained by using MLI in combination with (thermostat controlled) heaters and special coatings or paints.

In this way, the temperature of all the equipment can be kept within the qualification limits, except for the solar array which can reach a temperature of −184° C after a long eclipse (qualification limit is −170° C)

For payload cooling, four Stirling cycle coolers (2 operating, 2 in cold redundancy) are used. These coolers have been developed by Oxford university and BAe is presently producing and qualifying them for space applications. The configuration that has been proposed is shown in Figure 7.3 and has been discussed in subsection 7.3.2.

The heat dissipated by the coolers is transported to the radiator and main equipment platform

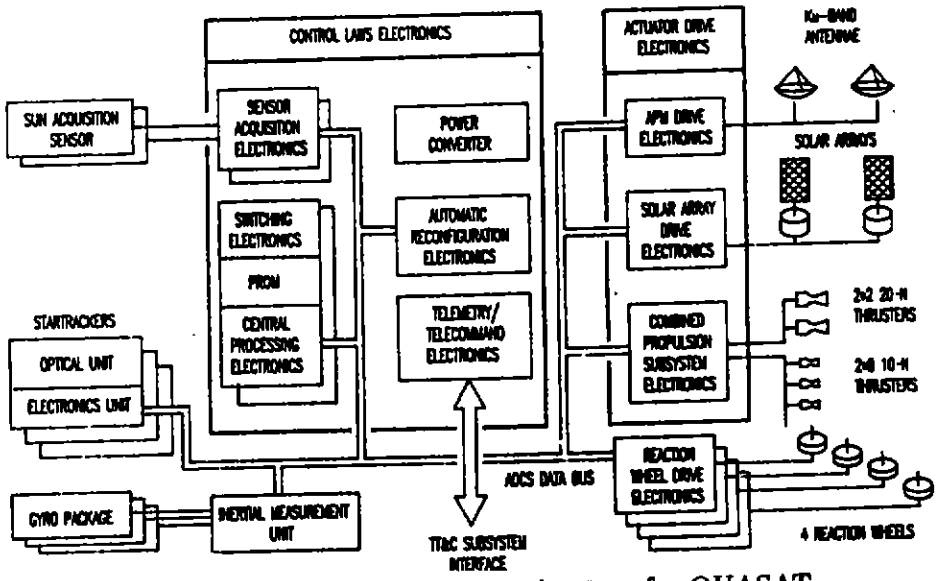

Figure 7.8: Overall AOCS arcnitecture for QUASAT

by 4 heat pipes (2 redundant). Two pipes join with the radiator pipes, the other two are joined to the cross pipes.

Predicted temperatures are 150 K for the C-band preamplifier and 95 K for K-band, with heat lift rates of 1550 and 900 mW, respectively. Although this does not meet the specification (80 K), the resulting 10 % loss in interferometer sensitivity was judged acceptable; the more so as improvement in the cooler efficiency can be expected in the near future. In addition, it is possible to operate all four coolers as long as the solar array delivers sufficient power and the thermal situation permits it (not in hot case). The preamplifier temperatures are 75 K and 110 K for K- and C-band, respectively.

7.4.5 Attitude/Orbit Control and Measurement Subsystem

The major requirements to be satisfied by the AOCS were summarized in subsection 7.3.3. In addition the following tasks must be performed:

- initial attitude acquisition.
- acquisition and control of attitude necessary for orbit maneuvers.
- acquisition and control of safe attitude in case of failure
- communication antenna pointing.

During the operational phase the spacecraft will in general observe one target for long periods of time. During this fine pointing mode the inertial attitude and solar aspect angle shall be kept constant. Due to the large opaque reflector the spacecraft experiences large solar radiation pressure disturbance torques (up to 1.6×10^{-3} Nm). In addition there are gravity gradient torques, which on average are about an order of magnitude smaller than the solar pressure torques.

To compensate for these disturbing torques, reaction wheels will be used. This actuator concept is preferred because during a phase referencing mode, when the antenna boresight direction will alternate between the target source and a reference point source which might be up to 2° from the target, kinetic momentum transfer will accomplish the slewing without any fuel consumption.

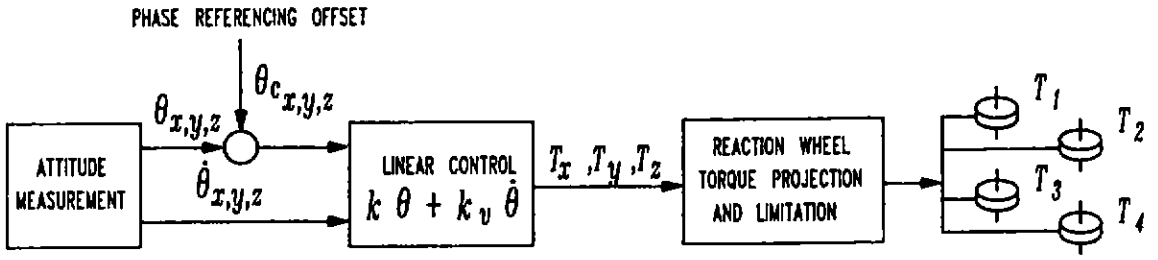

Figure 7.9: Simplified control law block diagram

The maximum kinetic momentum needs during one orbital period are 6.1, 70.6 and 6.6 Nms along the X, Y and Z axis, respectively. The wheel configuration and dimensions are chosen such as to limit off-loading to once per orbit. This leads to a configuration of four skewed wheels, nominally all working at the same time, supplying a large angular momentum storage capability along the Y-axis. The required wheel capacity is ±20 Nms allowing for a margin of 50 %. These wheels which are presently under development deliver a maximum torque of 0.1 Nm. In case of failure of one wheel the kinetic momentum storage capability is divided by two and the time between subsequent off-loadings has to be halved.

Off-loading of the wheels is achieved with 10 N thrusters operated in open-loop with pulse modulation so that the average thruster torque is close to the maximum wheel torque. The duration of 70 Nms off-loading including tranquilization is about 400 s. During the first part of the off-loading, mispointing reaches a 1.5° peak and stabilizes later at about 1° until the end of the thruster pulse sequence.

The duration of a 2° phase referencing maneuver (including settling time) is 170 s in the worst case (slew about Z-axis with 3 wheels running). With four wheels operating this is reduced to 135 s. For a slew about the Y-axis the durations are 110 s and 90 s, respectively.

The simplified control law block diagram (during fine pointing, wheel off-loading or phase referencing) is shown in Figure 7.9. Phase referencing maneuvers are simply initiated by setting a bias on the angular attitude measurement error signal. During wheel off-loading the thruster torque appears as a perturbation to the reaction wheel control. A control bandwidth of 0.013 Hz has been selected so as not to excite the first flexible modes of the spacecraft.

The requirement for accurate control and measurement of the boresight axis of the antenna imposes that the reference about the Y and Z axes is provided by startrackers. The measurement of the third axis (rotation about boresight direction) could either be provided by sun sensors or by startrackers. The sun sensor solution has been rejected because of field of view implementation problems and the limit that would be imposed on the anti-boresight direction with respect to the sun.

Therefore a full startracker solution has been chosen based on a two-out-of-three sensor configuration. The sensors are placed along a cone centered on the anti-boresight direction. The half angle of the cone is determined by the ratio between roll accuracy and transverse accuracy and should be 3°.

The attitude reconstitution requirement imposes a maximum measurement error of 3 arcsec for the star tracker. For startrackers built around a 110000-pixel Thomson CCD, the maximum acceptable field of view is then 12 square deg. The Galileo sensor (developed for ISO) then is the best choice for QUASAT. This sensor has a field of view of 3° × 4°. The limiting visual magnitude is 8. The probability of having at least one star brighter than 8th magnitude in the field of view of

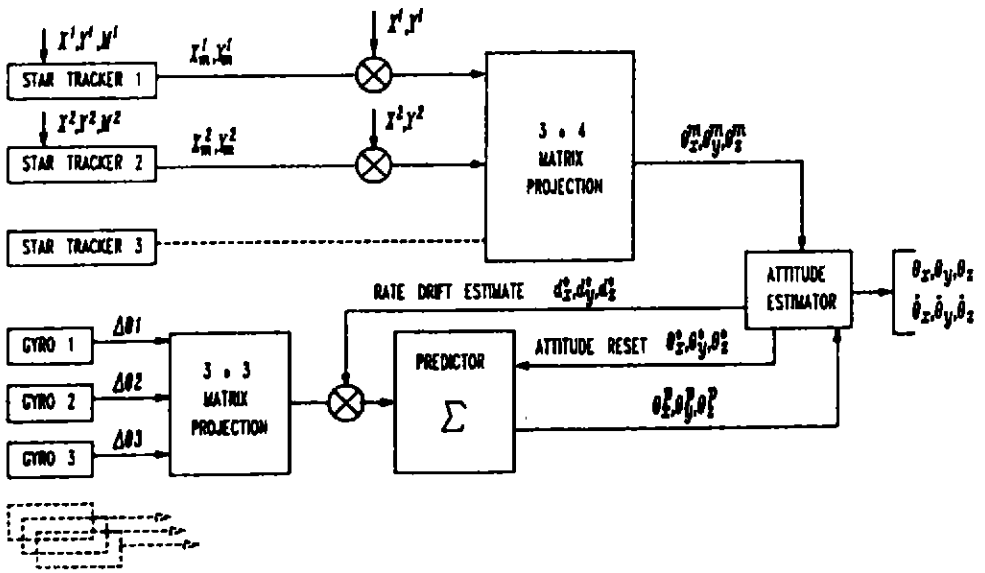

Figure 7.10: On board processing for attitude measurement

each of the two operating startrackers is 99.999 % on average and 99.51 % near the galactic pole.

To perform attitude maneuvers including phase referencing and momentum wheel off-loading, rotation must be controlled by a bias on the rates. Star sensors cannot measure the rates and thus gyrometers must be included. The six-gyro concept using three MATRA MAIA two-axis gyrometers in a two-out-of-three operating mode is selected for reliability reasons.

A schematic representation of the attitude measurement processing in the operational mode is shown in Figure 7.10. The attitude estimator is used both for gyro drift calibration and for attitude updates when startracker data are available. It is a simple linear filter.

For initial acquisition and during safe modes the residual rates are reduced using thrusters and gyro measurements after which the Sun acquisition phase starts. Two internally redundant Sun acquisition sensors (MATRA) are mounted on the solar panels in such a way that the same sensors are used to point the Y-axis towards the Sun during initial acquisition with the solar arrays in stowed position, and the X-axis toward the Sun for antenna curing and safe modes.

A final task of the AOCS is communication antenna pointing. The required pointing accuracy is 0.5°. Taking into account misalignments, pointing mechanism errors, thermoelastic deflections and flexible mode vibrations, an error of 0.2° can be allocated to command generation. The maximum angular rate that is required is 0.09°, leading to an update of the command angle every 2 sec. These updates can be generated on ground and sent to the spacecraft on the telecommand uplink. Another possibility which has not been investigated in detail yet is to use a closed-loop RF tracking system.

The overall AOCS architecture is shown in Figure 7.8. The total AOCS pointing accuracy is 14.6 arcsec. The pointing budget is shown in subsection 7.5.4.

7.4.6 Propulsion Subsystem

The fundamental design drivers for the propulsion subsystem are:

- execute perigee raise and inclination change maneuver (843.7 m s^{-1}; 2 impulses)
- execute apogee decrease maneuver (366.2 m s^{-1}; 4 impulses)
- momemtum wheel off-loading (8 kg/year)

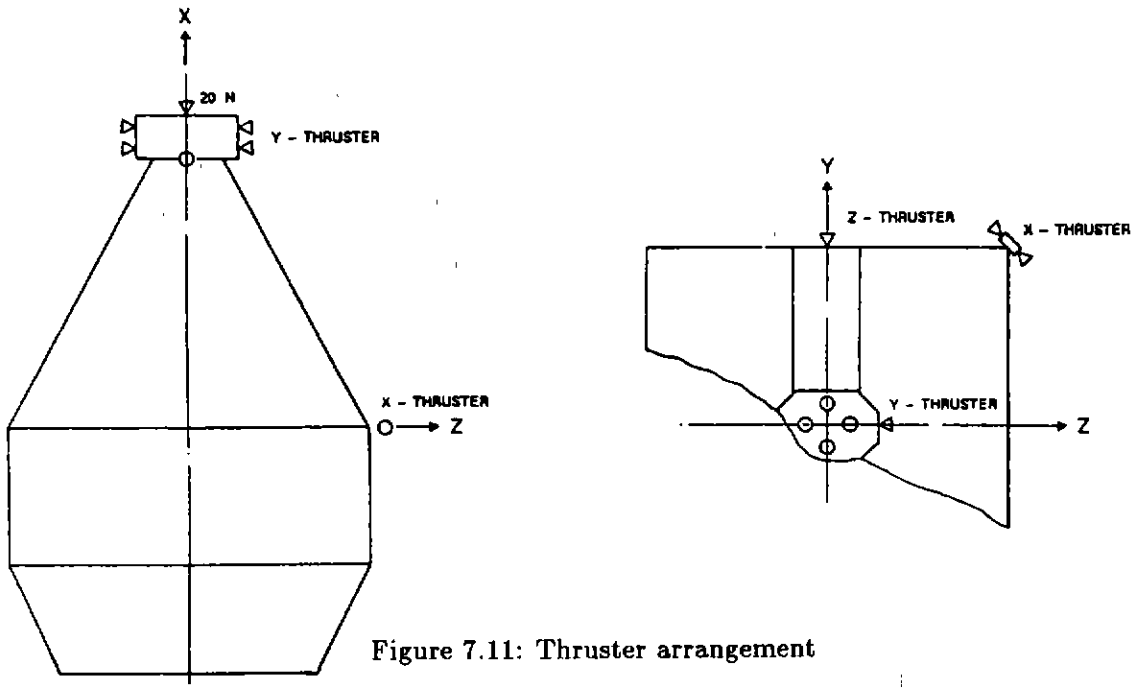

Figure 7.11: Thruster arrangement

Three propulsion system options were traded-off (subsection 7.2.2) and a monopropellant hydrazine system was selected.

The system is designed so as to utilize existing and qualified hardware to the largest extent to minimize development risks and cost.

The system, which is operated in blow-down mode (22/5 bar) consists of:

- four spherical diaphragm tanks from TRW-PSI
- two fully redundant thruster branches each containing two 20-N thrusters and eight 10-N thrusters and cross- coupled by four latching valves

The 20-N thrusters are used for injection into the two operational orbits and have been developed and qualified for Eureca.

The 10-N thrusters, used for AOCS tasks are those used in the METEOSAT program.

The thruster arrangement is shown in Figure 7.11 and has been selected to minimize plume impingement effects. The maximum plume impingement effect is caused by the X-thrusters giving a local energy flux of < 100 W m^{-2} on the antenna radome and < 350 W m^{-2} on the side walls.

The propellant budget is given in subsection 7.5.2.

7.4.7 Solar Array

The solar array has to be designed for:

- 710 W end of life (no margin)
- 820 W after two years (15 % margin)

Particle radiation effects in the QUASAT orbits cause a strong degradation of the solar cells. For this reason GAs cells have been compared with Si cells and different coverglass thicknesses have been considered. For both types of cells the end of life requirement is the sizing factor and a

A.4 Canadian Participation

From the start of the ESA/NASA studies on Space VLBI, Canada has shown a strong interest to participate in a possible programme. As a result of this, Canada has been invited to participate in the ESA Phase A study and, if the QUASAT mission is selected, in the spacecraft development. The National Research Council (NRC) of Canada has established that a potential Canadian contribution is the provision of some part of the telemetry downlink package for the radio astronomy (science) data and of the phase transfer system.

During the ESA Phase A study, Canada has cooperated with ESA by conducting a Phase A study on these RF packages. This Phase A study has been conducted by COM DEV under contract with the Canadian National Research Council. Both the X-and Ku-band option have been studied and analogue as well as digital modes of encoding have been examined. These trade-offs favoured a digital Ku-band system and a preliminary design of such a system, including power, mass, volume and cost estimates has been established and presented to ESA.

In the anticipated ESA/NASA/Canada cooperation scenario, for which NASA's contribution has been presented in the previous Appendices Canada could provide the space-part of the science data telemetry and phase transfer system, which represents a significant cost saving to ESA.

Figure 1.- Ground Segment Overview for the DSN Support Option

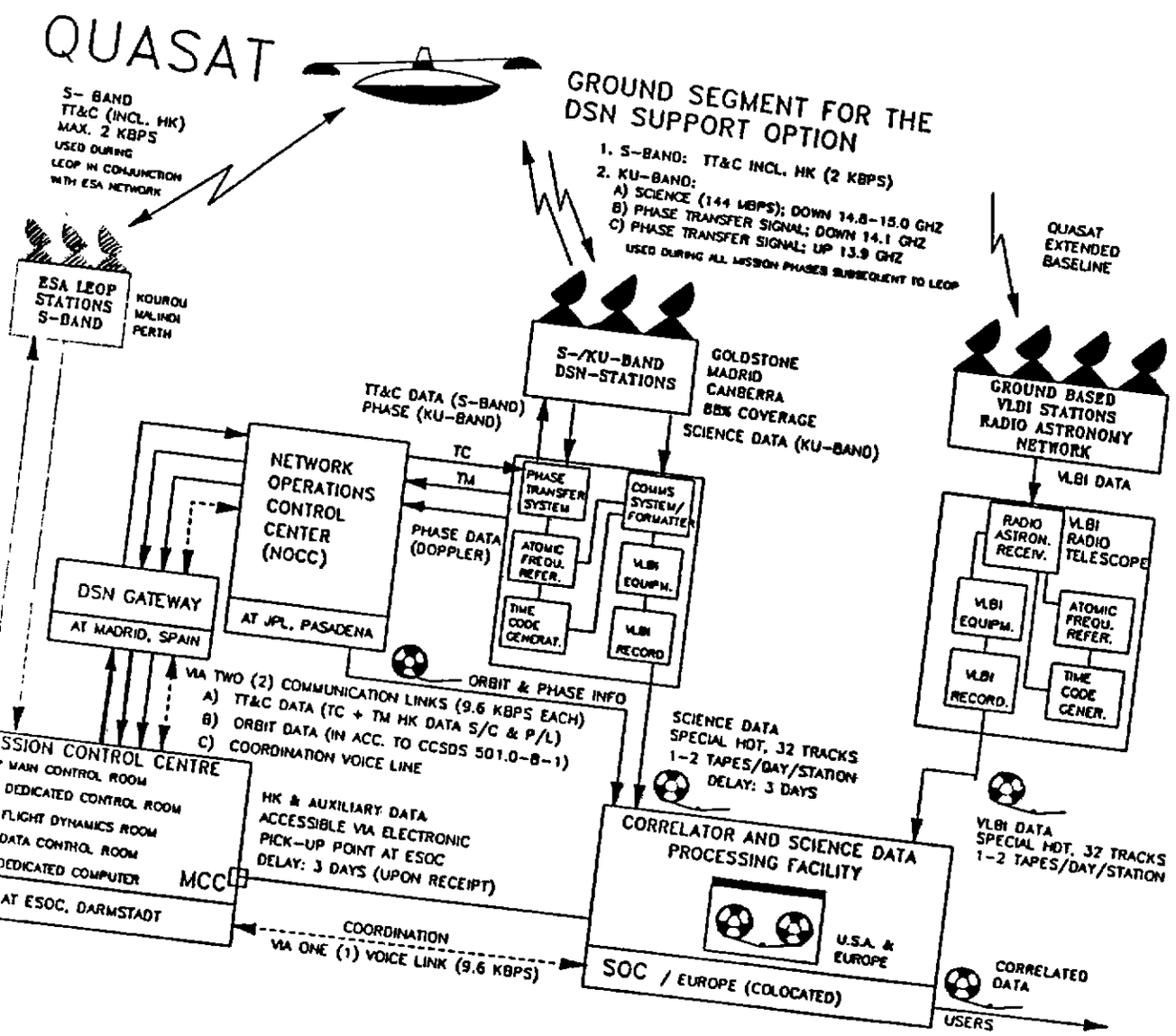

c) For the 'sequence of events generation' the coordination planning function made by ESOC is redundant to the similar function at JPL. JPL has control over planning of the network (sharing QUASAT/other missions).

The ESOC/JPL task distribution would therefore have to be negotiated with a view of ensuring ESOC's leading role in this mission, even if DSN has a major support function.

For the basic DSN support option a number of derivative versions have been identified, which could give ESOC additional tasks of more technology content. These are:

1) Precise orbit determination by ESOC from outputs of the phase transfer system, whereby pre-processed metric data are provided by JPL. H/ECD confirmed that this task can be accommodated within the cost estimated for the basic DSN support option.

2) Design, procurement and delivery to JPL/DSN of the phase transfer system.

3) Procurement and operation of one Ku-band ground station in addition to the DSN for improved data acquisition coverage (location Malindi, TBC).

6. Analyze metric data to determine precision orbits for the S/C.

7. Route phase delay information and precision orbital information to the European and U.S. correlation facilities.

8. Route state vectors based on the precision orbits to ESOC.

9. Generate predicted S/C trajectory information and compute DSN station predicts.

10. Analyze all S/C observational sequences and advise the science scheduling facility of ground tracking station readiness and constraints relative to the sequence and/or alternative suggestions to optimize the ground station performance relative to that sequence.

11. Represent QUASAT requirements to the JPL antenna scheduling conflict resolution process and secure the needed tracking allocations.

12. System engineer the end-to-end phase transfer system, furnishing only the ground portion of the system, but coordinating the Canada-furnished S/C electronics, ground testing, and performing the in-flight link performance analysis.

13. Furnish representation to the QUASAT Policy Management/ Operations Steering Group.

-2.3. ESOC analysis of proposed split of responsibilities

The above proposed split of tasks and responsibilities reflects the low cost approach preferred by the project, however, does not follow exactly the spirit in which ESOC would define this scenario. In particular, the following potential problems can be identified:

a) During the routine operations phase ESOC communicates with the DSN stations via the Robledo gateway and the JPL/NOCC. For real-time operations this is not the best system, since ESOC would have no control over the transmission delays to the satellite. If the system therefore would operate off-line only, this would be a major limitation in case of a satellite emergency.

b) The orbit reconstitution performed at ESOC for S/C control on the basis of 'state vectors' is redundant with the same function performed at the NOCC using data derived from the phase transfer. It has to be noted that the orbit reconstitution made at NOCC would be more accurate than that possible at ESOC, since it is based on data derived from phase transfer processing instead of 'state vectors'.

- Orbit Change Maneuvering
- Earth Antenna Orientation Maneuvering

3. Generate "on line" commands for payload and S/C testing and commissioning during LEOP and emergency corrections during Scientific Operations Phase (SOP).

4. Route all SOP commands to DSN/NOCC through Madrid I/F for S-band transmission to S/C through DSN antennas.

5. During LEOP, route all commands to ESA S-band stations for transmission to S/C.

6. Receive and log S-band transmitted housekeeping telemetry data from ESA stations during LEOP and from DSN interface during SOP. Convert data to engineering units and analyze data to assess S/C and instrument performance, including verification of radio source acquisition and computation of pointing offsets.

7. Deliver required instrument and S/C calibration data to the European and U.S. science data processing facilities.

8. Generate predicted S/C trajectory information and plan and compute all S/C maneuvers.

9. Analyze all S/C observational sequences and advise the science scheduling facility of S/C readiness and constraints relative to the sequence and/or alternative suggestions to optimize the S/C performance relative to the sequence.

10. Furnish representation to the QUASAT Policy Management/ Operations Steering Group.

2.2 NASA/JPL Responsibilities

1. Provide S/Ku band tracking during science operations mission phase (SOP). Two-way S-band will carry command and telemetry, and two-way Ku band will carry the phase transfer and science data.

2. Record all VLBI science data received from the S/C.

3. Mail recorded tapes (in VLBA format) to the European and U.S. correlation facilities. JPL will furnish the tapes and provide for tape transport.

4. Route through the NOCC all ESOC-bound telemetry and ESOC-generated S/C commands (normally store and forward, but in real time if needed).

5. Generate metric data from the Ku carrier signal.

A.3 ESOC: NASA Support Option

DSN SUPPORT OPTION

General

The objective of this appendix is to provide a brief summary of the ways and means by which a cooperation between ESA and NASA could be conducted within the framework of the QUASAT mission operations planning and execution and to compile the related assumptions hereto. The potential scenario has been proposed by NASA/JPL and ESTEC/PF and was outlined in the course of the final presentation (April 15, 1988 at ESTEC). A discussion took place at NASA-HQ (July 6, 1988) and subsequently a proposal was forwarded by JPL (MSG: HGII-3082-5473, 07/18/88).

It should be noted that the DSN Support Option has not yet been finalized nor was approved by either party.

Compared to the ESA stand-alone baseline, the DSN support option would be mainly characterized by the fact, that the ESA KU-band ground stations are replaced by the DSN network (34 m) during the operational phase of the mission, and that NASA/JPL provides the QUASAT unique processing equipment required within the ground stations.

An additional difference is that DSN provides for simultaneous S/Ku-band support during the Scientific Operations Phase (SOP), and hence the TC and HK-TM will be transmitted in the S-band frequencies only. Furthermore DSN will provide support for the second 'LEOP' maneuver during transfer from orbit 1 to orbit 2.

The operations scenario will be such that during all mission phases the overall responsibility for the mission will rest with ESA, and that all spacecraft control activities will be performed from the MCC located in Darmstadt, W-Germany.

Responsibilities of NASA/JPL will encompass the provision of the DSN, processing of the science data and phase transfer data, preprocessing of orbit data, as well as the distribution of science data (recording of science data and shipment of VLBI tapes) to the Science Operations Centre (SOC) / Correlator.

-2. Responsibilities (To Be Confirmed)

-2.1 ESOC Responsibilities

1. Provide S-band tracking during launch and early operations mission phases (LEOP).

2. Generate all S/C commands (nominal mode - "non-real time") during Science Operations Mission Phase (SOP) for:
   - Instrument Activity Control
   - S/C Orientation Maneuvering

b. Facilitation of the purchase and acquisition of VLBA compatible data recorders by the DSN.

c. Co-observer of astronomical objects (approximately 30% of the time) with QUASAT.

d. VLBI data correlation and archival of results.

e. Radio source image processing.

f. Participation in the QUASAT Operations Steering Group and to the European Experiment Proposal Evaluation Process at the Host European Institute.

NASA's funding of NRAO QUASAT activities, and therefore JPL's coordinating interest, would be limited to cover only modifications to the VLBA correlator for Space VLBI processing and operations functions incremental to the normal VLBA operations imposed by the presence of QUASAT as an observing telescope.

Reference 1. QUASAT, a VLBI Observatory in Space, a proposal to the National Aeronautics and Space Administration from the Jet Propulsion Laboratory, July 31, 1986.

(1) The execution of a flight antenna materials testing and evaluation program to aid ESA flight readiness.

(2) General, but limited, mission analysis and systems engineering support to the ESA QUASAT Project.

(3 Coordination of the use of the DSN tracking facilities, including participation in the tracking schedule conflict resolution process and the analysis and evaluation of alternative schedules when required and schedule coordination with the European Host Institute science experiment schedule.

(4) Generation of requirements on the DSN for support of the project. THis support could include the following functions:

a. System engineering of the end-to-end signal phase transfer system, including ground and space elements.

b. Tracking of the QUASAT spacecraft. Two-way S-band will carry command and telemetry (from and to ESOC), and two-way K_u band will carry the phase transfer signal, science data, and doppler and range observables.*

c. Recording VLBI science data received from the spacecraft and delivery to correlation facilities in Europe and the U.S.

d. Precision determination of the QUASAT spacecraft orbit.

(5) Development and operation of an image processing support and guest investigator facility in the IPAC.

(6) Participation in the QUASAT Operations Steering Group.

(7) Coordination and funding for the U.S. membership in a joint ESA-NASA Science Working Team. U.S. members will be selected from the list of proposers of the NASA-ESA QUASAT Mission; see reference 1. Functions of the team will include:

a. Defining the science requirements on the mission during the mission development phase.
b. Defining the scientific experiments for the core program.
c. Analyzing the data obtained during the core program.

(8) Coordination of the NASA funded activities by the NRAO in support of the QUASAT mission. The expected NRAO activities for QUASAT, both NASA and NSF funded, are listed below:

a. Peer review, prioritization, selection of, and scheduling for experiment proposals which involve observation by NRAO facilities.

*Here we assume that ESA will operate the spacecraft from its control center in Darmstadt, West Germany, the basic control being to point the antenna at the selected radio sources and observe at selected frequencies.

A.2 NASA: Support of QUASAT

Introduction

This appendix presents a proposed plan for NASA's participation and support of the ESA QUASAT mission. It provides a summary of NASA's potential participation in both the development and operations phases of the mission which could be carried out if QUASAT is selected by ESA as its next science mission.

U.S. Participation Overview

U.S. participation in the ESA QUASAT mission could consist of the following technical functions:

By JPL:

- Tracking, data recording and precision orbit determination - carried out by the Deep Space Network (DSN).
- Technical support to ESA in the ground testing and evaluation of flight antenna materials.
- Image processing support at the Caltech Infrared Processing and Analysis Center (IPAC).

By the National Radio Astronomy Observatory (NRAO):

- Observing astronomical objects simultaneously with QUASAT by the VLBA and other NRAO telescopes.
- Data correlation and image processing.
- Experiment proposal scientific evaluation and selection.

By the U.S. Science Community:

- Membership and participation in a joint ESA-NASA Science Working Team (SWT).
- Individual proposals, in response to an AO, and data analysis in the later mission phases.

Technical & Management Plan

NASA would implement its role in QUASAT activities through a flight project management structure at the Jet Propulsion Laboratory. The Project would coordinate the QUASAT activities of the NRAO, the DSN and the U.S. science community. Functions which the U.S. QUASAT Project would carry out in coordination with ESA, could include:

Appendix A

Collaborative scenario

A.1 Introduction

Ever since QUASAT was proposed to ESA it has been conceived as a collaborative project. The current scenario is the result of discussions over the last few years with NASA, Canada and Australia. Representatives from all three countries have participated as full science team members in both scientific and technical discussions. The current report have profited greatly from these interactions for instance making it possible to take into account the experience gained from the TDRSS experiment.

The NASA involvment could consist of JPL and DSN ground support. Canada could build part of the Ku band system on-board the spacecraft.

The potential use of the large (34 m) DSN antennas would impact on the spacecraft design in the sense that the diameter of the Ku-band link antennas and/or the transmitter power could be reduced. This could enable the use of for instance solid state transponders and reduce the overall power requirement. The cooperation with the DSN would have the advantage that groundstations are already designed for phase coherence. Furthermore a lot of the infrastructure for VLBI is already in place. The DSN is often involved in VLBI experiments (in addition to the TDRSS) and have accumulated considerable experience in this area. The non-use of Ku-band for command and telemetry (only S-band) has the further advantage that it simplifies the Ku-band data handling system and also the design of the link antenna control system.

Canada has carried out a complete study of the spacecraft segment of the phase- and data link system. The ESA Phase A study profited from this and results from the Canadian study where taken into account. This part of the spacecraft offers a clean interface and would represent an important contribution to the program.

This collaborative scenario is the result of extensive discussions and although still awaiting formal agreements has the support from all parties. The following sections describe this scenario as regards: NASA, ESOC and Canada. The Australian participation is belived to be limited to the ground VLBI system (the AT) and is documented in the main report.

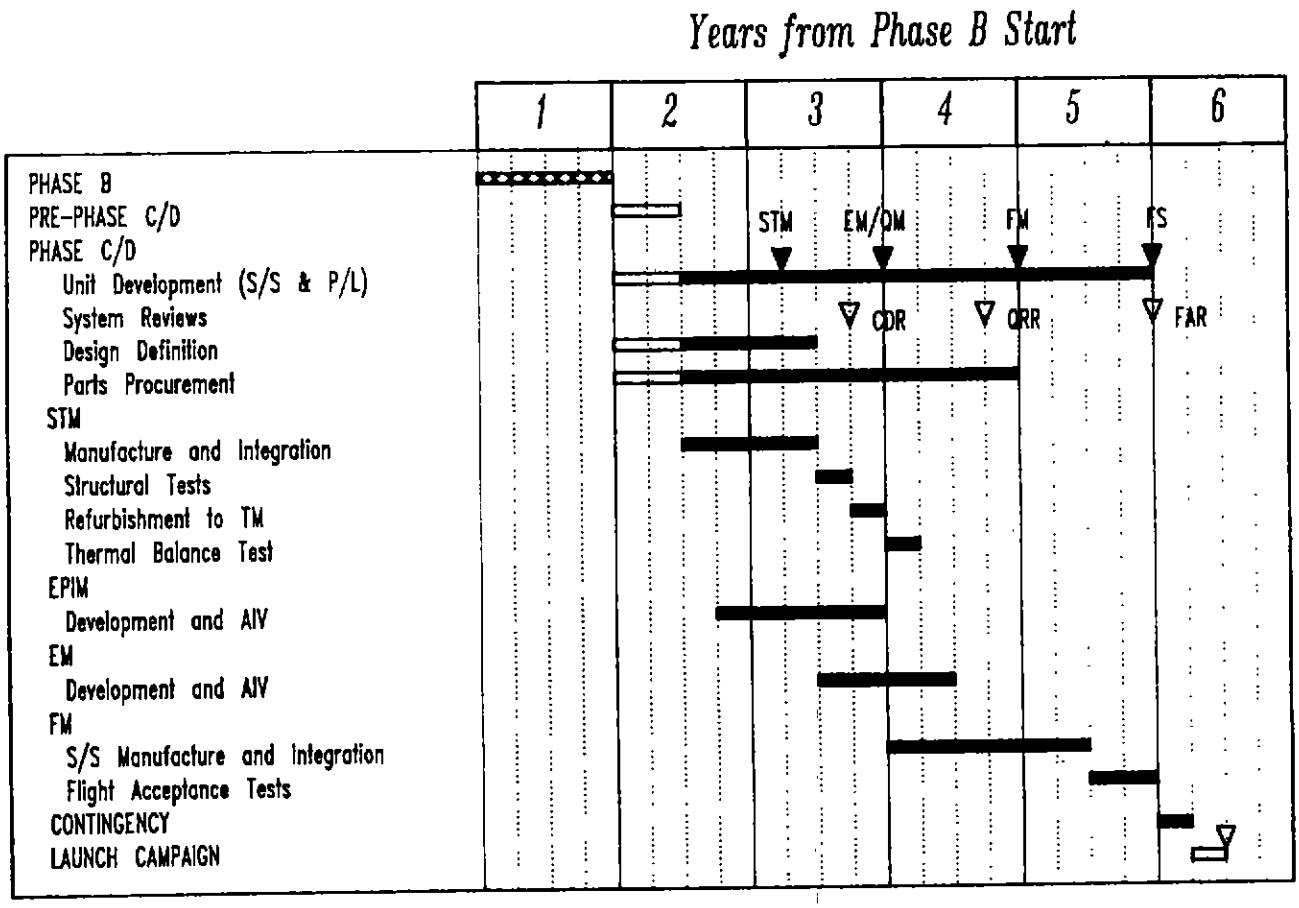

Figure 11.2: Overall programme schedule

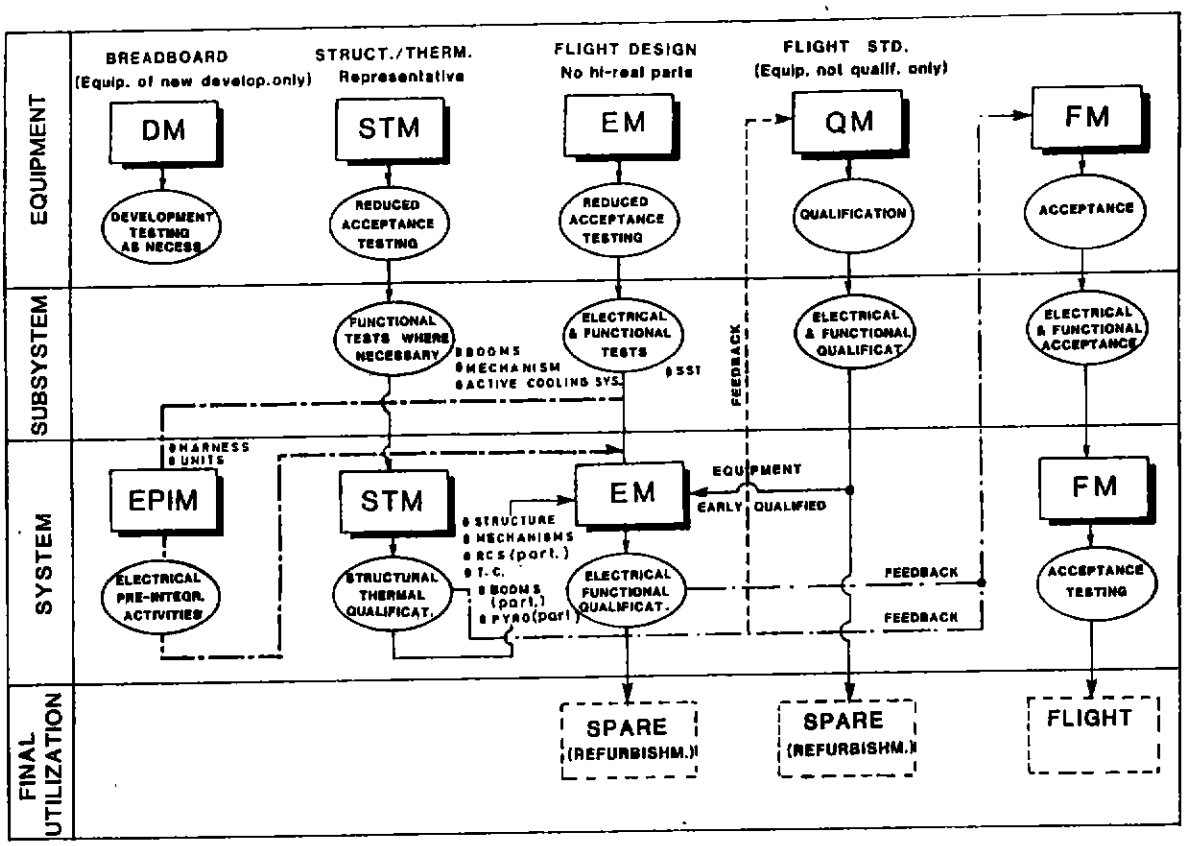

Figure 11.1: Model Philosophy

11.4.1 Development Philosophy

The proposed model and test philosophy chosen for QUASAT is shown in Figure 11.1 and is based on a protoflight approach where only one model, the flight model (FM) is built to flight standard. In order to minimize the risks associated with this approach, a development plan is proposed in which the FM is preceded by one complete spacecraft development model (STM/EM).

The complete structural/thermal qualification campaign is conducted on the structural/thermal model (STM), which has two main configurations: structural (SM) and thermal (TM). The SM is flight representative with respect to structure, mechanisms, booms and parts of the RCS and thermal control. All other units are structurally/thermally representative dummies.

After structural tests, the SM is refurbished into TM by integration of the complete thermal control hardware.

The engineering model (EM) is constituted by the refurbished flight-standard STM parts plus a flight design set of units and functional subsystems (without Hi-rel parts). At the end of the EM test campaign, complete qualification is achieved and the feedback to FM equipment production is completed.

A complete set of new flight standard hardware is integrated to form the FM which will be subjected to the acceptance test campaign prior to delivery.

Units used for qualification of hardware will be used as flight spares after refurbishment. For already qualified hardware two flight models are proposed and the first of them will become flight spare after its use for EM system testing.

The overall programme schedule based this model philosiphy is shown in Figure 11.2.

patibility between instruments and common payload equipment is thus imperative and methods to maintain compatibility during the detailed design, development and calibration phases should be described. The responsibility for these procedures will rest with the PI.

Selection of the instruments will take place via the normal procedure which includes a technical evaluation by the Executive, a scientific evaluation by ESA's scientific advisory bodies and approval by the SPC. The selected PI with co-investigators will then be responsible for obtaining the necessary funding from the appropriate national authorities.

11.2.3 Instrument Development

Following selection of the instruments, refined resource allocations and instrument interfaces would be negotiated with principal investigators prior to the start of the spacecraft Phase B. These resources and interfaces would be frozen at the end of Phase B.

The development schedule of the instruments is shown in Figure 11.2. For each instrument/unit, the PI groups would be required to supply the following models:

- 1 dummy model for the spacecraft Electrical Pre-Integration Model (EPIM) and the Structural/Thermal Model (STM)
- 1 engineering model (electrically and thermally representative but with no Hi-rel parts) for the spacecraft Engineering Model (EM)
- 1 qualification model (QM) for instrument/unit qualification and use as flight spare
- 1 flight model (FM)

Special items of mechanical ground support equipment and electrical check-out equipment would also have to be supplied by the PI groups.

During the development phase of the instruments, the QUASAT project would conduct, with the PI groups, a preliminary design review, a critical design review and a flight model review.

The QUASAT Science Working Team comprising the PI representatives and the ESA project scientist will monitor this development.

11.3 Programme management

11.4 Industrial Procurement

Subject to the approval of the ESA's Committees, it is proposed that the spacecraft development is carried out by an industrial prime contractor. In principle, the selection will be made according to a two-step procedure:

1. An open Invitation to Tender will be issued after completion of the pre-phase B studies and selection of the payload. Two contractors may be chosen for carrying out competitive Phase B1 studies.
2. After a short bridging phase during which the prime contractor and the main subcontractors are identified, Phases B2-C-D are initiated.

These industrial contracts will be funded and placed by ESA and responsibility for monitoring the contracts and provision for liaison between the contractor(s) and PI groups would be with the ESA project team.

Chapter 11

Spacecraft Development

11.1 Procurement policy

The proposed procurement scheme for the spacecraft is to consider the complete radio astronomy package, including feeds, low noise amplifiers, frequency converters, synthesizer, switching matrix, calibration and total power detection system and science data formatter, but excluding the radio astronomy reflector, as experiments which are to be provided through principal investigators (PI) with national funding. ESA would be responsible for overall spacecraft and mission design, experiment integration, system testing, launch, operations, and acquisition and distribution of the data and would procure the radio astronomy antenna and service module.

11.2 Instrument selection and development

11.2.1 Science Team

After approval of the mission, ESA will issue an Announcement of Opportunity (AO) calling for proposals for the Mission Scientists. They will be selected on the basis of scientific expertise and will together with representatives of the PI of the Scientific Payload and the Project Scientist form a QUASAT Science Team (QST). This team will be responsible for monitoring the QUASAT system development and advising ESA on the progress. The QST will also be responsible for a core observing program to be carried out during the early phase of operation. The team will only exist up to and including the early operational phase after which its functions are carried out by the QPEC and the QSOC.

11.2.2 Instrument Selection

ESA will also issue an AO calling for proposals for the instrument development. This AO will be explicit in terms of spacecraft mission and resources, technical interfaces, schedule, deliverable items and responsibilities of the parties. ESA will expect the proposal to cover the complete instrument.

Scientific collaborations or individual groups are expected to respond with proposals, describing in detail the design and development of the instrument. The proposals should describe the management structure within the collaboration and show how responsibilities for the scientific, technical, operational and analysis aspects will be discharged.

The standard procedures mentioned above must be implemented with care in order to satisfy certain special requirements of QUASAT. These special requirements result from the fact that different "experiments" (different frequencies) use common equipment (feeds, synthesizer, etc.). Com-

10.7 QUASAT Proposal Evaluation Committee (QPEC)

Announcements of opportunity for observing time on QUASAT will be made twice a year by QSOC and will be open to the world-wide community. Proposals submitted will fall into two categories:

1. proposals for global (combinations of EVN, VLBA, AT, and other non-affiliated telescopes) observations with QUASAT, and

2. proposals for observations with individual ground arrays and QUASAT.

QPEC will review the proposals at meetings twice per year, and rate them according to the scientific merit of the proposal and its technical feasibility. In carrying out this task, QPEC will be advised on the technical feasibility of the proposals by experts from the operations groups of the ground VLBI systems and from spacecraft operations. Proposals requesting the use of the US VLBA and other US telescopes as the sole ground array operating together with QUASAT will be reviewed by the US NRAO before meetings of the QPEC. Proposals selected by the NRAO will be forwarded to QPEC for inclusion in the overall review.

Membership of QPEC should comprise appropriate representation from the ground-based VLBI systems, from the scientific community at large, the QSOC Manager, and from the operations managements of the ground VLBI systems. The Chairman of QPEC should be selected by the QSG from amongst the scientific community at large.

10.8 Division of responsibility for QUASAT operations

- The QSG is responsible for reviewing the overall performance of the QUASAT system (spacecraft, telemetry stations, ground VLBI systems and all other activities related to QUASAT), and for initiating action where necessary.

- The EVN institutes are responsible for operating the EVN radio telescopes.

- The NRAO is responsible for operating the US VLBA.

- The CSIRO is responsible for operating the Australia Telescope.

- The ESOC MCC is responsible for the operations and control of the QUASAT spacecraft including its payload and the ESA ground station network. The MCC will monitor the performance of the spacecraft-ground signal link required fro acquisition of the science data from the QUASAT spacecraft.

- ESA staff at QSOC is responsible for issuing AO's for observing proposals, the formulation and distribution of the observing schedule to the appropriate parties, and monitoring the status of QUASAT as a radio telescope.

- The EVN and NRAO will carry out the correlation, initial editing and archiving (including calibration information) of the QUASAT VLBI data.

- The EVN and NRAO will monitor the VLBI performance of QUASAT, and relay information on this to QSOC and, via the MCC, to the Telemetry Station Network.

- QPEC is responsible for selecting observing proposals which will maximise the science return from QUASAT. QPEC will advise the QSG on matters related to scientific performance.

The QSOC team lead by the ESA science operations manager (or project scientist) will report to SSD/SA. ESA will support QSOC within the environment of the host institute by appointing staff to carry out the following functions:
- Management
- Secretarial assistance
- Scheduling
- Monitoring QUASAT payload status and overall function (with PI support)

NRAO and CSIRO intend to second staff to QSOC in order to facilitate liaison between themselves and QSOC.

10.5 VLBI Data Processing Facilities

Data recorded in joint observations by QUASAT with the EVN alone will be correlated at the European DPF. Data recorded in joint observations by QUASAT with the US VLBA alone will be correlated at the VLBA Array Operations Center. Data recorded by global ground arrays will be assigned to a correlator facility by a mutually acceptable procedure to be developed by the major ground arrays. Each of the major DPF's will consider correlating other QUASAT observations, if requested.

QSOC via the MCC will instruct the telemetry stations to send their VLBI tapes to the appropriate processor, and via the block observing schedule will similarly inform the ground VLBI systems operations managements. QSOC will distribute the necessary calibration information to the correlators to enable the correlation to take place. Copies of the output data tapes should be archived at QSOC to ensure uniformity.

Both NRAO and CSIRO will consider hosting QUASAT Science Support Centres in the USA and Australia respectively, to provide facilities for constructing and processing images from QUASAT data. Such centres may also be established either on a national or pan-European basis in Europe.

10.6 Ground VLBI Systems

The tasks of the Ground VLBI Systems are:

- carry out the observations scheduled by QSOC.
- dispatch video tapes recorded at individual telescopes to the correlator assigned by the ground networks.
- dispatch information on the calibration of the telescope performance to the correlator and to the user.
- correlate the QUASAT data tapes with the ground VLBI data tapes.
- monitor the VLBI performance of VLBI systems including QUASAT and relay information on this to QSOC.

The day-to-day operations of the ground VLBI arrays will be supervised by the EVN Coordination Group in Europe, by the NRAO Director for Socorro Operations in the USA, and by the AT Head of VLBI Operations in Australia. QSOC will communicate directly with the Chairman of the EVN Coordination Group and with his NRAO and AT counterparts.

Membership of the QSG should comprise appropriate representatives of the ground-based VLBI networks and the participating space agencies.

10.3 QUASAT Operations Management

There are five elements to the operational management of QUASAT:

1. QUASAT Science Operations Centre (QSOC)
2. Mission Control Centre (MCC)/ ESA Ground Station Network
3. VLBI Data Processing Facilities
4. Ground-based VLBI Systems
5. QUASAT Proposal Evaluation Committee (QPEC)

Elements 1), 3), 4) and 5) will be described in terms of the tasks to be carried out in support of QUASAT observations. The MCC and ESA Ground Station Network have been described in sections 8.4 and 8.3.

10.4 QUASAT Science Operations Centre (QSOC)

Following a competitive selection, after an announcement of opportunity, the QSOC will be located at a host scientific institute preferably, but not necessarily, at the European VLBI Data Processing Facility. The Space Telescope European Science Institute established within ESO Garching as host institute may be an example. It will carry out the following tasks:

1. issue "announcements of opportunity" for observations with the QUASAT system, and carry out the administration of the proposal evaluation process.
2. following advice from the QPEC on the observing proposals, and after consultation with spacecraft and ground VLBI system operations managements, construct observing schedules bearing in mind spacecraft, telemetry station and ground-based radio telescope constraints, and send to the ground-based VLBI systems and to the MCC.
3. receive and assimilate house-keeping and auxilliary data (e.g. phase- transfer link information and performance data on the radio astronomy receivers on board the spacecraft). Communicate phase transfer and receiver performance information to the Data Processing Facilities (DPF) of the ground VLBI systems.
4. following correlation of the QUASAT data with that of the ground VLBI systems at the DPF assigned by the ground systems, QSOC staff will check QUASAT end-performance by producing "quick-look" images for the astronomer proposing the observation.
5. receive feedback from the User Community on the performance of QUASAT.

Chapter 10

QUASAT Science Operation

10.1 The Scientific User and QUASAT

Opportunities to use the QUASAT obervatory will be open to any competent scientist. Following the twice-yearly Announcements of Opportunity for submission of observing proposals, an investigator may submit proposals for QUASAT observations with any of the ground-based VLBI systems, to the QUASAT Science Operations Centre (QSOC) in Europe. Evaluation of the proposals will take place in the QUASAT Proposal Evaluation Commitee, and the results communicated to the investigator. If successful, the proposal will be scheduled for observation at a time dependent on its priority, and on the constraints of the spacecraft, the telemetry station network, and the ground VLBI systems. Observations will be carried out for the astronomer "in absentia", that is, without requiring the presence of the investigator either at the QUASAT Mission Control Centre at ESOC or at any of the telescopes of the ground VLBI systems. Following the observation, the science data tapes from the participating ground telescopes and from the telemetry station network will be correlated absentee at either the European or US VLBI Data Processing Facility (DPF).Scheduling of the correlation will be carried out by the individual DPF. An investigator will receive a computer tape from the DPF containing calibrated interferometric data in a standard format (e.g. FITS), which can then be analysed in the usual manner for ground-based interferometric data sing standard software (e.g. the Astronomical Image Processing Software, AIPS, developed for e VLA, but also including VLBI-specific tasks). QUASAT Science Support Centres are under sideration in Europe, USA, and Australia to provide advice on analysing QUASAT data. The ASAT system contains a number of disparate elements — a space radio telescope and telemetry on network under control of a space agency and ground VLBI systems operated by national ies. The smooth functioning of the system "behind the scenes" is essential for a high scientific and for ease of use for the individual investigator. The remainder of this Chapter is devoted ning the operations management and the interactions between, and responsibilities of, the elements of the system.

10.2 QUASAT Steering Group

The QUASAT Steering Group (QSG) Space-Earth VLBI system will be operated under the auspices of the QUASAT Steering Group. The QSG will review operations of the complete space-ground VLBI system and its scientific performance twice a year. It will have authority for non-fiscal policy decisions concerning current and future operations of the system. Fiscal questions will be referred to the sponsoring organisations. The QSG will select the Chairman of the Proposal Evaluation Committee (QPEC).

experiments using the NASA Deep Space Network and other stations, and by system tests and maintenance. About 10 percent of the time the system will not be in use, no telemetry station being in view of the satellite.

The EVN Consortium and NRAO each agree to make a minimum commitment of 30 percent of ground VLBI array time to joint use with QUASAT. The AT agrees to make a minimum commitment of 15 percent of ground array time available for use with QUASAT. These commitments hold for an initial period of two years. In the event of a major spacecraft failure that impacts the main scientific goals of the mission, the commitment of observing time will be reconsidered.

During the first three months, the European VLBI Consortium, the US NRAO and the AT agree to conduct a QUASAT observing programme that has been planned by a QUASAT Science Team with appropriate representation from Europe, USA, Australia and Canada.

4. The specifically space-related elements of the QUASAT mission are to be funded by ESA and collaborating national space agencies. This means that satellite, telemetry, and spacecraft operations are to be paid for by the space agencies.

5. The costs of developing, building, operating, and maintaining the individual radio telescopes and the correlators in the earth-based VLBI systems – will continue to be funded by the national and international agencies supporting the EVN, the VLBA and AT.

   Additional operational costs necessary to the operation of the EVN with QUASAT are to be supported by the appropriate national space agencies.

   Additional systems costs and operational costs necessary to the operation of the VLBA with QUASAT are to be supported by NASA.

   Additional operational costs necessary to the operation of the AT with QUASAT are to be supported by the appropriate national agencies.

6. In coordinating QUASAT and ground operations, the favourable collaborative experience VLBI astronomers gives confidence that similar collaborations will be successful between various ground VLBI systems and between the ground systems and QUASAT. The rou project operations, as noted in point 1, are naturally separable, with the ground sy being operated by the ground-based agencies and QUASAT being operated by ES construction phases, similarly, will be under the supervision of the appropriate agenci QUASAT Science Team will monitor the interface problems that might arise and their solution.

7. The EVN, NRAO and AT endorse the concept management plan for QUASAT put forward in Chapter 10 of this report.

Table 9.4: USSR VLBI Network

Name	Antenna diameter	Latitude	Longitude
Simeiz	22m	44°	−34°
Evpatoria	70m	+45°	−33°
Pushino	22m	+55°	−38°
Bearlake	64m	+56°	−43°
Samarkand	70m	+39°	−66°
Ulan UJde	25m	+52°	−107°
Ussurusk	70m	+43°	−132°

9.7 Commitment of Observing Time on the Ground VLBI Systems

The following paragraphs has been subscribed to by the following official representatives of the ground arrays:

R. Wielebinski Chairman, Board of Directors, European Consortium for Very Long Baseline Interferometry, for the European Very Long Baseline Interferometry Network (EVN).

P.A. Vanden Bout Director, National Radio Astronomy Observatory, for the US Very Long Baseline Array (VLBA).

R.D. Ekers Director, Australia Telescope, for the Australia Telescope (AT).

1. This document will refer to the VLBI systems now in preparation for Europe and the US, to a combination of the two, and to the AT. It is reasonable to expect, based on current VLBI experience, that other arrays and individual radio telescopes outfitted for VLBI participation, will also be part of VLBI operations that use the QUASAT orbiting station.

   The European VLBI Network will be operated under agreements set up by the various national authorities. The US VLB Array will be operated by the NRAO under contract from the National Science Foundation (NSF). The Australia Telescope will be operated by the Commonwealth Scientific and Industrial Research Organisation.

2. The EVN Consortium, the NRAO, and the AT agree that the QUASAT orbiting VLBI station will enhance the scientific power of VLBI observations greatly since (1) it will allow interferometry with much longer baselines than available with earth-based arrays with image quality equal to the best now achieved on Earth and (2) it will allow the study of low-declination and southern hemisphere sources that cannot be studied with high two-dimensional resolution using ground-based arrays that are currently planned.

3. It is clear that all of the available QUASAT observing time will be utilized for observations with the EVN, VLBA, combinations of these two arrays, and with the other arrays such as the AT. As an initial target, the QUASAT Science Team has proposed that about 20 percent of the time be used by each northern hemisphere array operating independently, for a total of 40 percent, and a further 20 percent will be used by a combination of the two arrays. Of the remaining 40 percent of the observing time, 20 percent would be used in conjunction with the AT and other Southern Hemisphere radio telescopes, and 10 percent by special-purpose

and the VLA from a new operations centre in Socorro, New Mexico.

9.5 The Southern Hemisphere Array

Centre piece of the Southern Hemisphere Array will be the Australia Telescope (AT) currently under construction. The AT is a long baseline array consisting of a local linear array of six 22-m antennae at Culgoora, a new 22-m antenna at Siding Spring, and the existing 64-m telescope at Parkes. Within Australia, additional telscopes at Tidbinbilla (NASA) and Hobart (University of Tasmania) will be able to operate with the AT to form a north-south array with good baseline coverage from 100 to 1500 km. All of these antennas will be QUASAT compatible. VLBA tape recorders have been specified for all sites and the preferred local-oscillator distribution scheme is transmission via the Australian domestic satellite, AUSSAT3.

Studies of the imaging potential of space VLBI have shown that QUASAT can provide very good images of sourthern sources if the orbiting station observes in conjunction with the Australian array augmented by stations in Brazil, South Africa and (depending on the declination) in Japan. QUASAT will provide the only means of making good VLBI images of objects at declinations below −45°. Table 9.3 lists the stations of the Southern Hemisphere Array.

Table 9.3: The Southern Hemisphere Array

Name(country)	Antenna diameter	Lat.	Long.
Culgoora (Aus)	54m*)	−30°	−150°
Mopta (Aus)	22m	−31°	−149°
Parkes (Aus)	64m	−33°	−148°
Tidbinbilla/Canberra (Aus)	70m	−35°	−149°
Hobart, Tasmania (Aus)	26m	−42°	−148°
Hartebeesthoek (SA)	26m	−26°	−28°
Itapetinga (BR)	15m	−23°	−47°
Nobeyama (J)	45m	+36°	−139°
SEST, Swedish/ESO (Chile)	15m	−29°	−70°

*) equivalent diameter of tied array

9.6 Other Telescopes

Besides the three networks in Europe, the USA and the Southern Hemisphere there will be about a dozen other radiotelescopes operational by 1995. These are stations in the USSR, China, India and Japan (see Figure 9.1).

In the Soviet Union there is a network of seven antennas under construction or in the process of being equipped for VLBI use. Observing time with this network is decided by the Soviet Academy of Sciences.

There will be three 25 m telescopes in China by 1995. The locations are near Shanghai, Kunming (SW China), and Urumchi (NW China). The observing time with this network is decided by the Chinese Academy of Sciences.

The maximum east-west and north-south spacings between the European antennas are about 2700 km and 1500 km respectively. Studies of the imaging potential of space VLBI have shown that the EVN provides excellent aperture plane coverage with QUASAT if only two further stations on the east coast and the west coast of the USA are added to the array. The requirement for the addition of more distant antennas to the EVN comes from the fact that the shortest baselines from satellite to ground-based telescopes are about 6 000 km, considerably more than the 2 700 km on the ground, which leaves a large annular gap in the aperture plane for the EVN alone with QUASAT.

The unique advantage of the EVN is the considerable number of large diameter antennas with high frequency capability which results in a VLBI system of unparalleled sensitivity. By 1995 there will be seven antennas with effective diameters $\geq$ 30 m and capable of observing at 22 GHz, among them the 100-m telescope and not counting the 70-m DSN antenna near Madrid. There will be a total of 13 antennas with diameters $\geq$ 20 m with 22 GHz capability.

The European VLBI Data Processing Facility is planned to handle the simultaneous correlation of multi-station data including that from QUASAT.

9.4 The US Very-Long-Baseline Array

A new dedicated VLB Array (VLBA) is now under construction by the NRAO in the USA. The array will be available for astronomical and astrometric/geodetic observations. When completed in 1992 it will consist of ten new 25 m antennas located at sites throughout the United States, ranging from Hawaii to the Caribbean; see Figure 9.1 and Table 9.2.

The configuration of the array is optimized to provide both high angular resolution and a large field of view, with as uniform two-dimensional aperture plane coverage as possible, over a wide range of declination. Observations will be possible in nine frequency bands from 330 MHz to 43 GHz. The fundamental recording specification requires continuous, unattended operation at 128 Mbit/s for 12 hours.

For the observations of weak sources and observations with QUASAT the sensitivity of the VLBA can be enhanced by adding the VLA (equivalent diameter $\approx$ 130 m) and other large telescopes in the USA and in Europe.

The VLBA correlator is planned as a 20-station system, to accommodate extended-array observations, i.e. global and/or Space VLBI observations. NRAO plans to operate both the VLBA

Table 9.2: VLBA stations

Location	N Latitude	W. Longitude
Pie Town, New Mexico	34°	108°
Kitt Peak, Arizona	32°	112°
Los Alamos, New Mexico	36°	106°
North Liberty, Iowa	42°	92°
Fort Davis, Texas	31°	104°
Brewster, Washington	48°	120°
St. Croix, Virgin Islands	18°	65°
Owens Valley, California	37°	118°
Mauna Kea, Hawaii	20°	155°
Hancock, New Hampshire	43°	72°

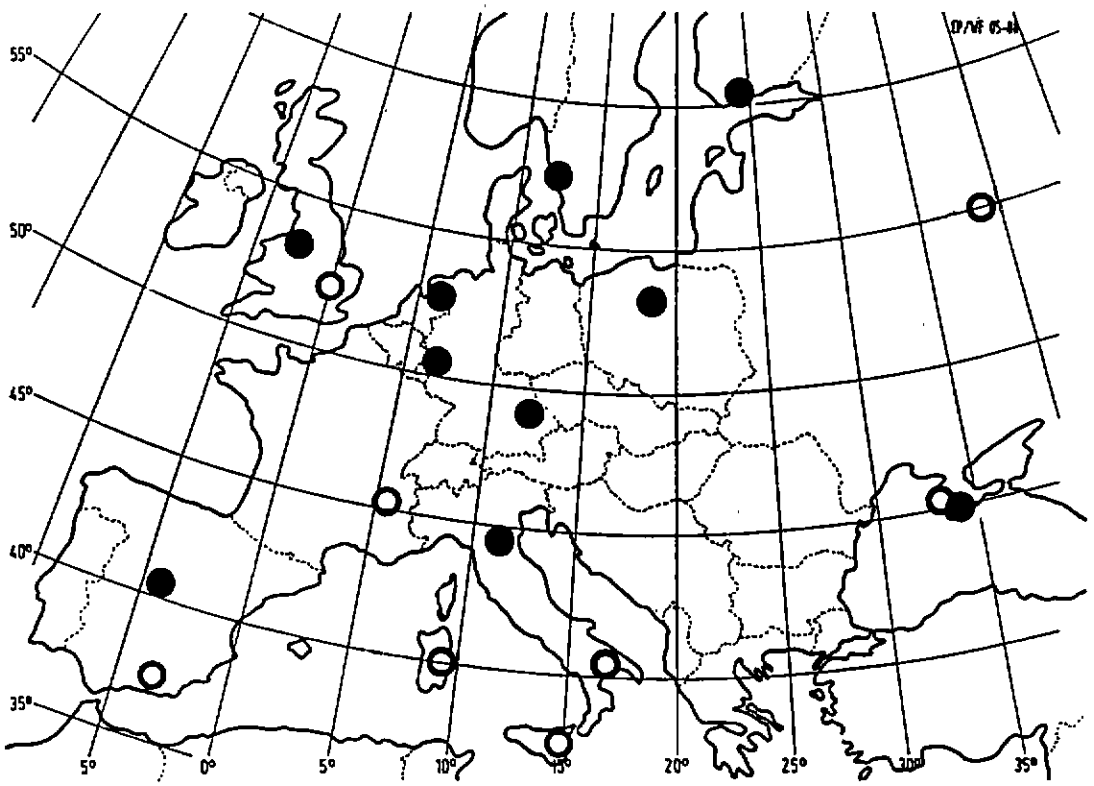

Figure 9.2: The European net of VLBI stations

European VLBI stations currently in operation (full circles) or expected to be operational by 1995 (open circles).

Table 9.1: European VLBI Stations

Location (country)	Antenna ⌀	VLBI status	Institute
Jodrell Bank (UK)	76m,26m	EVN station	Univ. of Manchester
Cambridge (UK)	32m	funded, EVN+MERLIN station	Univ. of Manchester
Robledo/Madrid (E)	70m	DSN station, occasional VLBI	DSN
Pico Veleta/Granada (E)	30m	mm-ant. to be equipp. VLBI	IRAM Grenoble
Plateau de Bure (F)	30m*	mm-ant. to be equipp. VLBI	IRAM Grenoble
Westerbork (NL)	93m*	array, EVN station	NFfRA, Dwingeloo
Effelsberg/Bonn (D)	100m	EVN station	MPIfR, Bonn
Wettzell, Bavaria (D)	20m	astrometric/geodetic VLBI	Satellitengeodäsie, Bonn
Medicini/Bologna (I)	32m	EVN station	Istit. di radioastr., Bologna
Noto, Sicily (I)	32m	under construction, for VLBI	Istit. di radioastr., Bologna
Sardinia (I)	≥32m	planned, for VLBI use	Istit. di radioastr., Bologna
Matera, Cabria (I)	20m	under constr., astro/geo VLBI	
Onsala/Göteborg (S)	26m,20m	EVN station	Onsala Space Observatory
Torun (PI)	15m,32m	EVN station, 32m under constr.	Torun Rad. Astron. Obs.
Metsähovi/Helsinki (SF)	14m	mm-ant., occasional VLBI use	Univ. of Helsinki
Simeiz, Crimea (USSR)	22m	EVN station	Crimea Astroph. Observ.

*) equivalent diameter of phased array

New developments:

- the construction of new and the activation of existing radio telescopes for VLBI use (England, Italy, Poland, Spain, China, India, Japan) or the construction of whole VLBI networks in the USA, the USSR and in Australia;
- the implementation of advanced receiving systems permitting quasi-simultaneous multi-frequency observations in both polarizations;
- the implementation of user-friendly automated operation of the interferometer elements allowing for remote control of individual stations by an array control centre;
- the development and implementation by the VLBA of an advanced VLBI system, for recording, playback and correlation based on high-density recording techniques developed at the Haystack Observatory. In its final form, the new recording system will permit recording at a rate of 128 Mbits/s for 12 hours on one tape. For reasons of compatibility the VLBA standard will be adopted in all networks.
- the construction of advanced correlators, the 'foci' of the networks, in Europe and in the USA permitting simultaneous correlation of data from up to 20 stations including one or more orbiting stations.

9.2 Current Status

Current astronomical VLBI observations are carried out using telescopes located on both sides of the North Atlantic Ocean making up the European and US VLBI Networks. Both networks are administered by consortia of institutions engaged in radio astronomy. The EVN has eight members from seven European countries and the US consortium consists of eight members from the USA and two from Europe. VLBI is one of the major, if not the major, activity at most of the consortium member institutes and up to one third of all possible observing time is set aside for this work.

Starting in the late 1970's these networks have turned into facilities run like single observatories and open to any user from the international community. Characteristic functions of the network operations are: evaluation of observing proposals through programme committees, coordinated scheduling of VLBI block time four times per year, and 'absentee observing' at network stations. VLBI processing centres are in Bonn (FRG), Haystack (MA., USA) and Pasadena (CA., USA). Software packages are available for 'post-processing' and image reconstruction. The European and US networks interact closely for the organization of global observations with up to 18 telescopes and baselines ranging from a few 1000 to about 8500 km.

9.3 The European VLBI Network

Figure 9.2 shows the geographical location of twenty radio telescopes in Europe which are either active VLBI elements or are under construction or are planned for VLBI use. Table 9.1 lists the locations of these telescopes along with their diameter, their VLBI status and the operating institution.

Chapter 9

Earth-based VLBI Systems

9.1 Overview/Goals for 1995

The ground-based VLBI systems constitute the other major element of the QUASAT mission. The European VLBI network augmented by associate stations, the US VLB Array (VLBA) augmented by the VLA and other large telescopes, and the Ssouthern Hemisphere Network will be the main partners of the orbiting element; but other networks in the USSR and in Asia (China, India, Japan) are likely to participate as well. Figure 9.1 shows the geographical location of 44 major VLBI stations which will be operational by 1995.

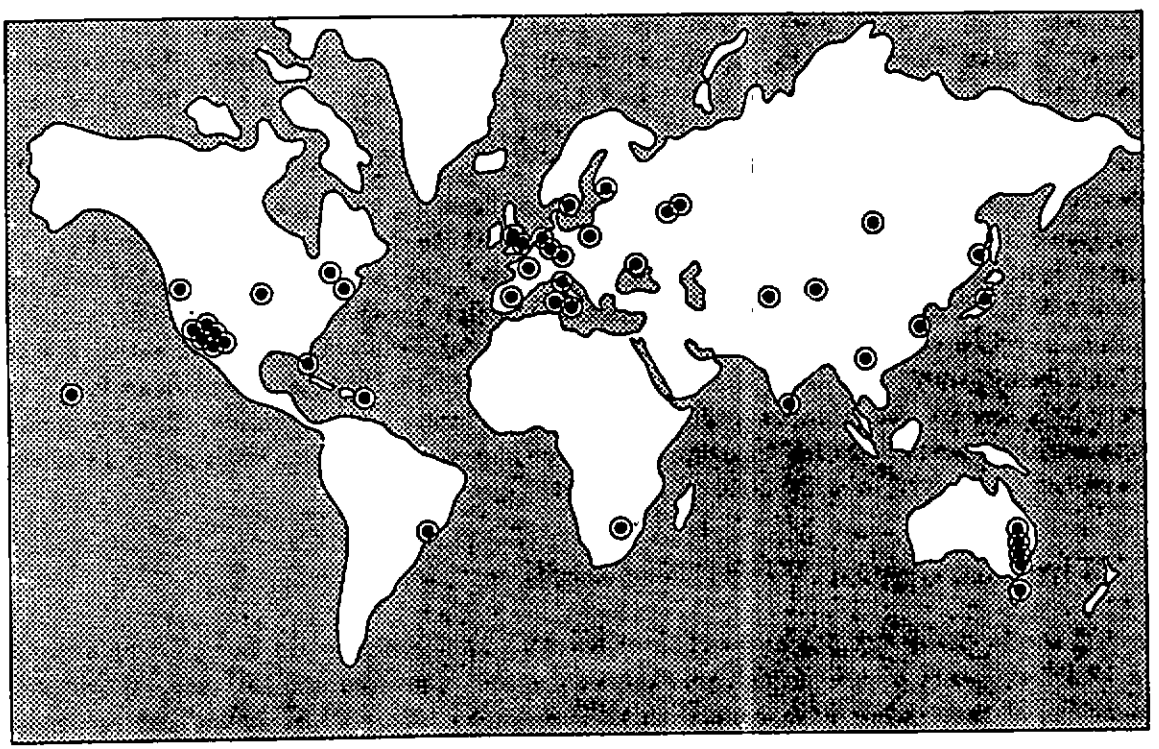

Figure 9.1: The global net of VLBI antennas

44 major VLBI stations expected to be operational by 1995. The radio telescopes are located in Australia, Brazil, Canada, China, England, Finland, France, W-Germany, Italy, India, Japan, the Netherlands, Poland, South Africa, Spain, Sweden, USA and USSR.

(b) *Off-line Computer System*, used for non-time-critical tasks. The TBD off-line system, which will basically be used during the operations phase, will handle all Flight Dynamics tasks. In addition the system will be used for the Spacecraft Performance Evaluation System (SPES) tasks, the project dedicated non-time critical processing activities, and any mission analysis activities prior to launch.

(c) *Simulation Computer*(TBD), used as a simulation system pre-launch and during the operational phase.

In view of the relatively low data rates to the MCC - only HK data - it is intended to satisfy the computer requirements with existing hardware to the maximum extent possible.

The **Mission Software** needed to fulfill the mission requirements and to support the operational concept can be described as follows:

(a) *Mission Analysis Software.* Existing in-house mission analysis software will be used to support the necessary mission analysis activities prior to launch which include mission studies, concept evaluation and trade-off evaluations for e.g. launch window calculations, launch and injection strategies, and nominal operational orbits.

(b) *Data Processing Software.* Data Processing software is required to handle the HK-telemetry and telecommand data streams and to support the mission as regards: mission planning subsystem, satellite monitoring subsystem, control subsystem, on-board software support, and off-line activities.

(c) *Flight Dynamics Software.* Flight Dynamics software is required in support of attitude determination and control, orbit determination and control, supported by related system and quality assurance

(d) *Simulator Software.* Satellite simulator software will be developed to model the satellite subsystems, the satellite environment and the relevant parts of the ground segment. The satellite simulator software will represent for both nominal and contingency situations the satellite on-board behaviour, and the interaction of the satellite and its space environment.

8.3 Ground Station Network

(a) *Launch and Early Orbit Phase (LEOP) Network.* The standard ESA LEOP network with stations located in Kourou, Malindi and Perth will support the mission from approximately 8 hrs prior to launch until acquisition of the first operational orbit, until begin of the commissioning operations. The LEOP network will also be used to support the transfer phase from the first to the second operational orbit. The LEOP stations will only be capable of supporting the S-band operations with low speed housekeeping data.

(b) *Routine Operations Network.* The routine operational orbit phases will be supported by Ku-band telemetry Stations to be installed and located in Kourou, Malindi and Perth. The functions of the ground station(s) are those described in subsections 8.2.1 and 8.2.2.

In order to meet the mission requirements each telemetry station needs to be provided with a Ku-band up/down link system including a 10m ground dish, a hydrogen maser as the atomic frequency reference, and a specially designed phase transfer system. Furthermore, unique QUASAT equipment will be required for recording of science data, i.e. an interface unit to synchronize and format data prior to recording and VLBI recorders.

Each telemetry station required in support of spacecraft operations will be linked to the Mission Control Centre through a fully redundant pair of digital communication links which will provide sufficient capacity (9.6 Kbps) to handle the combined load of HK-telemetry, telecommand, ranging and doppler data.

8.4 Mission Control Centre

The **Mission Control Centre** (MCC) for the mission will be located at ESOC, Darmstadt in West Germany. The operations conducted from the MCC include:

(a) *Scheduling and planning* of satellite operations on the basis of block observing schedules issued by QSOC and scheduling of ground segment facilities in line with satellite operations schedule, pass characteristics, user product requests and facility performance.

(b) *Monitoring and control* of the status and proper functioning of the satellite by analysis of housekeeping telemetry data, and monitoring and coordination of ground segment facilities which are actively participating in the mission.

(c) *Execution of flight control* including orbit and attitude maneuvers and reconstitution and prediction of flight dynamics data, including handling of any anomalies detected by satellite monitoring.

Due to the requirement to correlate the science data acquired from QUASAT with the data obtained by the Earth based VLBI telescopes in order obtain the scientific results, and taking into account that no science data will be sent to the MCC, the QSOC will not be co-located at the MCC, but at a host institute preferably, but not necessarily, at the European VLBI Data Processing Facility.

However, there will be a QSOC representative at the MCC during all mission phases to maintain the interface to the QSOC.

The MCC will be connected to the QSOC via a dedicated voice link required for coordination purposes.

The **Computer Facilities** used in support of the mission will basically consist of the following systems:

(a) *Mission Dedicated Computer System* (MDCS), used as real time and/or near-real time monitoring and control system, which will comprise two VAX computers with identical CPU's, whereby one machine will be used as prime computer, and the second one as back-up.

tapes (special High Density Tapes (HDT's), 32 tracks. Approximately 1 to 2 tapes per day and per ground station are expected. Science Data Tapes will be sent directly from the ground station(s) to the SOC (Correlator) on a daily basis, and will be available at the VLBI data processing facility within 3 day. No science data will be sent to the MCC. Further processing (correlation) of science data is considered to be fully a VLBI data processing facility responsibility and will not be performed by the MCC.

Housekeeping Data HK-telemetry data comprising either full spacecraft and/or reduced payload status data will be decoded and time tagged with an accuracy of $\pm 25\mu$seconds relative to UTC at the ground station(s). The HK data need to be matched to the orbital parameters to define the transfer time between S/C and ground station. The capability will exist to convert housekeeping data to engineering units, to enable assessment of system performance. HK data will be routed via communication lines directly to the MCC and are available at the MCC within TBD hrs of receipt at the ground station. Housekeeping data will be supplied off-line to QSOC within 3 days together with interpretation files allowing the end user to process any data required for his purposes.

Phase Transfer Data Phase Transfer will be measured and pre-processed at the ground station(s) by a specially designed phase transfer system to yield the doppler data required for orbit reconstitution, and the information on the phase behaviour of the on-board local oscillator for correlation purposes. These data will form part of the auxiliary data (see below) provided to the QSOC.

Auxiliary Data The auxiliary data provided will comprise data not contained in the HK-telemetry data, and will include e.g. orbit and attitude data (position and velocity data with reference to the pointing direction), command log (e.g. command history, error reports, etc.), phase information, etc.

8.2.3 Data Distribution / Archiving

The Data Distribution performed by the MCC will be as follows:

1. VLBI Tapes containing science data acquired by QUASAT will be send directly from the ground station(s) to the VLBI data processing facility on a daily basis, and will be available with approximately 3 days delay time.

2. HK- and Auxiliary data will be sent to the QSOC on Computer Compatible Tapes (CCT's) with 6250 bpi, 9 tracks approximately 3 days after the observation. QSOC will forward the necessary information to the VLBI data processing facility.

Distribution of data to the end user is a QSOC responsibility. The Archiving Functions can be summarized as follows:

1. Raw HK-telemetry data and auxiliary data will be archived by the MCC for a period of 10 years from the end of the mission. A table of contents of the archive will be available in form of an on-line catalogue. The archive medium will allow retrievals by optical disc and/or magnetic tape and/or electronic means, as required.

2. Raw science data will not be archived. Archiving of processed (correlated) science data is a VLBI data processing faility responsibility and will not be performed by the MCC.

Payload real-time commanding will be supported during commissioning and contingency operations only. No real-time and / or near real-time commanding by users outside MCC will be performed. In general all commands will be validated before transmission from the MCC and verified subsequent to the uplink via housekeeping. The required operational modes and user requests (e.g. observing times, sources, etc.) should be available at the MCC not later than 2 weeks prior to required execution.

8.2.1 RF and TT&C Interfaces

On the basis of the mission requirements the following Radio-Frequency- (RF-) and Tracking, Telemtry and Command (TT&C) link interface baseline has been established:

Spacecraft TT&C The use of S-band frequencies is only foreseen for the support of the satellite TT&C (2 Kbps) during LEOP and the Transfer Orbit Phase (TOP). Furthermore contingency situations during the operational phase of the mission may be supported in S-band, however, no hot redundancy can be guaranteed.

The use of the Ku-band frequencies (13.9 and 14.1 GHz - see below) is foreseen for the support of the satellite TT&C (2 Kbps) during the operational phase of the mission.

Science Data down link Ku-band (14.8-15.0 GHz) for the digital transmission of the science data to ground is selected from a frequency management point of view and allows the observation bandwidth of 64 MHz to be digitally transmitted at 144 Mbps without use of polarization multiplexing. The transmission modulation scheme is assumed to be QPSK directly modulated on the carrier.

Phase Transfer up/down link The possibility of selecting two relatively close frequencies (13.9 and 14.1 GHz) for relaying the phase transfer signal in Ku-band is based on the assumption of link reciprocity, i.e. the phase shift on-board the satellite is half the phase shift measured on-ground. Under this assumption, there is no need to correct the ionospheric error using a coherent carrier in a different frequency band.

In order to meet the stability requirements associated with the phase transfer data, coherency between station up- and down-link will be required as a fundamental station design criterion. In turn this requires the development of an on-board transponder which fulfills the phase stability- and spread spectrum requirements. The latter is required to avoid interference with military radars operated in the same frequency band. The influence on the phase transfer of the on-board antenna booms for the S/C to ground station antennas is yet to be determined and may require up-link correction for each attitude.

To meet the stability requirements the phase transfer uplink will be continuously updated, based on smoothed orbital parameters to keep the up-link within the transponder range. Updating will be performed approximately every 2 to 3 seconds based on orbit prediction / reconstitution.

The properties of the phase transfer data (phase tracking of a coherently transponded signal) will also be used for orbit determination purposes.

Preliminary telemetry and telecommand link budgets have been established (subsection 7.5.5) and show adequate margins.

8.2.2 Mission Products

Science Data Upon receipt of the science data at the ground station, data processing will be limited to frame synchronization, recoding and subsequent recording of the data on VLBI

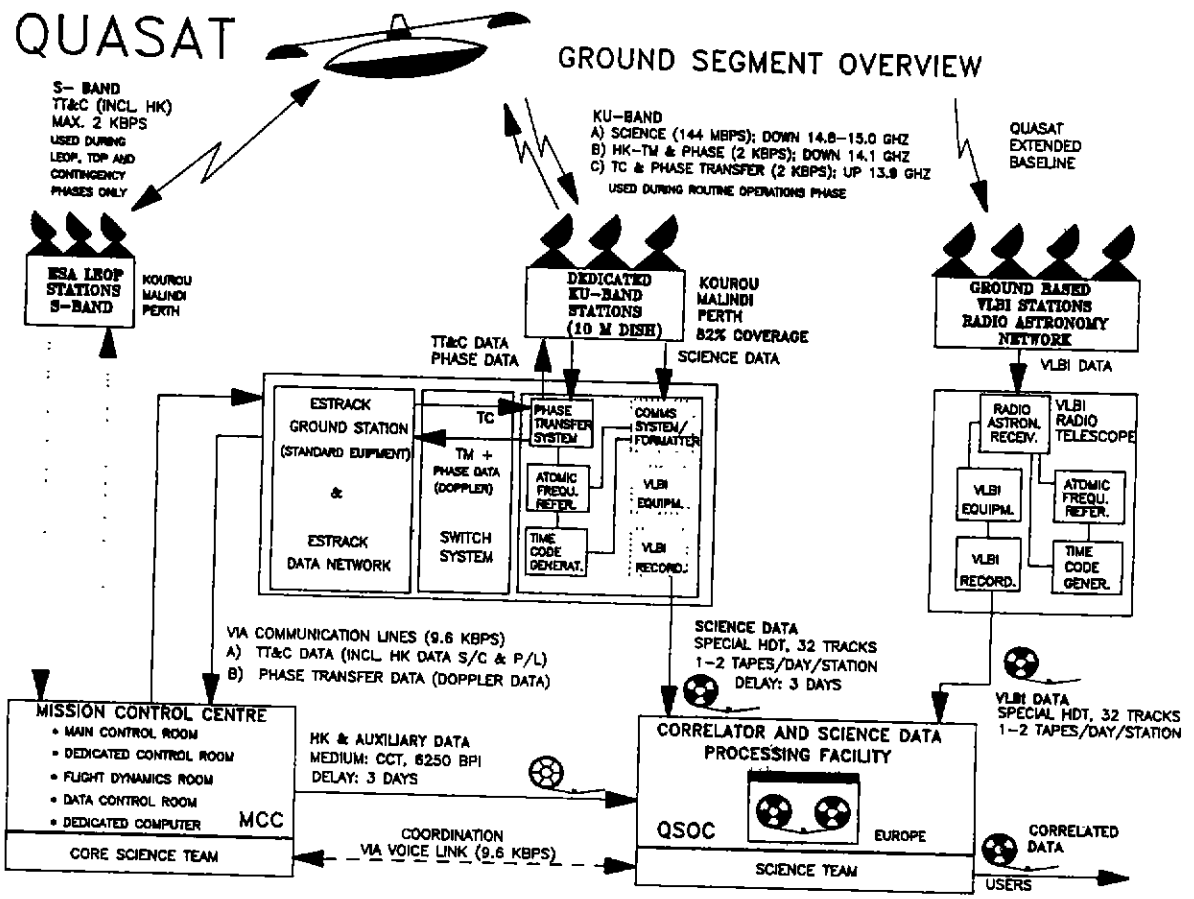

Figure 8.1: QUASAT Ground Segment Overview

Chapter 8

Flight Operations and ESA Network

8.1 Introduction

An overview of the Ground Segment required to support the mission during the various mission phases i.e. Launch and Early Orbit Phase (LEOP), Transfer Orbit Phase(s), Commissioning and Verification Phase(s), and the Mission Operations Phase(s) is provided in Figure 8.1 The ground segment consists of the following essential elements:

- Launch and Early Orbit Phase (LEOP) Network
- Routine Operations Phase Network
- Mission Control Centre (MCC)
- QUASAT Science Operations Centre (QSOC)
- VLBI Data processing facility
- Ground VLBI Networks

8.2 Operational / Technical Concept

The overall responsibility for mission rests with the ESA Directorate of Scientific Programmes. Control of flight operations, however, will be delegated to the Directorate of Operations. All mission operations will be conducted according to mission timelines, Flight Control Procedures (FCP's), and Contingency Recovery Procedures (CRP's) which are all part of the Flight Operations Plan (FOP).

The concept for controlling the satellite is based on the use of a single control centre in conjunction with three ESA ground stations. During the Routine Operations Phase (operational orbits) the nominal mode to operate the satellite is 'Non Real Time'.

Contacts between the satellite and MCC are primarily used for the pre-programming of those autonomous on-board operations requiring subsequent near term execution, and for data acquisition during periods of telemetry station coverage.

During any critical operations (LEOP, Commissioning- and contingency phases), however, the satellite will be on-line with the MCC, which will assess in real time the execution of commanded operations down to the level of activated units, and assess in real time the overall performance situation on-board the satellite.

in case the S-band system is made to operate during science observations, which in the baseline system design it is not.

Analysis of service module equipement showed potential noise sources in the power subsystem (array power toggling, BDR operation) causing interference in the 327 MHz band. EMC requirements will have to be imposed on these circuits to achieve compatibility.

Finally, conducted emissions caused by digital or power circuits might be a cause of interference. Carefull harness design (single point grounding, geometrical layout, screening) to suit payload requirements will therefore be necessary.

7.6.3 New Developments

Although in the spacecraft design conventional solutions have been selected wherever possible and have been shown to meet the specification; the following areas remain, where substantial new (technology) developments are required.

- REFLECTOR.The ISRR concept has been developed by Contraves under ESA contract. A 3 m offset model has been built and tested, and a 6 m centre-fed model is presently being manufactured and will be subjected to extensive testing in the near future. Apart from these tests on scaled-down models, a materials characterization test program is foreseen for the materials used in the ISRR in order to determine its dimensional stability in the space environment.

- BOOMS. Although the design of the long booms is based on proven technology and the development can take advantage of mechanism designs that have evolved for other space applications, a considerable effort will be required in this area.

- Ku-BAND SYSTEM. Ku-band transponders are presently being developed by ATES for Eutelsat and ERS-1. However, the high- stability and spread spectrum requirements imposed by QUASAT certainly will necessitate additional development. This will also be required for the Ku-band waveguides, although the same technology as used for the (space-qualified) C-band and X-band carbon fibre waveguides (developed by Dornier) can be applied.

Table 7.9: Antenna efficiency budget

Power Loss due to:	K-band 22 GHz	C-band 5 GHz	L-band 1.7 GHz	UHF 0.3 GHz
Illumination, Spillover, Phase	0.70	0.71	0.72	0.65
Blocking	0.937	0.937	0.937	0.937
Central Support Attenuation	0.977	0.997	0.999	>0.999
Surface Error	0.57	0.972	0.997	>0.999
Attenuation of 3 Membranes	0.981	0.997	>0.999	>0.999
Reflector Mismatch	1.0	1.0	0.999	0.984
Anti-Static Coating	0.977	0.988	1.0	1.0
Axial Defocussing	0.99	0.99	0.99	0.99
Transverse Displacement	0.99	1.0	1.0	1.0
Thermal Deformation	0.94	0.99	1.0	1.0
Mispointing ($\leq$ 30 arcsec)	0.955	0.977	1.0	1.0
TOTAL	0.31	0.61	0.66	0.59

Concerning electronics, especially in payload and OBDH subsystem equipment, special radiation-hardened components and/or appropriate shielding have to be provided (to be analyzed in Phase B).

Another area of concern is the total dose seen by the CCD matrices of the startrackers. Presently not enough is known about this problem but since the same problem exists for ISO and XMM a better understanding can be expected in the near future. In any case, appropriate shielding of the CCD's will have to be stipulated.

7.6.2 EMC

An EMC analysis has been carried out in order to identify the main sources of interference and evaluate their impact on spacecraft design. It was found that the major interference is caused by radiated emissions generated by the following sources:

- Ku-band antenna system
- S-band antenna system
- Service module and solar array

Concerning the radiated emission from the Ku-band antenna, it is assumed that the feeds provide enough rejection of out-of- band radiation. In-band unintentional radiation may be produced as sub-harmonics of the 14 GHz frequency. Assuming the level of these harmonics at -60 dBc (standard), an additional 30 dB suppression is necessary to meet the payload EMI requirements. The Ku-band system design shall provide for this attenuation.

The S-band antenna might cause interference problems due to the second harmonic which is within the tuning bandwidth for C-band. A total attenuation of 90 dB of this second harmonic shall be provided by the S-band system to satisfy payload requirements. This constraint only applies

Table 7.7: Ku-band science data down-link budget summary

Function	Nominal/Adverse Margins (dB) Down-link
Carrier Lock	29.2/24.7
Telemetry Recovery	6.0/1.5

7.5.6 Phase Transfer Coherency Budget

Table 7.8: Phase transfer coherency budget

Perturbation Source	Coherence
Propagation Terms	
- Ionospheric Scintillation	0.9980
- Tropospheric Scintillation	0.9980
Receiver Error	0.9983
Multipath	0.9992
Mechanical Instabilities	0.9980
Higher-Order Phase Rates	0.9875
Overall Coherence Factor (over T = 300 sec)	0.9791

7.5.7 Antenna Efficiency Budget

See table 7.9. Note that power loss due to thermal deformation is for worst case and no refocussing.

7.6 Special Aspects

7.6.1 Particle Radiation

In the proposed orbits, QUASAT will experience severe radiation environments since it is continuously within the Earth's radiation belts. Particles fluxes and doses resulting from geomagnetically trapped energetic protons and electrons and from solar flare induced protons have been computed at Estec. The resulting doses are extremely high (5 to 10 times the typical communication satellite dose after 5 years).

A major effect of this environment is the degradation of the solar cells leading to an efficiency loss of about 40 % after 5 years.

In addition, charge accumulation on the large (dielectric) Kapton-covered radome could be a potential hazard to the spacecraft. The resulting discharges could be a source of interference and cause damage to the thin aluminium layer of the reflector. Predicted potential differences for a dielectric radome are as high as 15 kV. Therefore it is necessary to cover the radome with a (semi) conductive material (Indium Tin Oxide) to leak out the dc charges.

7.5.4 Pointing Budget

Table 7.4: Pointing budget

ERROR SOURCE	3σ error (arcsec)
Star tracker	
- bias error	3
- noise equivalent angle	0.8
Star tracker support	
- thermoelastic bias	calibrated
Measurement RSS	3.8
Control	10.8
Pointing accuracy (AOCS frame)	14.6
Reflector thermoelastc bias	calibrated
Calibration error estimate	20
Pointing accuracy after calibration	24.8

7.5.5 RF Link Budgets

Table 7.5: S-band link budget summary

Function	Nominal/Adverse Margins (dB)		
	Up-link	Down-link	Up + Down
Telecommand	3.8/-0.3	-	-
Telemetry	-	4.4 / 0.9	-
Ranging	31.3/25.1	-	16.2/5.9

Table 7.6: Ku-band phase transfer/TT&C link budget summary

Function	Nominal/Adverse Margins (dB)	
	Up-link	Down-link
Carrier Lock	5.0/2.5	8.2/3.7
Telemetry Recovery	-	15.9/11.4
Telecommand Recovery	9.5/7.0	-

7.5.2 Propellant Budget

The propellant budget in Table 7.2 is based on the dry spacecraft mass including contingencies. There is no additional contingency on the propellant mass

Table 7.2: Propellant budget

	Mass (kg)
Spacecraft dry mass	779
Ejectables	20.7
Helium pressurant	0.8
Residuals	7.2
Propellant mass	
AOCS (5 years)	40
Apogee maneuver	453.5
Perigee maneuver	143.1
Propellant consumed	636.6
TOTAL PROPELLANT LOADED	643.8

7.5.3 Power Budget

The power budget is shown in table 7.3. Three cases are considered: the science (operational) mode, the survival mode during long (> 1 hr) eclipses and the transfer orbit mode. In this last mode there is a distinction between the average power consumption and the power consumption during maneuvers, as well as between power in sunlight (sl) or in eclipse(ec).

Table 7.3: Power budget (Watts)

Load	SCIENCE		SURVIVAL	TRANSFER	
	aver.	max		aver.	maneuv.
Payload	47-67	67	-	-	
Data handling	35		15	30	
TT&C Ku-band	81		-	-	
TT&C S-band	7		7	29	
AOCS	126	178	42	100	
Power	29		9	29	
Coolers	80		80	-	
Heaters	97		130	150 sl 130 ec	138 sl 118 ec
Harness loss	12		5	5	
Propulsion	21		27	27	43
TOTAL	535-555	607	315	370 sl 350 ec	374 sl 354 ec

Table 7.1: Mass budget

Subsystem	Mass (kg)
Payload	44
Reflector	124
TT&C Ku-band	37
TT&C S-band	13
Data Handling	20
Power	68
Solar array	70
Harness	45
Structure and Mechanisms	98
Thermal control	132
AOCS	75
Propulsion	53
TOTAL DRY MASS	779
Propellant/Pressurant	644.6
TOTAL INITIAL S/C MASS	1423.6
Adaptor	85
TOTAL LAUNCH MASS	1508.6

For reasons of redundancy, the antenna pointing mechanism electronics are mounted in the spacecraft body. Transmitters and receivers are also body-mounted and the RF links along the booms are obtained via silver-plated carbon fibre waveguides. Such waveguides have been developed by Dornier for C-band (5.3 GHz) and X-band (9.6 GHz) and no major problems are foreseen in the possible development of Ku-band waveguides. The connection with the antennas is via rotary joints.

The 5 W (SSPA) Science Data transmitter (SDTX) and 0.1 W Phase Transfer transmitter (PTTX) which are on are connected to the antenna in use via the transfer switch in the Radio Frequency Distribution Unit (RFDU). The one Phase Transfer receiver (PTRX) that is on is connected to both transmitters enabling a healthy cross-coupling at the receiver output. Receiver input cross- coupling is made permanent with the 3 dB coupler.

The science data downlink budget summary and phase transfer link budget summary are given in subsection 7.5.5.

7.5 System Budgets

7.5.1 Mass Budget

The mass budget given in Table 7.1 includes the following contingencies:

payload and new equipment	10 %
minor modifications	5 %
existing hardware	0 %

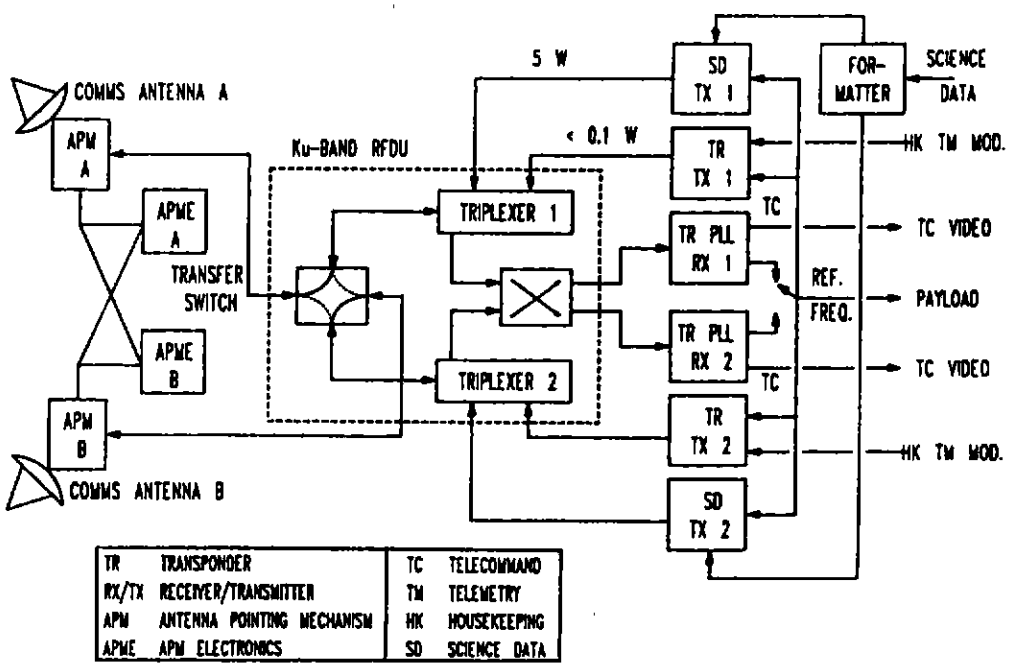

Figure 7.15: On-board Ku-band baseline

The Ku-band system encompasses the following links and functions

1. *Phase transfer uplink (13.9 GHz)*
   - ultra stable phase transfer (frequency derived from ground station hydrogen maser)
   - spread spectrum required to avoid interference with military radars.
   - transmitter frequency continuously updated to compensate for the predicted up-link Doppler shift.
   - telecommands are to be sent via this link almost continuously because of communications antenna pointing requirements (2 kbps)
2. *Phase transfer downlink (14.1 GHz)*
   - coherent with uplink, minimizing phase stability degradation.
   - spread spectrum required
   - housekeeping telemetry modulated on this link (4 kbps)
3. *Science data downlink (14.8 - 15.0 GHz)*
   - digital transmission of radio astronomy data (64 MHz bandwidth) to ground.
   - QPSK modulation directly on carrier
   - transmission bit rate is 144 Mbps.
   - bit error rate $< 6.6 \times 10^{-3}$

A block diagram of the Ku-band system baseline is shown in Figure 7.15. The 0.5 m Ku-band antennas with the hemispherical antenna pointing mechanisms (APM) are mounted on the booms.

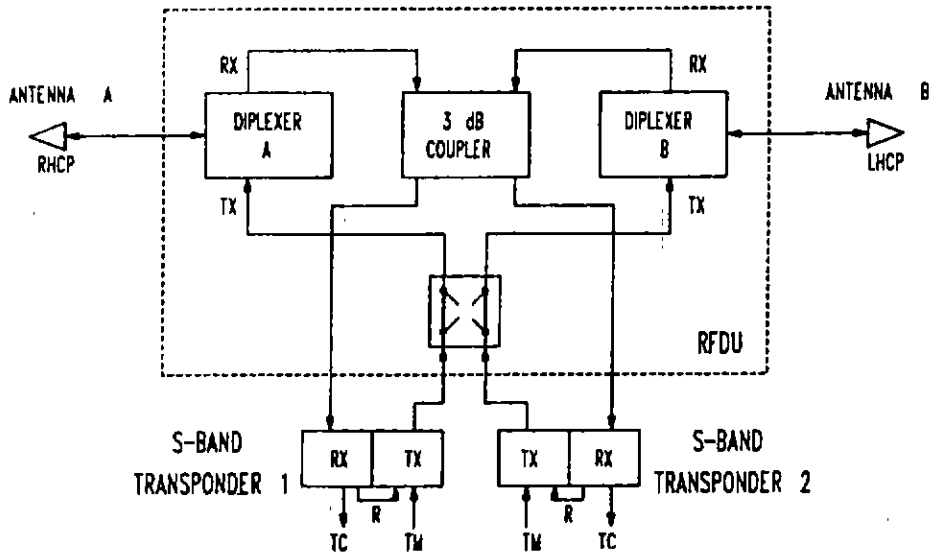

Figure 7.14: S-band configuration

To fulfill these tasks a straightforward OBDH subsystem, based on a possible Cluster DH is foreseen and shown in Figure 7.13

Telecommand reception is handled by the decoder which contains two PSK-demodulators and one protocol handler that selects either S-band or Ku-band. Valid telecommand frames are either executed directly in the decoder or sent to the Central Terminal Unit (CTU) for further processing and distribution over the OBDH bus.

The CTU also handles the housekeeping data collection using the OBDH bus and the Remote Terminal Units (RTU). The data are serialized and passed to the Science Data Formatter for inclusion in the Ku-band TM data or to the S-band for direct transmission.

On-board time keeping is another vital function of the CTU and the on-board time is distributed via the OBDH bus.

7.4.10 Telecommunications

QUASAT requires two telecommunications subsystems. A standard S-band system is used for tracking, housekeeping telemetry and command during LEOP, transfer orbit phases and in contingency situations. The block diagram is shown in Figure 7.14. The two hemispherical antenna are mounted on deployable booms which are attached to the outer edges of the solar array wings. The antennas are deployed automatically just after separation from the third stage of Ariane. The receivers, which are on all the time, are connected to both antennas, while for the transmitters a transfer switch is used to connect to either one antenna. The S-band link budget summary is shown in subsection 7.5.5.

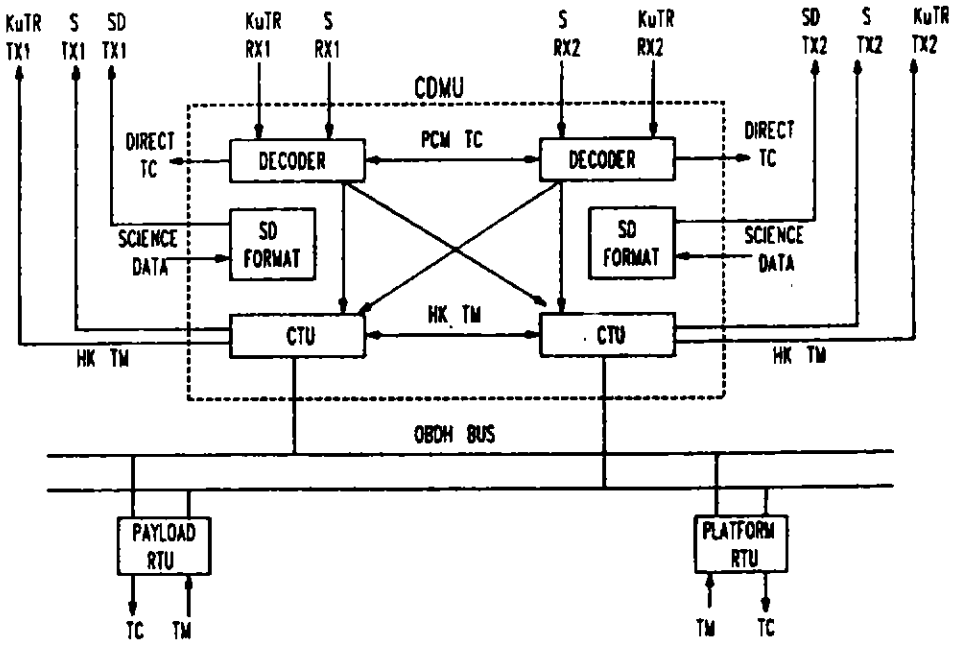

Figure 7.13: Data handling block diagram

The total power budget is shown in subsection 7.5.3 and the block diagram for the selected power subsystem is shown in Figure 7.12. It is based on the EUROSTAR/INMARSAT power subsystem providing a single regulated 42.5 V main bus connected to a star point for distribution to the spacecraft loads.

The Array Switching Regulator (ASR) provides the regulated bus in sunlight by the well established technique of sequentially switching solar array sections. It also provides control signals required by the other regulating elements of the subsystem: the Battery Discharge Regulators (BDR) and the chargers of the Battery Control and Interface Units (BCIU).

Eclipse regime regulation is also performed by the ASR which continually adjusts the BDR output current to meet the bus demand.

The BCIU's include the battery chargers, heater control and pyrotechnic circuits and an RTU interfacing with the OBDH bus for control and monitoring of the power subsystem.

Two 18 Ah NiCd batteries supply power in eclipse and during periods when the load exceeds the solar array capability, for instance, during a fuse clearing event.

Switching and protection of the main bus is accomplished within each individual load by means of relay switches, together with fuses and/or current limiters.

7.4.9 On-Board Data Handling Subsystem

The main functions to be implemented in the OBDH subsystem are:

- telecommand reception and distribution
- housekeeping data collection
- downlink housekeeping data stream generation
- science data formatting
- on-board time keeping and time distribution
- time-tag command handling

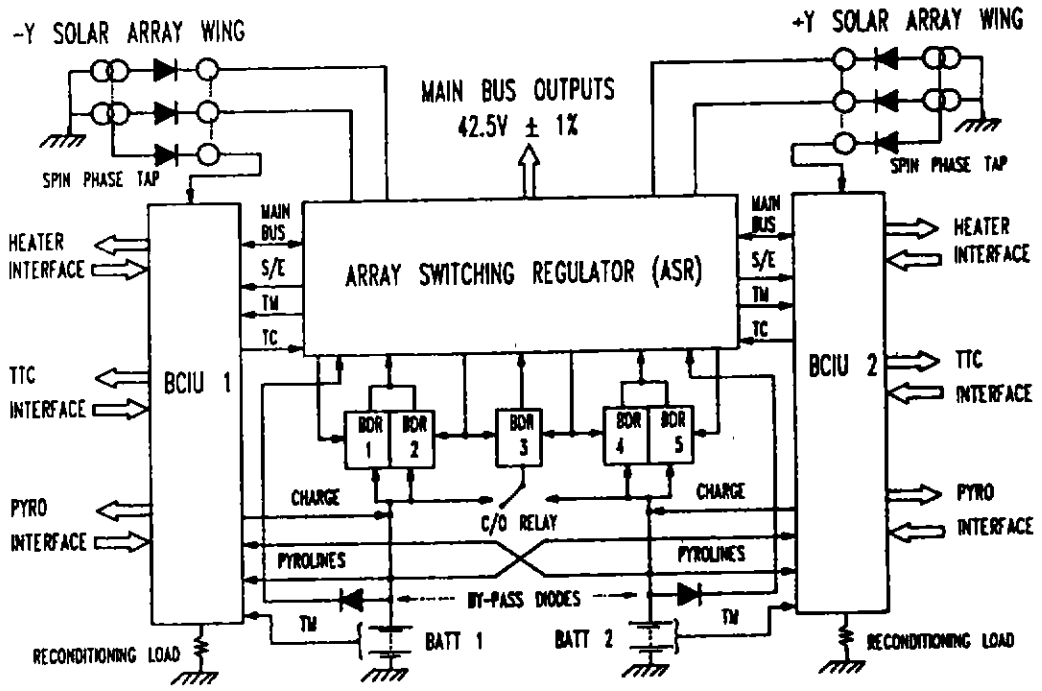

Figure 7.12: Power Subsystem simplified block diagram

GAs array will give a mass saving of about 15 kg. In addition, a GAs array would only require one panel per wing, while a silicon array has to be folded dual panel per wing. On the other hand, a GAs array would lead to cost increase of about 1 MAU and a qualification program would have to be started immediately.

These last considerations were the decisive factor for selecting a Si array with 500 micron coverglass and a total area of 11.8 m^2. The total maximum power degradation due to radiation of this array is 42 %.

To meet the power requirement in transfer orbit at minimum solar aspect angle (60°) one wing has to be deployed, supplying 425 W.

A qualification problem with today's generation of solar arrays is presented by the temperature reached after a long eclipse (−184° C). The qualification limit of present panels is −170° C and a delta-qualification on solar array components in a specially controlled facility appears necessary.

7.4.8 Power Subsystem

The power subsystem provides the following fundamental features:

- power distribution to the spacecraft loads
- battery management
- provision of pyrotechnic firing circuits and their control
- provision of heater controls
- telemetry and telecommand interfaces for both power subsystem and other subsystems